NG3-19948

SMITHSONIAN INSTITUTION
ASTROPHYSICAL OBSERVATORY

Research in Space Science

SPECIAL REPORT

Number 110

PROJECT CELESCOPE

An Astrophysical Reconnaissance Satellite

Edited

by

Robert J. Davis

OTS PRICE
XEROX $ 9.60
MICROFILM $ 3.74

December 14, 1962

CAMBRIDGE 38, MASSACHUSETTS

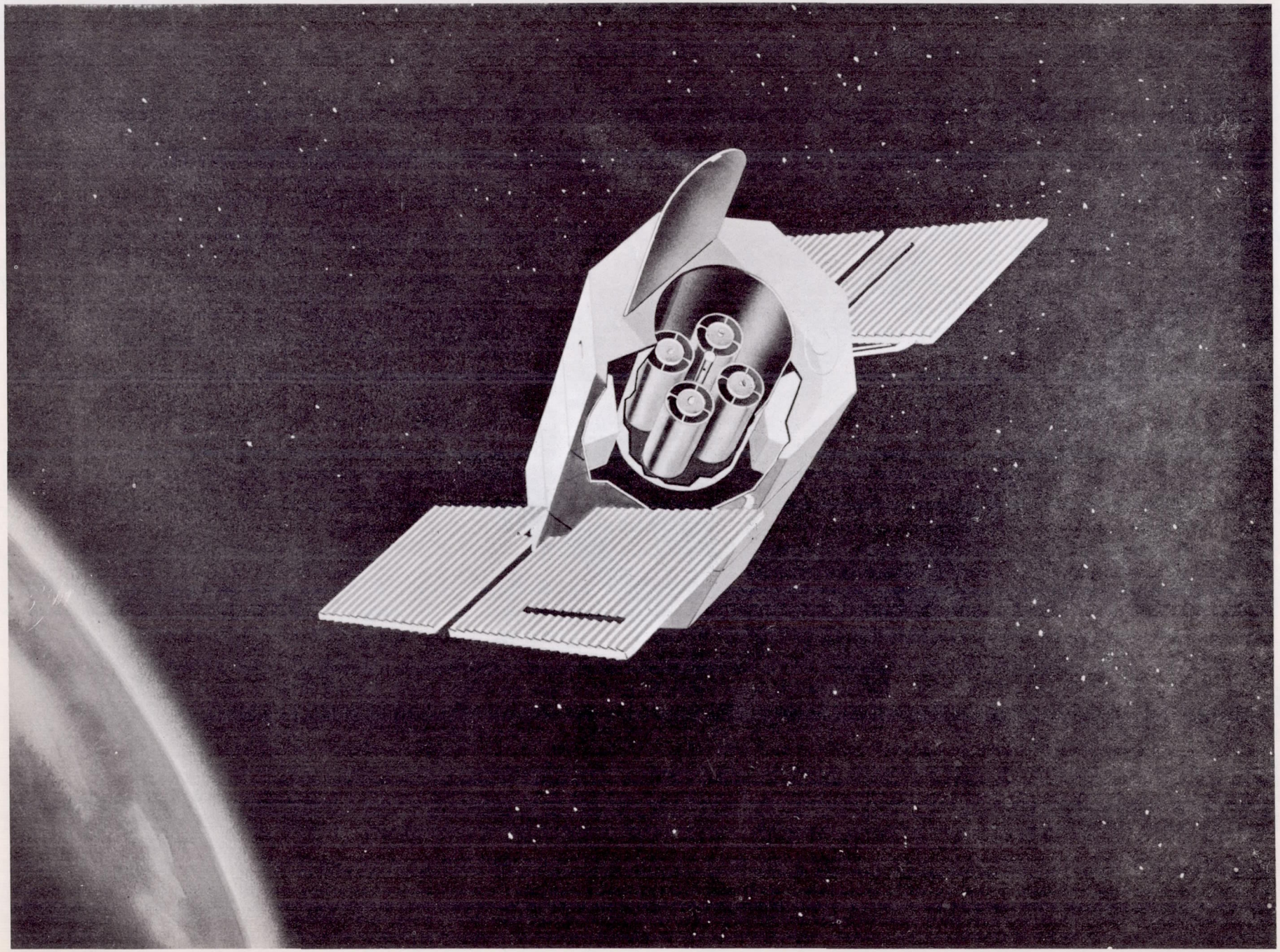

PROJECT CELESCOPE

An Astrophysical Reconnaissance Satellite

SAO Special Report No. 110

PROJECT CELESCOPE

An Astrophysical Reconnaissance Satellite

Edited

by

Robert J. Davis

Smithsonian Institution
Astrophysical Observatory

Cambridge 38, Massachusetts

PROJECT CELESCOPE

An Astrophysical Reconnaissance Satellite

Preface

In accordance with our stated intention to keep information about the Celescope Project up-to-date by issuing revisions as the design concepts develop, we present Special Report No. 110 It supersedes Special Report No. 83, published January 1962. The description now contains all those originally determined criteria and specifications of the program which have required no alteration, and incorporates details of construction that have undergone modification since the publication of the previous document. Our main purpose is to bring the latest developments to the attention of scientists, engineers, and others interested in the project, although not all the details discussed will necessarily be of concern to all readers.

Portions of this Report have been taken directly from progress reports prepared by Electro-Mechanical Research, Inc., the prime contractor for design and fabrication of the Celescope payload and ground-support equipment.

Robert J. Davis
Smithsonian Astrophysical Observatory

September 25, 1962

Table of Contents

List of Figures

List of Tables

Abbreviations used

AG	:	Analog gate
A-to-D	:	Analog-to-Digital
BC	:	Binary Counter
e.a.	:	elemental area
EFL	:	Effective Focal Length
EOS	:	Equipment in the Optical Space
NASA	:	National Aeronautics and Space Administration
OAO	:	Orbiting Astronomical Observatory
PCM	:	Pulse Code Modulation
PI	:	Pulse Inverter
UV	:	Ultraviolet

PROJECT CELESCOPE

An Astrophysical Reconnaissance Satellite

PROJECT CELESCOPE

An Astrophysical Reconnaissance Satellite

Introduction

The Smithsonian Astrophysical Observatory has long been interested in artificial satellites. Since 1955, one of our primary missions has been the precision optical tracking of such satellites. By these passive observing techniques we have gained valuable information concerning upper-atmospheric densities and the shape and structure of the earth.

Not only these satellites but also many recent rockets and balloons have contained active experimental apparatus for conducting observational programs above the atmosphere. Astronomers have three major reasons for making such observations. First, they want to overcome the problem of atmospheric absorption of electromagnetic radiation. The first solar spectrograms extending to wavelengths shorter than 2900 A were obtained from V-2 rockets flown in 1946. Water-vapor bands were first detected in an infrared spectrum of Venus obtained during balloon observations in 1959. The second reason is to increase angular resolution. Princeton's Project Stratoscope balloon program enabled Dr. Martin Schwarzschild in 1958 to photograph the solar granulation at improved resolution. The third reason is to decrease background illumination. There is as yet no example of extraterrestrial observations for this purpose.

On February 4 and 25, 1958, the scientific staffs of Harvard College Observatory and the Smithsonian Astrophysical Observatory met to discuss the most urgently needed astrophysical observations above the atmosphere. We concluded that the first should be ultraviolet studies, since infrared and high-resolution studies could at present be better done from balloons. We planned on using imaging techniques to allow us to study a maximum number of objects during the early phases of the program. Television offered advantages over other methods because it would enable us to control and change the program as the data were gathered.

In September 1958 the Smithsonian Astrophysical Observatory presented to the National Aeronautics and Space Administration a research proposal for these ultraviolet television studies. From it has grown Project Celescope, named for its pioneering of a truly celestial telescope, and applied especially to that division of the Smithsonian Astrophysical Observatory charged with the responsibility of designing, procuring, and operating the apparatus to be installed and orbited. The project is part of the NASA Orbiting Astronomical Observatories program (OAO), also termed the S-18 series. Other participating agencies are the University of Wisconsin, NASA's Goddard Space Flight Center, and Princeton University. The OAO program is more fully described by Ziemer (1961). The first OAO satellite, to be launched in 1964, will contain the Smithsonian Celescope and the University of Wisconsin's experiment.

Project Celescope now functions under NASA contract No. NAS5-1535.

I. Astrophysical Background

Short-wave electromagnetic radiation reacts strongly with matter. At wavelengths longer than 3200 A, the effects of the earth's atmosphere can be rather well eliminated from observational data by proper reduction procedure. Below 2800 A, no appreciable amount of radiation can penetrate the atmosphere to balloon altitudes (approximately 30 km) or lower. Altitudes of at least 100 km are necessary for making reasonably good observations between 1000 and 3000 A.

No optical materials are transparent to wavelengths shorter than 1050 A. Since transparent materials are necessary in our television camera tubes, this sets our short-wavelength limit.

1. Absorption by the Earth's Atmosphere

Tousey (1961) gives a chart showing the depth of penetration of incident ultraviolet radiation into the atmosphere. With the exception of a small, dusky "window" near 2100 A, the level to which 37 percent of the incident radiation penetrates is above 30 km for all wavelengths shorter than 3000 A. Between 2000 and 3000 A, the absorption is caused primarily by ozone (O_3). Although the maximum ozone density occurs near 20 km (Vigroux, 1960), appreciable amounts extending above 30 km effectively block the radiation between 2200 and 2800 A.

Between 1000 and 2000 A, the absorption is produced primarily by molecular oxygen (O_2). Throughout most of this region, 37 percent of the incident radiation penetrates to a level near 100 km. The vertical distribution of molecular oxygen is discussed by Kamiyama (1959).

2. Stellar Atmospheres

Since the preparation of Special Report No. 83, we have drastically revised our predictions concerning the ultraviolet fluxes to be expected from the hotter stars. For the reasons outlined below, we now expect the stars to be ten times fainter below 2000 Angstroms than we had predicted earlier. We have therefore had to repeat all the computations on which the design of the Celescope had been based. Fortunately, we had included in our original design a safety factor large enough to obviate changing the specifications for the broad-band television photometers. We have, however, had to eliminate from the system the slitless spectroscope.

Of the many problems to be attacked by the Celescope, only for the atmospheres of main-sequence early-type stars do we now have a reasonably clear picture of what to expect. One of Celescope's goals is the measurement of the brightnesses of at least 25 000 such stars in four spectral bands between 1000 and 3000 A.

The datum of interest is the shape of the spectral-energy distribution curves of the different types of stars. As was the case with the great sky surveys of the past--e.g., the Henry Draper Catalog and the Palomar Sky Atlas--we plan to acquire our data by a survey of the entire available portion of the celestial sphere, and thus increase our chances of making important unexpected discoveries. We are planning our instrumentation and observational program so as to balance the payload limitations of the Celescope with these scientific objectives.

The observational foundation for astrophysics is spectroscopy. Under close scrutiny, no two stellar spectra are identical. However, the great majority can be placed in a one-dimensional sequence based primarily on temperature. The coolest are the M stars, at about 3000° K. The K stars are at about 4200° K. (Both are also referred to as late-type stars, a relic of an obsolete theory of stellar evolution.) The G and F stars, intermediate types, are at about 6000° K. Early types are the A stars, at about 8000° K; the B stars, at perhaps 15 000° K; and the O stars, at perhaps 40 000° K. Each of these seven types is divided numerically, with the "0" (zero) subdivision being hottest and 9 the coolest. Thus, a B0 star at a provisional temperature of 32 800° K is nearly as hot as an O9 star at a provisional temperature of 37 450° K. The earliest O stars are classified as O5, and the latest M stars as M8. The sun is spectral type G1.5, at 5785° K.

To this one-dimensional temperature sequence may be added a second, less conspicuous, dimension involving atmospheric density. The giants and supergiants are less dense than the main-sequence (dwarf) stars, and therefore have sharper lines in their spectra. The giants and supergiants are much larger and more luminous than their main-sequence counterparts.

A third dimension in this scheme involves differences in chemical composition. Stars of types R, N, and S are cool stars of less usual chemical composition than the M stars. For the hotter stars, at least in the presently accessible region of the spectrum, these differences are not so obvious.

Many stars having somewhat peculiar spectra can still be fitted into the above scheme. Others, including the Wolf-Rayet stars, cannot. The Wolf-Rayet stars are apparently quite hot, exceeding 15 000° K, perhaps by a rather large factor. Their spectra consist primarily of emission lines and bands.

Recent experiments from rockets have given astronomers the first observational information concerning ultraviolet stellar spectra. Stecher and Milligan (1962) have obtained spectra of seven stars between 1600 and 4100 A. Alexander, Bowen, and Heddle (1962) have observed 22 stars at an effective wavelength near 1900 A. Byram, Chubb, and Friedman (1961, 1962) have observed 42 stars at effective wavelengths near 1250 and 1450 A. These observations indicate ultraviolet fluxes that are a factor of 3 to 10 lower than had been indicated by the model stellar atmospheres most widely used in predicting the spectra for the hotter stars. Since Celescope had been designed primarily on the basis of those models we have had to re-evaluate its expected performance in the light of the newer observations.

With the present design of the Celescope we expect to be able to measure the brightnesses of at least 25 000 stars with each of our broad-band television photometers. At the longer wavelengths, we shall observe statistically significant numbers of O, B, A, and F stars; at the shorter wavelengths, we shall be limited primarily to the O, B, and A stars. The small number of stars anticipated with the slitless spectroscope, however, has led to elimination of this instrument from the Celescope and its proposed replacement by a fourth broad-band television photometer.

Figures 1 through 5 compare the theoretical spectral distributions of stars of various spectral types with the provisional spectral distributions we are now using for our design. The effective temperatures used in the computation of these models were: O5, 44 600° K (Underhill, 1951); B0, 32 800° K (Traving, 1955); A0, 9200° K (Hunger, 1955); F0, 6720° K (Canavaggia and Pecker, 1953). If our provisional spectral distributions prove to be correct, these effective temperatures become: O5, 33 700° K; B0, 24 400° K; A0 and later, no change. The uncertainty of these provisional spectral distributions is pointed out by the factor of 5 difference at 2000 A between the flux from Beta and Epsilon Canis Majoris, as observed by Stecher and Milligan (1962). Both stars have been classified as type B1 II. This discrepancy might be explained by the fact that Beta Canis Majoris is known to be a pulsating variable star. Unfortunately, most of the slowly rotating giant stars between spectral types B1 and B3 are similar variables, and even some naked-eye stars in this spectral range have not yet been examined for pulsation or for rotation. (See McNamara and Hansen, 1961.) Nearly one-half of the stars so far observed in the ultraviolet from rockets lie in this spectral range. Perhaps Celescope will be able to separate the Beta Canis Majoris stars from their non-pulsating brethren.

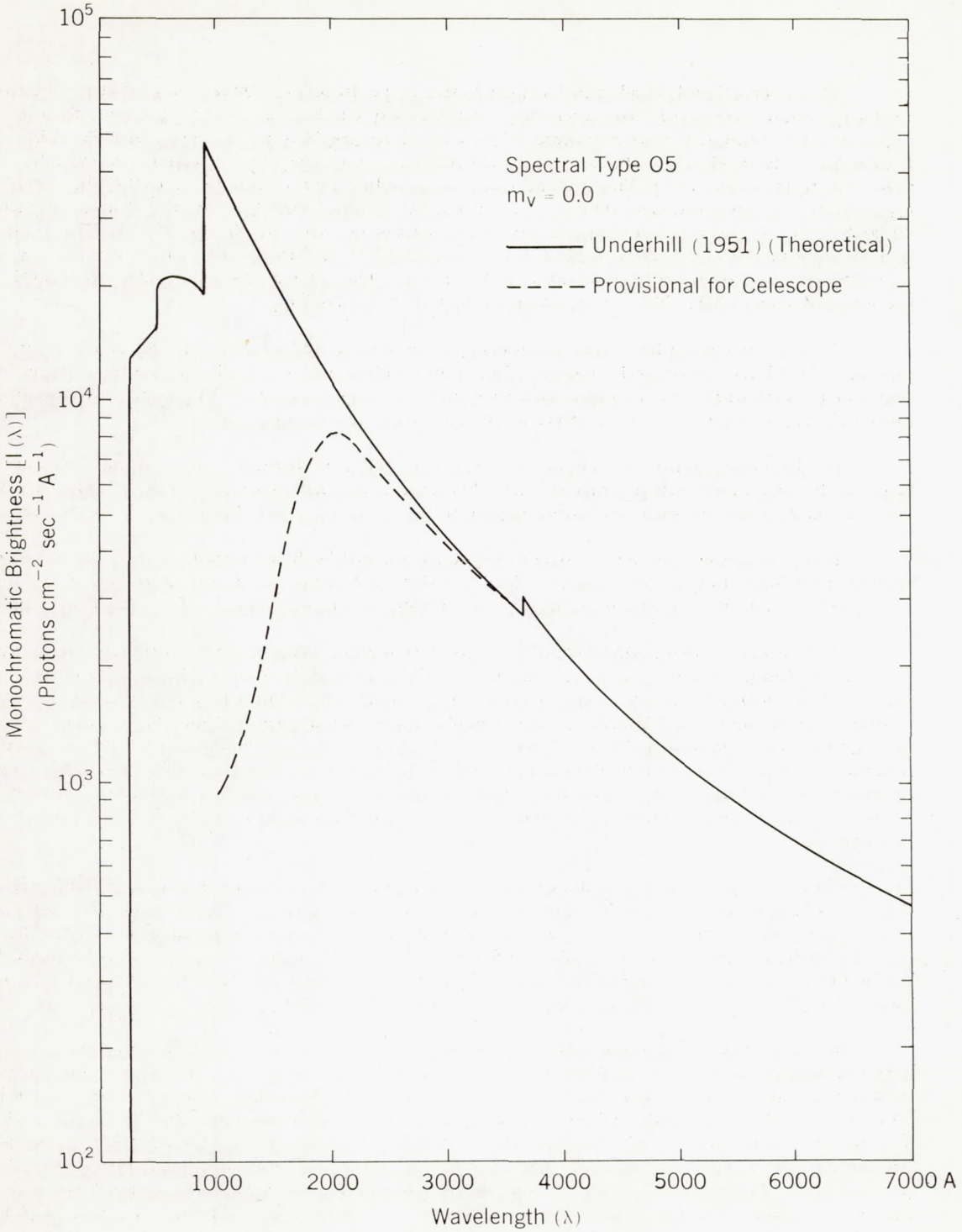

Figure 1.--Spectral distribution for an O5 star

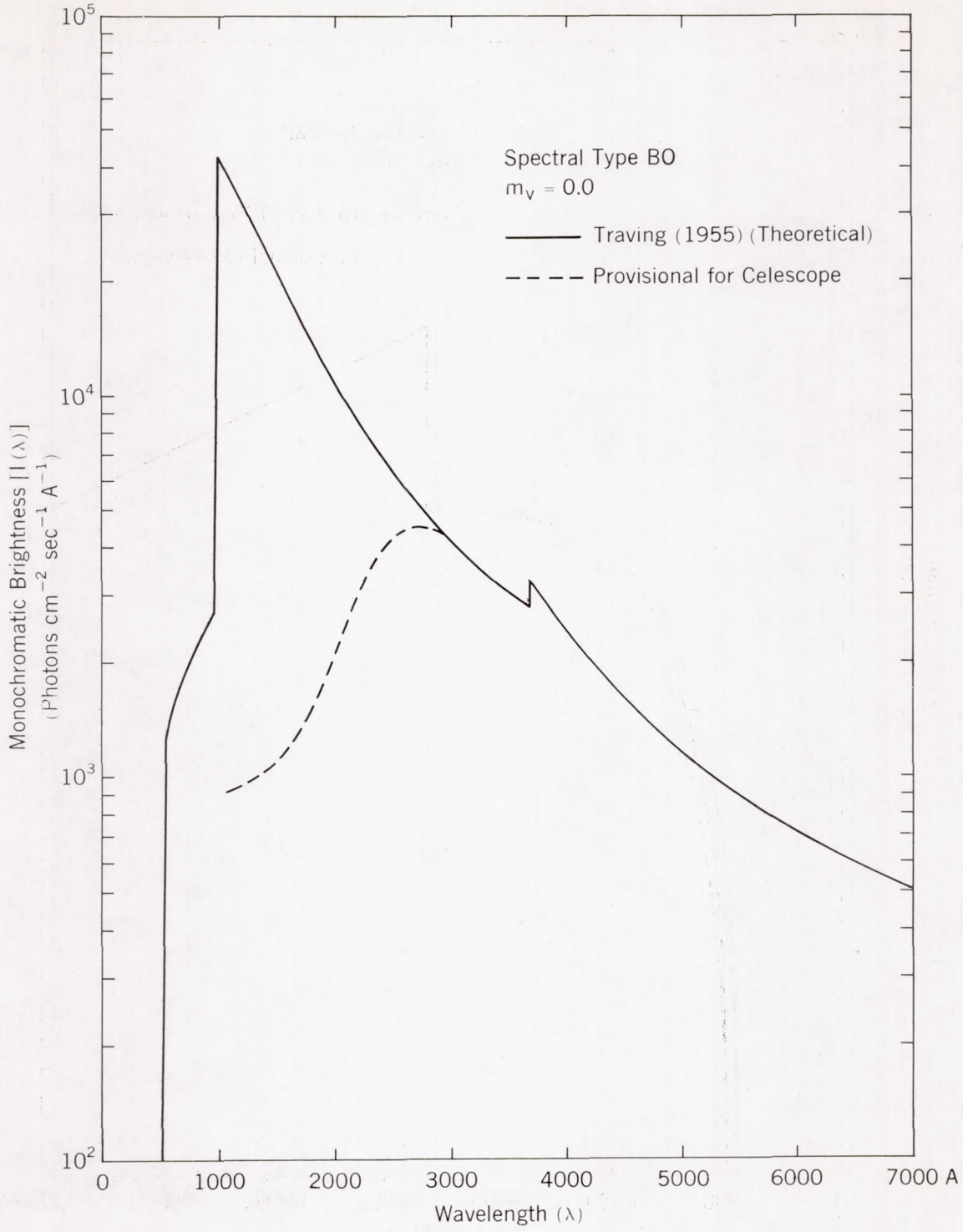

Figure 2.--Spectral distribution for a B0 star

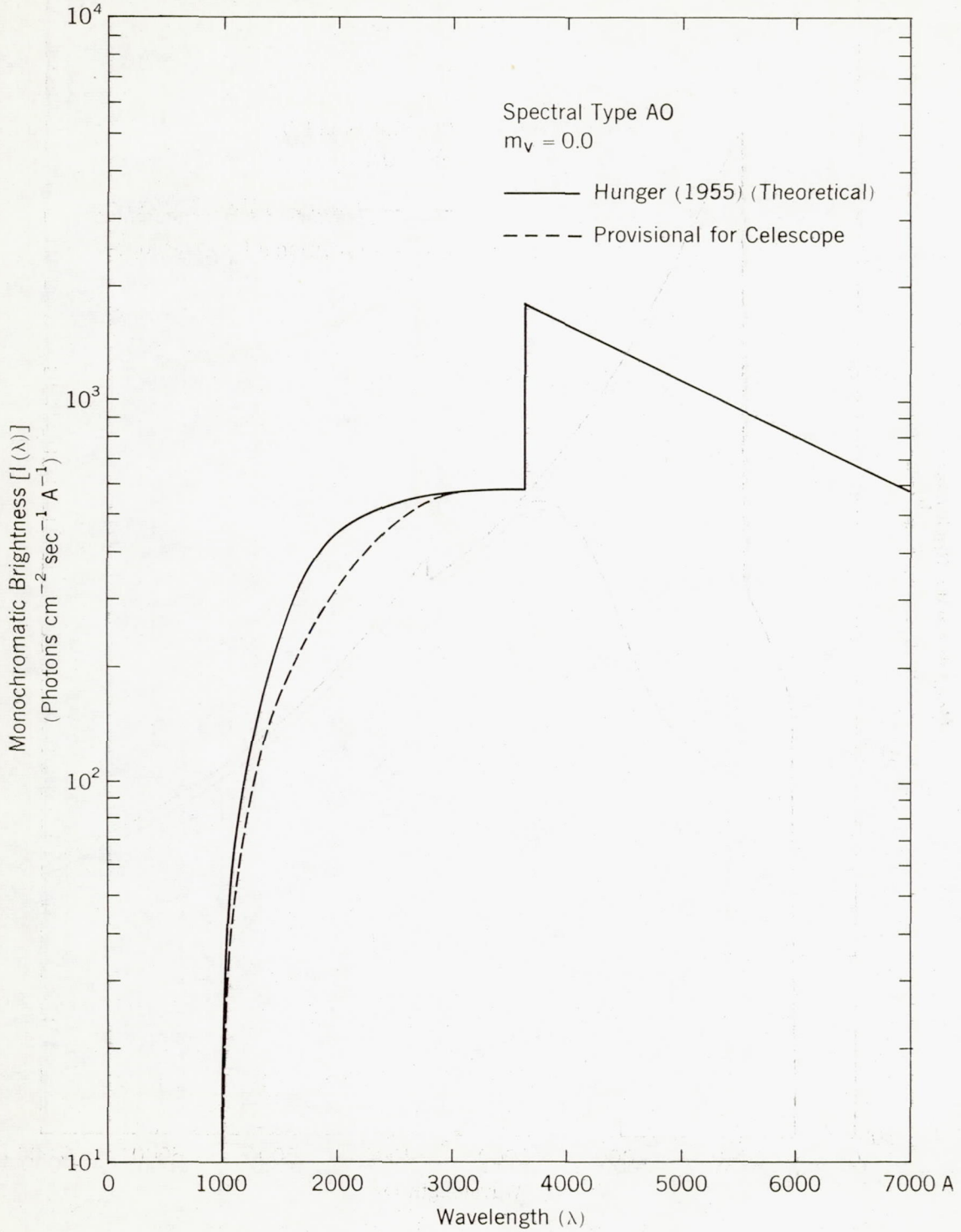

Figure 3.--Spectral distribution for an A0 star

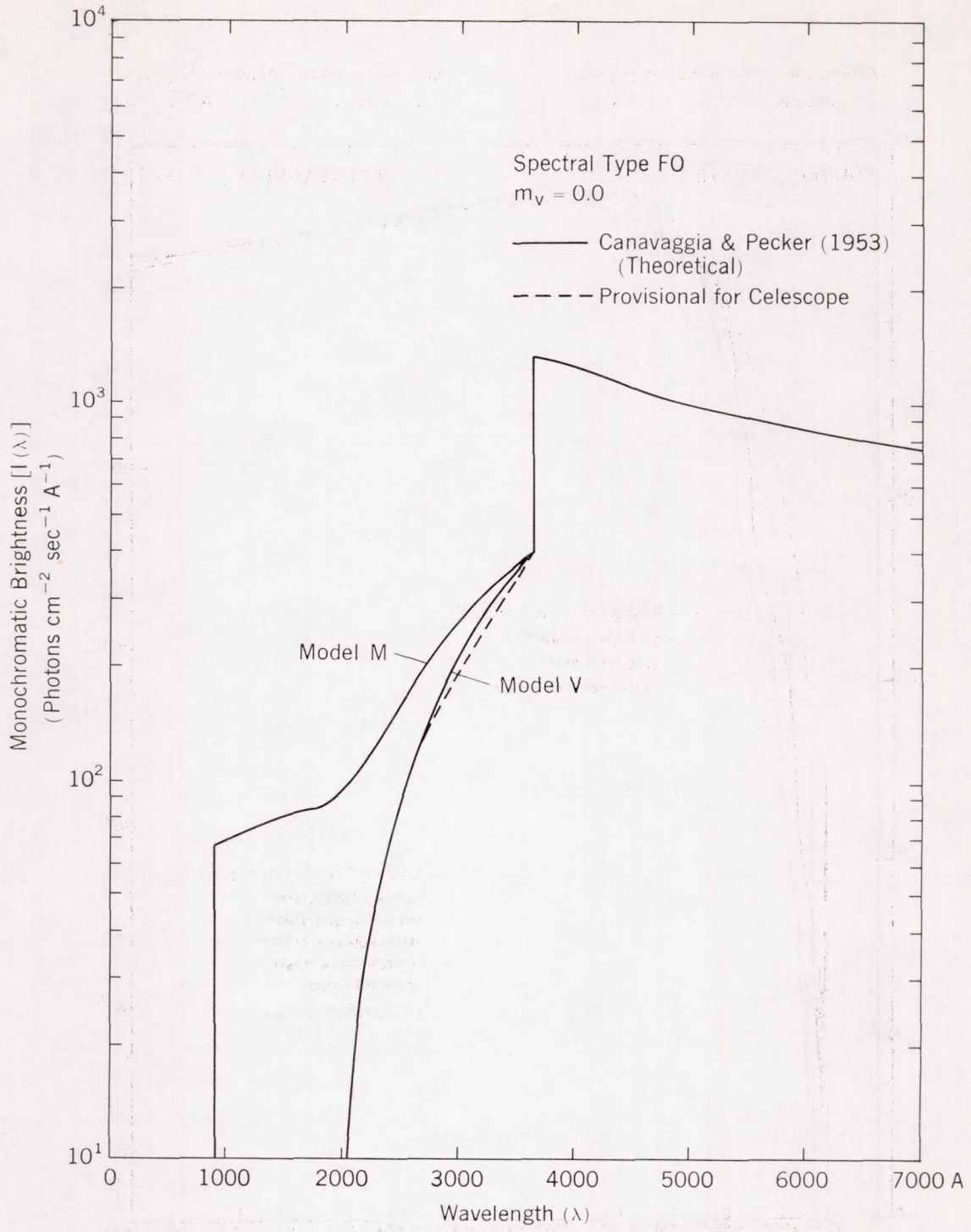

Figure 4.--Spectral distribution for an F0 star

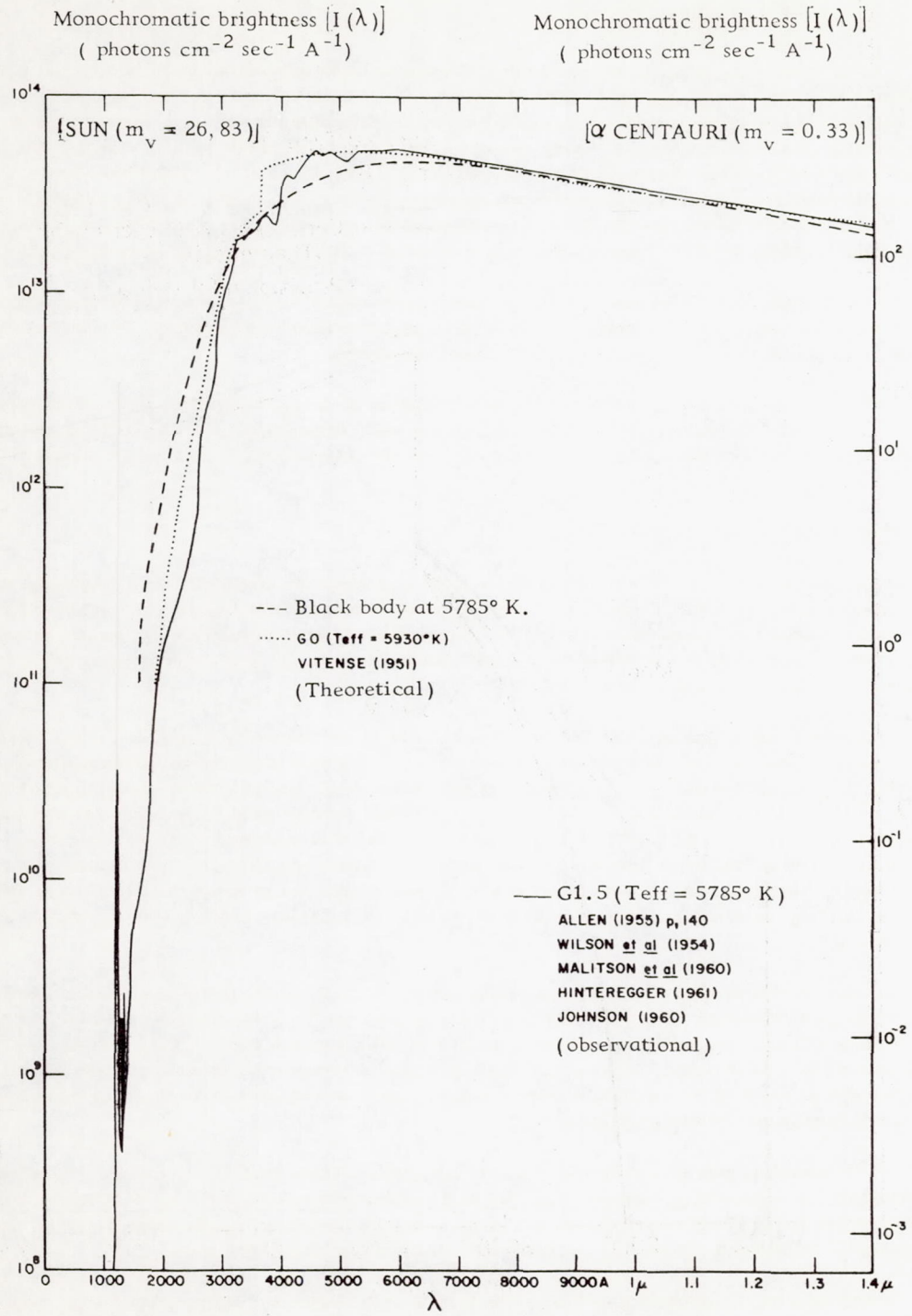

Figure 5.--Spectral distribution for the sun (G1.5 star)

The faintest stars we shall observe with Celescope will deliver about 0.04 photon per square centimeter per second per Angstrom to the optical system, the exact limit depending on which of the four broad-band wavelength regions we are considering. Celescope sensitivity is discussed more fully in Section III.1, "Sensory System." As we can see from figures 1 through 5, the brightest star in each spectral class A0 and earlier lies well above threshold, and we can expect to observe a large number of them with the Celescope. For the shorter wavelengths, however, the brightest stars of type F0 are only slightly brighter than the anticipated limiting magnitude of our survey. And at both the longer and the shorter wavelengths we should expect to see only a handful of stars of solar type (G1.5) and later.

Figure 6 indicates the number of stars of various spectral types that we expect to observe. The visual region is included for reference. As we shorten the effective wavelength of our photometric system, we get a smaller and smaller proportion of the later-type stars.

This problem of the ultraviolet flux from hot stars is of great importance to theoretical astrophysics. One goal of Celescope is to give it an observational foundation, and to chart the path for observing programs and instrumentation for future, more specialized satellites that are being planned.

3. Interstellar Absorption

Although Sir William Herschel made extensive studies of the irregularities in apparent stellar distribution caused by interstellar dust, it was more than a century later that this irregular distribution was correctly ascribed to interstellar absorption. And although Hartmann (1904) correctly ascribed certain narrow absorption lines in stellar spectra to interstellar gas, this explanation was not generally accepted until more than twenty years later.

The absorption spectrum of the interstellar medium is indicated in figure 7. The Lyman-alpha line at 1216 A and most of the absorption between 912 A and 504 A are caused by interstellar hydrogen gas. Since this gas is abundant, no ultraviolet radiation at the Lyman-alpha wavelength or at wavelengths shorter than 912 A can penetrate to the solar system. Thus we lose very little observational potential by limiting our optical system to 1050 A with the lithium-fluoride faceplate for the camera tube. The x-ray region of the spectrum, where we expect the interstellar medium to open up again, presents optical and astrophysical problems of an entirely different nature not presently the subject of specific planning by Celescope, but discussed in general terms by Baez (1960a, 1960b, 1961) and by Strom and Strom (1961).

The absorption at wavelengths longer than 912 A, except for the hydrogen Lyman-alpha line at 1216 A, is caused primarily by interstellar dust. The region of the curve between 3000 A and 912 A, as yet unobserved, is of importance to the theory of the interstellar dust particles. Celescope will make possible a study of this region. Greenberg (1960) discusses the important question of whether the interstellar dust consists of "classical" particles larger than a wavelength of light, or of "quantum-mechanical" particles of much smaller size.

The interstellar dust also polarizes the starlight passing through it. It is generally agreed that this polarization is caused by elongated particles aligned along or across the lines of force of an interstellar magnetic field. Although Celescope will be unable to measure polarization, future orbiting telescopes will undoubtedly study this important phenomenon in the ultraviolet.

Superposed on the general absorption spectrum shown in figure 7 are several sharp, faint lines not indicated in the figure, caused by atomic and molecular absorption. The study of similar lines in the ultraviolet will be made in the OAO satellite of Princeton University. In the visible region, there are additional absorption features, 200 A or so wide, as yet unexplained.

An important part of the reduction procedures for Celescope observations will be to disentangle the effects of the interstellar medium from those of stellar atmospheres.

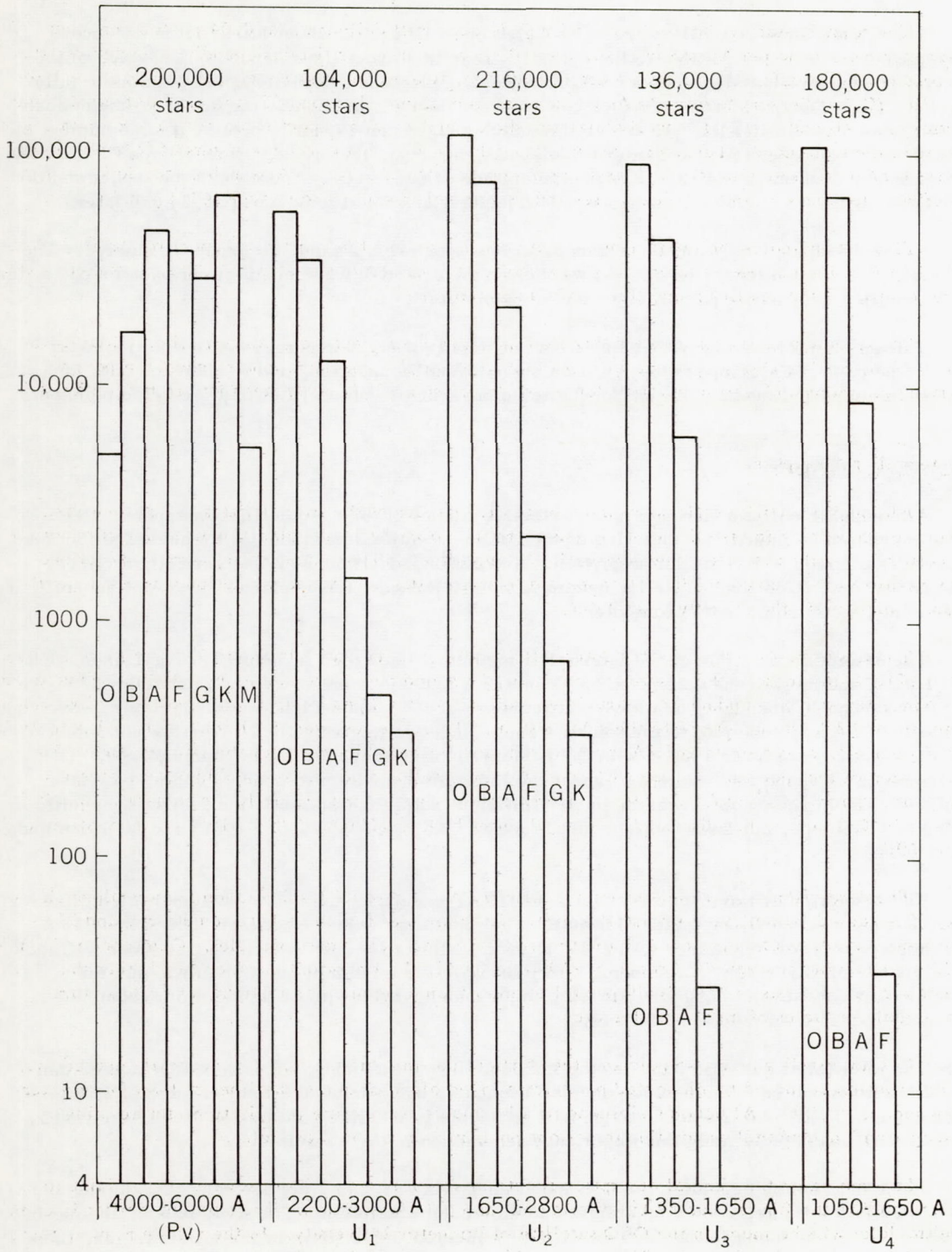

Figure 6. --Number of stars of various spectral types expected to be observed with Celescope

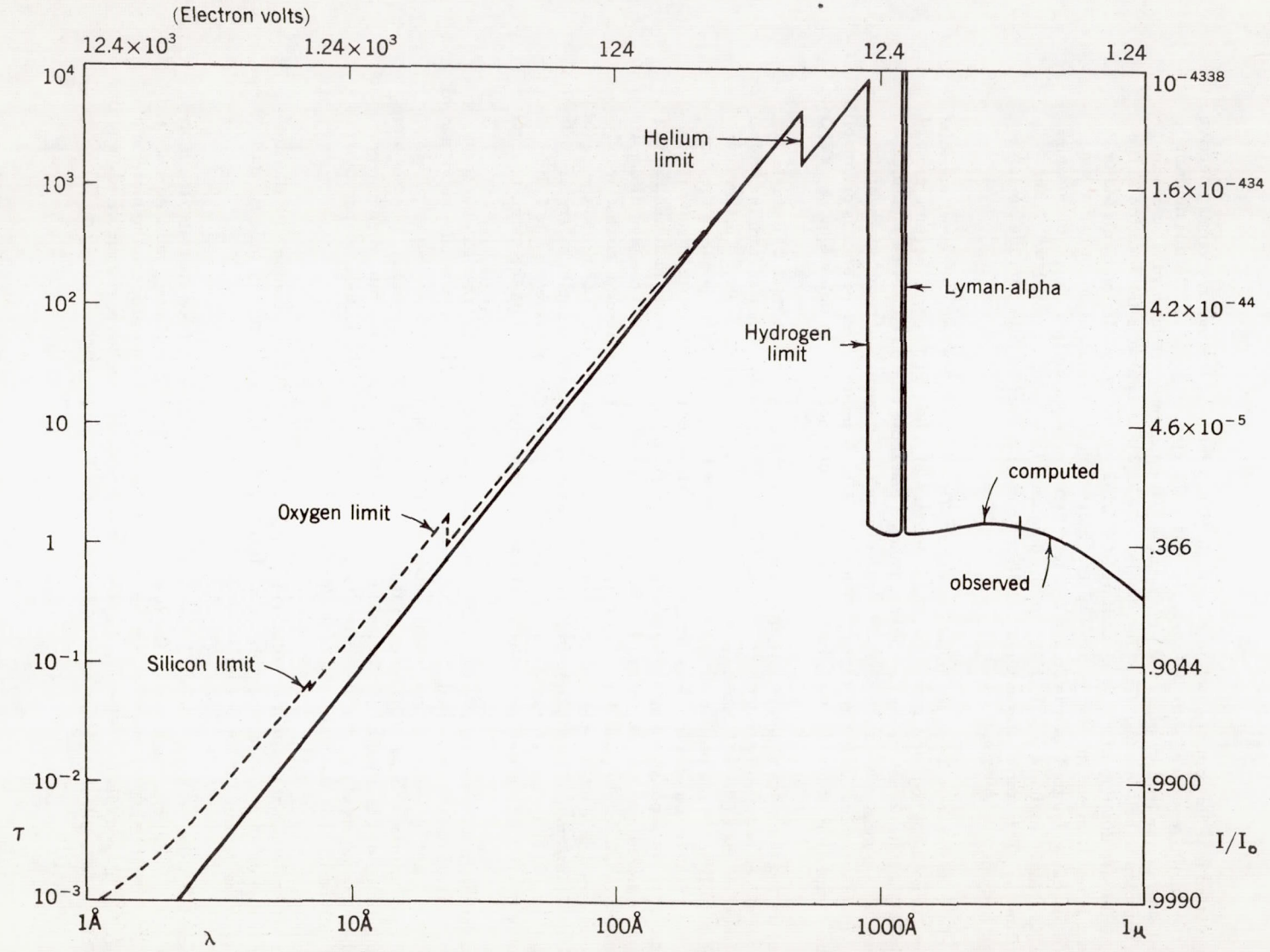

Figure 7.--Wavelength dependence of interstellar absorption

4. Stars

When plotted in a diagram of absolute magnitude (i.e., intrinsic luminosity) versus effective temperature, the "main-sequence" stars lie along the line so labeled in figure 8. In this diagram, the 100 nearest stars are marked by plus signs (+), and the 100 apparently brightest stars by crosses (x). Four stars are common to both groups. The line labeled "NGC 2362" indicates the location in the temperature-luminosity diagram of the group of stars NGC 2362, in the constellation Canis Major. This star cluster is less than one million years old; stars more than 8000 times as bright as the sun, however, have already exhausted their hydrogen and left the main sequence in a cluster of this age. The line labeled "M67" indicates the location in this diagram of the group of stars M67, in the constellation Cancer. This star cluster is about 5 billion years old; stars brighter than the sun have exhausted their hydrogen in this time.

Most of the nearer stars lie on the main sequence. The majority of these, however, are faint red dwarfs that cannot be recognized as such beyond a distance of a few light years. Because most of the apparently bright stars do not lie on the main sequence, and those that do cannot be measured accurately enough, we must rely on the study of physically related groups of stars and on theory to determine the main sequence for spectral types earlier than A0. A major source of error is our inability to separate the components of double stars; known double stars are indicated in figure 8 by circles (O).

To understand the main sequence, we must investigate the evolutionary track of a single star. In some manner as yet very poorly understood, gravitationally stable blobs of matter from the interstellar medium lose their excess rotational and magnetic energy to collapse gravitationally. This process continues isothermally until the pressure is great enough so that the gas becomes opaque to the long wavelengths that are carrying off the energy generated. At this point the temperature begins rising, rapidly at the center but more slowly at the surface, and the object becomes a star radiating most of its energy in the infrared. As the star contracts, it grows hotter and brighter until the central density and temperature reach a point at which nuclear reactions can occur. If the protostar consists wholly of hydrogen, this point is reached when the central temperature is about 13 000 000° K and the central density is about 83 gm/cm^3. The collapse from protostar to main sequence occupies a very small fraction of a star's lifetime, whereas the release of nuclear energy from the fusion of hydrogen into helium occupies a large fraction of its lifetime. It is for this reason that most stars lie on the main sequence.

A star on the main sequence evolves slowly, moving upward and to the left along the sequence until the supply of hydrogen is exhausted. At that point the star again collapses to release gravitational energy until the central temperature and density become high enough to release nuclear energy by the conversion of helium into carbon. This reaction is much faster than hydrogen burning, releases more energy per unit time, and thus produces a star of higher luminosity. The higher rate of energy production also causes the outer layers of the star to expand. Such a red giant has lower surface temperature and greater total luminosity than the main-sequence star from which it evolved.

After the helium-burning stage, evolution again proceeds very rapidly, ending with the star's collapsing to the white-dwarf stage. Because its nuclear fuel is spent and its surface area is small, the white dwarf releases its stored thermal energy slowly.

The position a star occupies while it is on the main sequence depends upon its mass, the more massive stars being hotter and brighter than the less massive. As figure 8 indicates, most stars are red dwarfs. Because of selection effects, however, most of the apparently bright stars are the hotter main-sequence stars and the red giants. When we observe in the ultraviolet, we favor even more strongly the hot stars. This is also evident in figure 8, in which the 27 theoretically brightest stars at 1250 A are indicated by squares (□).

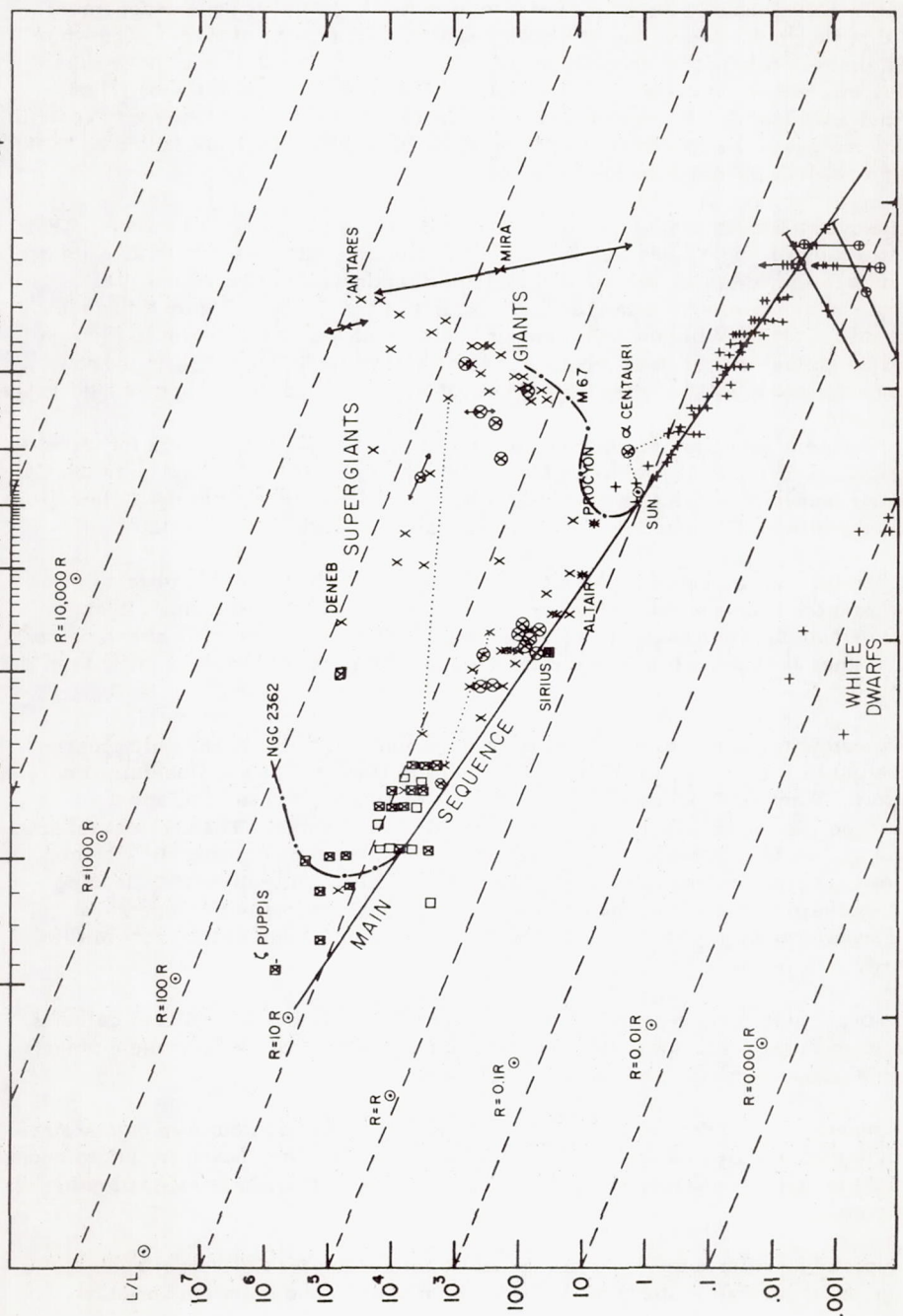

Figure 8.--Luminosity - temperature diagram for stars

Thus with Celescope we expect to observe primarily stars with effective surface temperatures in excess of 10 000° K. What of the other stars? If the sun is typical of the cool main-sequence stars, we would observe the chromospheric radiation from a handful of G stars (including Alpha Centauri) in the 2200 to 3000 A band. We might conjecture that the red giants have exaggerated chromospheres, and that we would observe the ultraviolet radiation from some of them. The white and red dwarfs would almost surely not be detected at all. If, however, the flare stars have flares similar to those on the sun, we might detect the ultraviolet radiation from some of them. Flare stars are red dwarfs that occasionally, for periods of a few minutes, increase their luminosity, especially in the yellow and blue regions of the spectrum, by factors from 10 to 100. They are indicated in figure 8 by vertical arrows proceeding upward from their symbols.

Several Wolf-Rayet stars will almost certainly be prominent on the Celescope survey. Their spectra consist almost wholly of bright lines and bands. Their effective surface temperatures are not well known. Their surface temperatures as indicated by ionization and excitation effects are comparable to or greater than the effective surface temperatures of the O stars. Figure 8 includes only one Wolf-Rayet star, Gamma Velorum. The proper location for Gamma Velorum in figure 8 is highly uncertain because neither the temperature nor the total energy output (luminosity) is known accurately. This star is plotted at $L/L_{\odot} = 10^5$, $T_{eff} = 30\ 000°$ K, below and to the right of Zeta Puppis.

The central stars of the planetary nebulae are similar to the Wolf-Rayet, but are intrinsically about 3 magnitudes (i.e., a factor of 16) fainter. Many of them are expected to show up in the Celescope survey. Only the nearer planetary nebulae have angular dimensions large enough for the Celescope to be able to separate the ultraviolet radiation of the central star from that of the nebula.

Novae and supernovae would certainly be interesting objects to observe in the ultraviolet, should any flare up during the course of the Celescope survey. In a nova outburst a star's light increases by about 12 magnitudes (or a factor of 65 000), and the star sheds a fraction of one percent of its mass. The nova stage is apparently related to the evolution of a star of moderate mass from the red-giant to the white-dwarf stage.

In a supernova outburst a star loses several percent of its mass, a truly catastrophic process. Type I supernovae are old stars that have too high a mass to allow them to change gracefully from red giant to white dwarf. When the nuclear fuel in the core is exhausted, the star collapses, heating up the nuclear fuels in the envelope to create a gigantic fusion bomb. The neutrons released in this explosion build up heavier elements from the core materials, beginning primarily with iron. The light curve of this type of supernova exhibits the same half-life as Californium-254, leading some authors to the hypothesis that a large amount of this isotope is generated in the supernova explosion. A Type I supernova has a peak intensity about 18 magnitudes brighter than that of the star before the outburst.

Type II supernovae must be young stars, since they are found only in those parts of galaxies where star formation is occurring. Blaauw (1961) describes a new theory that explains these objects as the explosions of protostars too massive to become stable stars.

Both types of supernovae are very rare objects, none having occurred in our own galaxy since the invention of modern photometric and spectroscopic techniques. They are, however, bright enough so that Celescope might be able to observe one should it occur in one of the nearer external galaxies. Novae are more common.

Many other types of peculiar stars might be especially interesting for Celescope, such as the P-Cygni stars and a group of peculiar A stars that includes the magnetic and spectrum variables.

5. Nebulae

In the interstellar gas and dust there occur concentrations, or nebulosities. Of special interest to Celescope are those gaseous nebulae that shine because of fluorescent excitation by early-type stars embedded in them. One category of such nebulae is represented by the Great Nebula in Orion, which is excited by the group of O stars called Theta Orionis. With Celescope's limited angular resolving power we will not be able to resolve the details of their structure as we do in visible light from a large earth-based reflector.

A second category is the planetary nebulae, smaller and more regular in shape than the diffuse nebulae. Under low magnification many of them resemble planets. They are created by the expulsion of matter from their hot, rather strange central stars, and rather rapidly expand and dissipate in interstellar space. The ultraviolet radiation from these objects is also of interest to Celescope.

A third category of nebulosity, of special interest to the astrophysicist and galactic astronomer, is the molecular-hydrogen (H_2) region. At least 90 percent of the matter in interstellar space is hydrogen gas. At present we can study atomic-hydrogen (H I) regions by means of radio astronomy at 21 centimeters, and ionized-hydrogen (H II) regions by means of optical astronomy at the H-alpha line (6563 A). There are no techniques in the presently available regions of the spectrum to study possible interstellar clouds of molecular hydrogen. There are several indications that such clouds exist, including indirect deductions from radio-astronomical data, and the discovery of ultraviolet nebulosities by means of rocket-borne detectors (Kupperian, Boggess, and Milligan, 1958). Dr. Max Krook, of Harvard College Observatory, has suggested that this latter radiation is caused by Raman scattering of Lyman-alpha radiation by molecular hydrogen. If so, the ultraviolet nebulosities radiate monochromatically at 1284 A and at 2.38 microns. We are now attempting to detect the 2.38-micron radiation, should it exist, from the ultraviolet nebulosities observed in Orion and Virgo. It should be pointed out that other authors (Shklovskii, 1959; Pikel'ner et al., 1959; Hayakawa, 1960; Scientific American, 1960) ascribe this radiation to other causes.

Celescope may be sufficiently sensitive to allow us to study the ultraviolet radiation from molecular-hydrogen regions. It is unfortunate, however, that except for the possible Raman line at 1284 A, the primary spectral lines of molecular hydrogen all fall below 1150 A under the anticipated interstellar conditions.

6. Galaxies

All of the objects discussed up to this point are members of our own Milky Way galaxy, and because of limitations imposed by interstellar absorption we expect most of them to lie within a few thousand light years of the earth.

Celescope is not specially designed to observe external galaxies, which according to most reasonable theories will not be bright enough in the ultraviolet for proper study. As was the case with radio astronomy, we might discover that some peculiar galaxies are bright sources for our new wavelength region.

Among peculiar galaxies of special interest in this regard are the radio sources Virgo A and Cygnus A. The first (M87) is an elliptical galaxy possessing a luminous jet. The light from this jet is polarized and may be generated by synchrotron radiation. Cygnus A, although the second-brightest radio source in the sky, is optically rather faint. Originally interpreted as a pair of colliding galaxies, it is now more commonly claimed to be a single galaxy with a rare, although not unique, peculiarity.

7. Solar System

The most important, most interesting, and most studied body in the solar system (excluding the earth) is the sun. Because of its great brightness, the sun will not be observed by Celescope, since equipment suitable for its study cannot be used for study of any other body. Ultraviolet study of the sun is, however, of special interest to Celescope, since at present the sun is the only star that has been well observed in the ultraviolet. Our knowledge of the sun's radiation can serve to guide us in our design studies.

Figure 5 shows the measured continuous spectrum of the sun. Below 1500 A the major portion of the energy is contained in the emission - line spectrum rather than in the continuum. However, at these short wavelengths no other star similar to the sun would be bright enough to be observed. If we are to observe any stars of G and later spectral type with Celescope, we will truly be probing the unknown and unexpected--the most exciting part of science.

The sun's ultraviolet radiation comes primarily from the chromosphere, a layer of tenuous gas lying above the visible solar surface. The chromosphere is raised by mechanical agitation to a temperature approximately twice that of the visible surface, or photosphere. Just below the photosphere, the sun is in a boiling, bubbling state of convective energy transport. In and beyond the photosphere, the primary energy transport mechanism is radiation rather than convection. However, the momentum carried by the convection is transported through the photosphere into two regions, the chromosphere and corona, where the gas density is so low that thermodynamic equilibrium no longer holds even approximately. The temperature as expressed by the kinetic energy of the electrons, ions, and atoms--i.e., the electron temperature T_e--rises in the chromosphere to 10 000° K, whereas the radiation temperature falls below the 5785° value maintained just below the photosphere where the gases cannot "see" the cold of outer space. And since the overlying gases are hotter than the photosphere, the ultraviolet picture of the sun will be brightest at wavelengths where those gases are opaque, thus causing the far ultraviolet radiation of the sun to be generated primarily in the chromosphere.

The sun is continually expelling clouds of particles. Optical evidence of this activity is furnished by the prominence photographs being taken at the world's great solar observatories. Such clouds carry ions, electrons, and magnetic fields. These particles and fields interact with the earth's atmosphere and magnetic field to produce ionospheric disturbances, magnetic storms, and aurorae.

The earth's upper atmosphere interacts not only with the solar corpuscular but also with the electromagnetic radiation. Rocket observations have shown that both the daytime and nighttime skies are strong emitters of Lyman-alpha radiation (Kupperian, Byram, Chubb, and Friedman, 1958). The daytime illumination indicates that the earth's outer atmosphere reflects 70 percent of this radiation. The mechanism is resonant scattering by neutral hydrogen atoms. The nighttime illumination, which is much fainter, is caused by recombination of ionized hydrogen. This hydrogenic component of the atmosphere fades into the interplanetary gas, which, being composed of hydrogen, is also bright in Lyman-alpha. Lyman-alpha is not the only ultraviolet line to be expected in the spectrum of the upper atmosphere. Oxygen, nitrogen, and carbon compounds will also be strong emitters.

By observations taken with a rocket-borne photometer, Crosswhite, Zipf, and Fastie (1962) have obtained an ultraviolet spectrum of an aurora of intensity II^-. They have observed the following flux levels:

Table 1. Ultraviolet auroral flux levels

Wavelength range	Auroral flux
1100-1800 A	0.5 to 2.0 erg sec^{-1} cm^{-2} $steradian^{-1}$
1800-2600	0.02 to 0.08
2600-3400	0.07 to 0.28

Celescope should be able to observe aurorae brighter than 0.002 erg sec^{-1} cm^{-2} $steradian^{-1}$. It should therefore easily be able to study the aurora in the ultraviolet region of the spectrum. For comparison, the brightest ultraviolet nebulosities observed by Kupperian, Boggess, and Milligan (1958) were 0.003 of these units.

Heddle (1962) has observed the moon at a wavelength of 2200 A, where it is 17.5 magnitudes fainter than the sun, corresponding to about 1.6×10^4 photons cm^{-2} sec^{-1} A^{-1}, or 0.002 erg cm^{-2} sec^{-1} A^{-1} $steradian^{-1}$. Over the 1300-A bandwidth of the Celescope spectral response curve that covers the 200-A region, the moon's brightness is 2.5 ergs cm^{-2} sec^{-1} $steradian^{-1}$. The moon should thus be easily studied by Celescope at the longer ultraviolet wavelengths.

Ultraviolet radiation is also to be expected from other planetary atmospheres. However, the Lyman-alpha component is expected to be masked by the interplanetary background, and the longer-wavelength components may be too faint to be detected with Celescope.

II. Experimental Objectives

1. All-sky Survey

The minimum objective of Celescope, as presently stated, is to obtain all-sky maps in four ultraviolet colors to a limiting stellar magnitude of 8.0. This limit should provide us with four-color data on about 25 000 stars, virtually all of F-type or earlier. It would also provide us with two-color data on the G and K stars. At this sensitivity, we should be able to study any nebulosities whose brightness exceeds about 8×10^{-3} ergs sec^{-1} cm^{-2} $steradian^{-1}$ over the pass band of the photometer, corresponding to 8th magnitude per elemental area. The elemental area is about 45 seconds of arc in diameter.

Our presently contemplated sensitivity is four times better than this minimum requirement.

We plan to transmit our video signal solely by digital techniques. The normal mode of operation will be a real-time pulse code modulation (PCM) in which the signal amplitude at each elemental area is encoded as an 8-bit binary word. This mode gives us 7-bit accuracy in measuring the brightnesses of both stars and nebulosities. A stellar-scan back-up mode using digital techniques allows us to employ the facilities of the spacecraft Experimenters' Data Handling Equipment if real-time operation over the wide-band transmitter should become impossible or highly inefficient. In this mode the positions and intensities of all stars in the picture are converted into a series of 25-bit binary words. A second back-up mode using analog techniques allows us to obtain information at reduced accuracy on both stars and nebulae.

Our operational techniques will undoubtedly be modified by actual experience with the Celescope in orbit; however, our present plans are to begin by using one 60-second exposure on each camera for each position, the information on the target of the television camera tube being read out by the digital-direct (PCM) mode of scanning. We describe these plans more fully near the beginning of Section III. 4, and in figure 26.

Any analog transmissions will be converted on the ground to a PCM format similar to that used by the digital-direct mode; all of our data reduction will make use solely of digital techniques.

The nebular information will be converted into isophotal contour maps for publication and further study, whereas the stellar information will be printed in catalog form. Although these final reductions will use automatic computing techniques, a "quick-look" console at NASA's OAO control station will allow us to display the information in the form of ordinary television pictures. We will thereby readily be able to ascertain their quality and correct the operating adjustments of the Celescope accordingly.

2. Slitless Spectra

As explained above , we no longer plan to install a slitless spectroscope.

3. The Solar System

As mentioned above, Celescope will not be used to study the sun. The OAO spacecraft is programmed so that the optic axis will never come within 45° of the sun, and a sun shield should close to keep the direct rays of the sun from entering the Celescope tube should this limit be passed. Direct solar illumination would destroy the detector.

The earth's atmosphere is expected to be a strong and interesting source of ultraviolet radiation that Celescope may well be suited to study. We plan to look downward at both the illuminated and dark portions of the atmosphere. An intensive study will be made only if it does not interfere with the celestial observations, or if Celescope proves unsuccessful in its celestial mission. Looking upward, we expect to find no atmospheric emission or absorption other than the Lyman-alpha emission at 1216 A.

The other planets are not expected to be bright in the ultraviolet, but Celescope will definitely look for them, and surprises are to be anticipated. We will also make a special effort to observe the interplanetary medium. By observations made near the sun when direct sunlight is blocked by the earth we hope to be able to observe clouds of gas expelled from the sun. These observations would complement those now being made of the effects on the earth's magnetic field and ionosphere of clouds of ionized particles expelled by the sun.

4. Objects of Special Interest

We anticipate that many objects of interest will not be detected on the sky survey. We are now compiling a list of special and peculiar objects that would be of interest even if they are below the threshold of Celescope's normal operation. Since the slewing capabilities of the spacecraft will not always allow us to use the entire communications contact time, we will be able to take additional long exposures on regions containing these objects. Among such objects will be the radio sources 3C48, Cygnus A, Virgo A, and Taurus A; selected OB associations such as Perseus II that are near enough and uncomplicated enough for convenient study; a few selected planetary nebulae; a selection of Wolf-Rayet stars; and additional classes of objects too numerous to mention here.

5. Calibration Techniques

Proper calibration of the Celescope is so important that we anticipate spending as much as half of our entire effort to ensure proper calibration of adequate quality. Our techniques for the calibration of the various Celescope components are growing to keep step with the camera-tube development program. Although the spectral response and the sensitivity of each tube are calibrated by the manufacturer, we recheck all tubes when we receive them and again when they are mounted in prototype and flight equipment. Figure 9 is a photograph of our calibration equipment.

We begin by calibrating a hydrogen-arc ultraviolet source. This lamp is placed at the entrance slit of a vacuum monochromator, and a nitric-oxide photon counter is positioned at the exit slit. The monochromator is set to isolate the Lyman-alpha radiation of the lamp. We know the efficiency of the counter from the absorption cross-section of nitric oxide at this wavelength. This arrangement gives the absolute flux of Lyman-alpha emerging from the exit slit.

We now replace the nitric-oxide detector with a photomultiplier tube coated with sodium salicylate. The fluorescent quantum efficiency of this material is constant over the spectral range of 1000 to 3500 A. By scanning the monochromator through this range, we obtain the relative spectral output curve of the monochromator under our standard calibration-scanning conditions. The absolute output is determined from the response at Lyman-alpha.

We also calibrate the spectral response curve of an ASCOP solar-blind photomultiplier against this standard in order to have a standard detector less subject to change with time.

For calibrating a television camera tube, we place the tube at the exit slit of the monochromator and scan the spectrum in the standard manner. We record the video output on an oscilloscope to obtain the video output signal as a function of wavelength and position on the faceplate of the tube. Since the exit slit will be .05 x 8 millimeters and the photocathode is used over a 25-mm-square area, this mapping of the spectral sensitivity of each tube is a time-consuming operation.

The calibration is not complete until the other elements of this system, and the assembled system itself, have been calibrated. To measure the reflectivities of our mirrors, we coat a small test-plate when we coat each mirror surface. A special attachment at the exit slit of the monochromator allows us to measure in quick succession the direct and the reflected beam. We can thus determine the effect of mirror reflectivity on our system response. The same apparatus allows us to measure the transmissivity of each optical filter.

We can calibrate our electronic systems (video amplifiers and communication link) by impressing electronically generated video signals of known amplitude at the signal input electrodes.

For the system test, we must go to the vacuum optical bench to be built at NASA's Goddard Space Flight Center for OAO use. Its ultraviolet source must be calibrated by means similar to those used on our equipment. If the system calibration does not agree with the sum of the calibrations of the parts, we must again look for and remove the sources of error.

It is highly important to protect all of our optical elements, i.e., mirrors, filters, and detectors, from any environment that would tend to change the system's spectral response curve, since once the Celescope is assembled, re-measuring these quantities to the desired accuracy becomes very difficult, if not impossible. After assembly of the Celescope we will, therefore, rely on calibrated point sources to check the sensitivity calibration . Once the satellite is in orbit, it may be impossible to differentiate between sensitivity changes caused by the optics and those caused by the electronics.

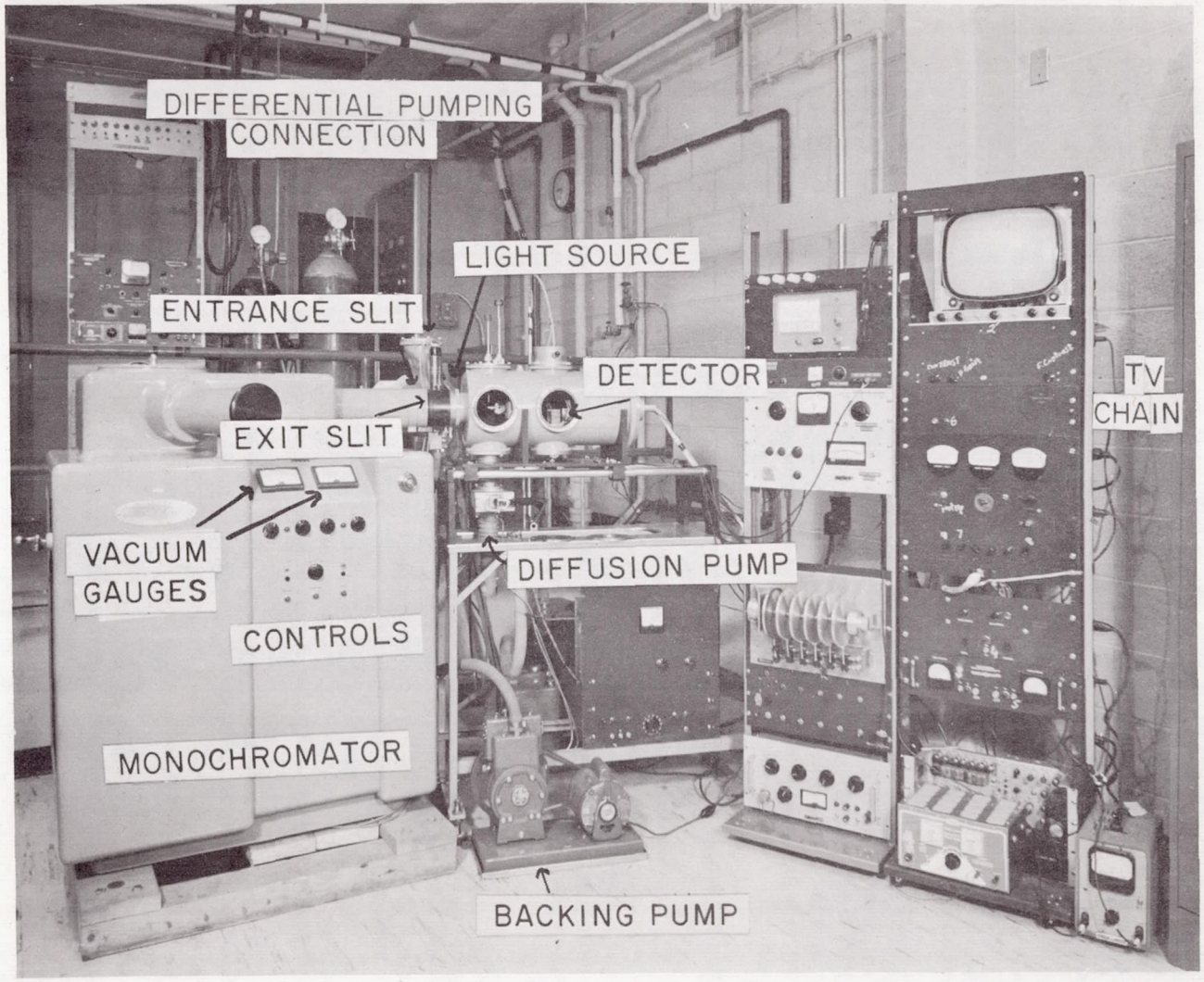

Figure 9. --Celescope spectrophotometric calibration equipment

Using these techniques, we have calibrated several detectors and light sources as secondary standards of ultraviolet radiation. Our standard detectors--two nitric-oxide photon counters obtained from Geophysics Corporation of America , and one from the Naval Research Laboratory--are recalibrated periodically against primary standards at Geophysics Corporation, Naval Research Laboratory, and NASA. We thus maintain our intensity standard to within $\pm$ 5 percent of these primary standards, which, we find, agree with one another to within our $\pm$ 5 percent error of measurement.

We have standardized these detectors at 1216 A; we compare them at that wavelength against photomultipliers of known spectral response characteristics and use those photomultipliers at other wavelengths.

We have procured several light sources to be used as secondary standards. These have consisted of mercury-vapor lamps operating at 2537 A. The calibrated source includes a holder where we may insert a selection of pinholes of various sizes. A quartz lens images or collimates the 2537-A light coming from the pinhole, depending on the adjustment of the system. There is a calibrated iris diaphragm near the lens.

We are presently evaluating two types of calibrator lamps for use in the orbiting Celescope. For our two shorter wavelengths, we are testing xenon discharge lamps developed especially for us by the ASCOP division of Electro-Mechanical Research. We plan to operate them at 0.5 milliampere, under which conditions they radiate about 3×10^{11} photons sec^{-1} cm^{-2} $steradian^{-1}$ in the forward direction at 1470 A. Radiations at other wavelengths contribute less than 1 percent to the television signal and can be neglected. With these lamps and an appropriate array of pinholes, a pattern of artificial stars can be focused onto the uvicon photocathode with brightnesses ranging between 2×10^3 photons sec^{-1} and 3×10^4 photons sec^{-1}--that is, between 0 and 3 magnitudes brighter than the faintest stars we hope to measure.

The xenon lamp requires three minutes after turn-on to reach full intensity. Although its output variations caused by variations in input voltage are negligible, its output does change with time. Figure 10 shows the aging curves as measured for three of these lamps. Our calibration procedure must include a correction for this aging. These lamps can be fired at low temperatures. By appropriate potting with thermal-insulating material, we hope to be able to mount them so that no temperature correction will be required.

For our two longer wavelengths, we are evaluating mercury-vapor lamps available commercially from Black Light Eastern Corp. The lamps would be operated at 0.5 milliampere, radiating about 4×10^{12} photons sec^{-1} cm^{-2} $sterad^{-1}$ in the forward direction at 2537 A. Radiations at other wavelengths again contribute less than 1 percent to the television signal and can be neglected. With these lamps and an appropriate array of pinholes, a pattern of artificial stars can be focused onto the uvicon photocathode with brightnesses ranging between 4×10^3 and 4×10^5 photons sec^{-1}-- that is, between 0 and 5 magnitudes brighter than the faintest stars we hope to measure. The mercury lamp requires only one minute after turn-on to reach full intensity. As mounted in the Celescope, its output variations arising from variations in input voltage are negligible. This lamp, however, has an undesirable variation output versus bulb temperature that has not yet been overcome.

Figure 11 shows the xenon calibration lamp. Figure 12 shows the mercury-vapor calibration lamp.

Each step in the calibration is performed as near as possible to the time of the first observation. By making our first observations in Orion, where there is a large number of stars expected to be bright in the ultraviolet, we hope to locate early a field suitable as a photometric standard. We will then return to that field frequently while we set up secondary standards. We will observe some standard field at least once per day, and use the internal calibration at least twice per orbit. Thus, we will be using our artificial standard as an aid to interpolation only. The calibration sequence will be varied as necessary during operation.

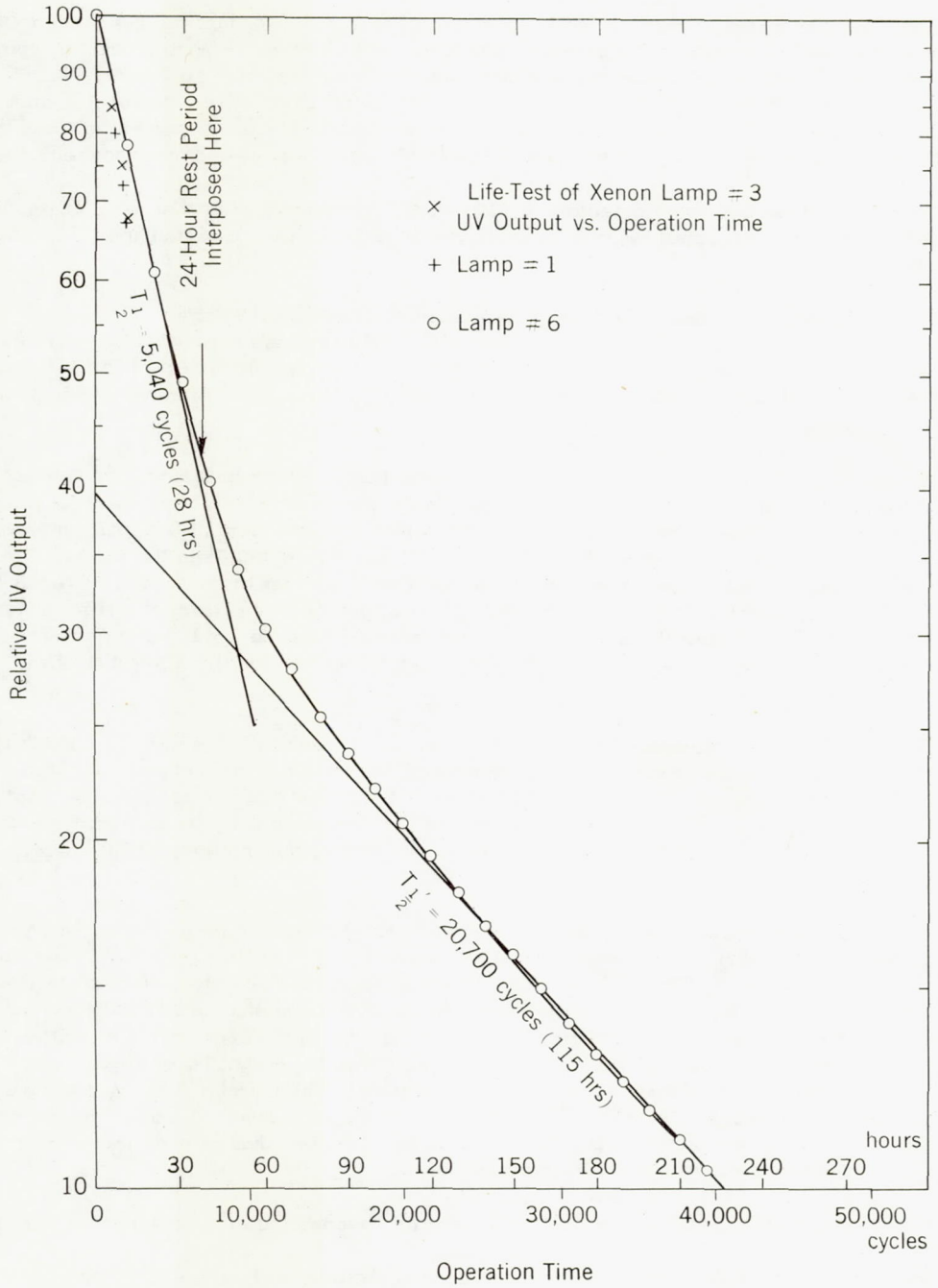

Figure 10. --Aging curves of ASCOP xenon calibrator lamps

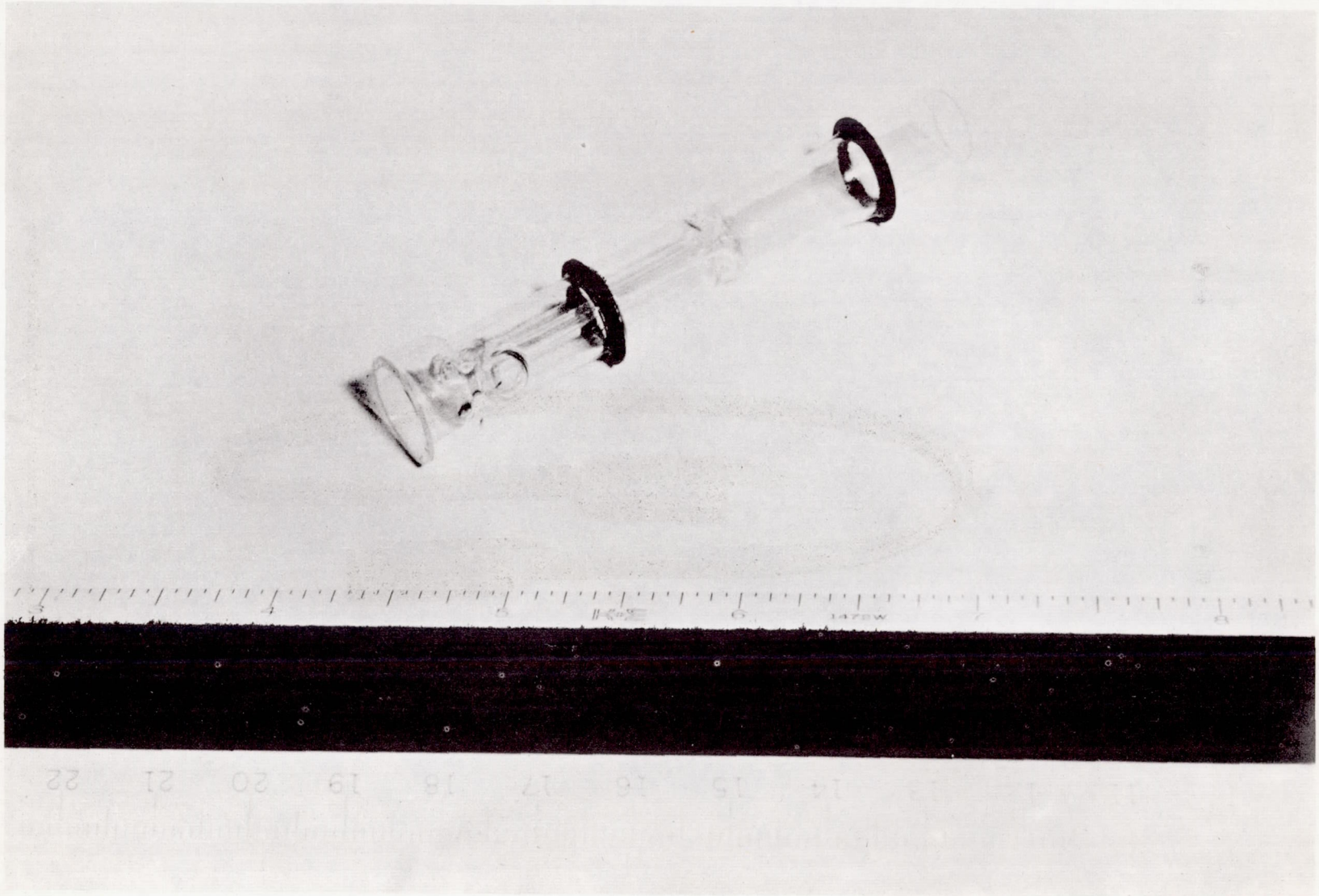

Figure 11.--Photograph of ASCOP xenon calibrator lamp for space-borne applications

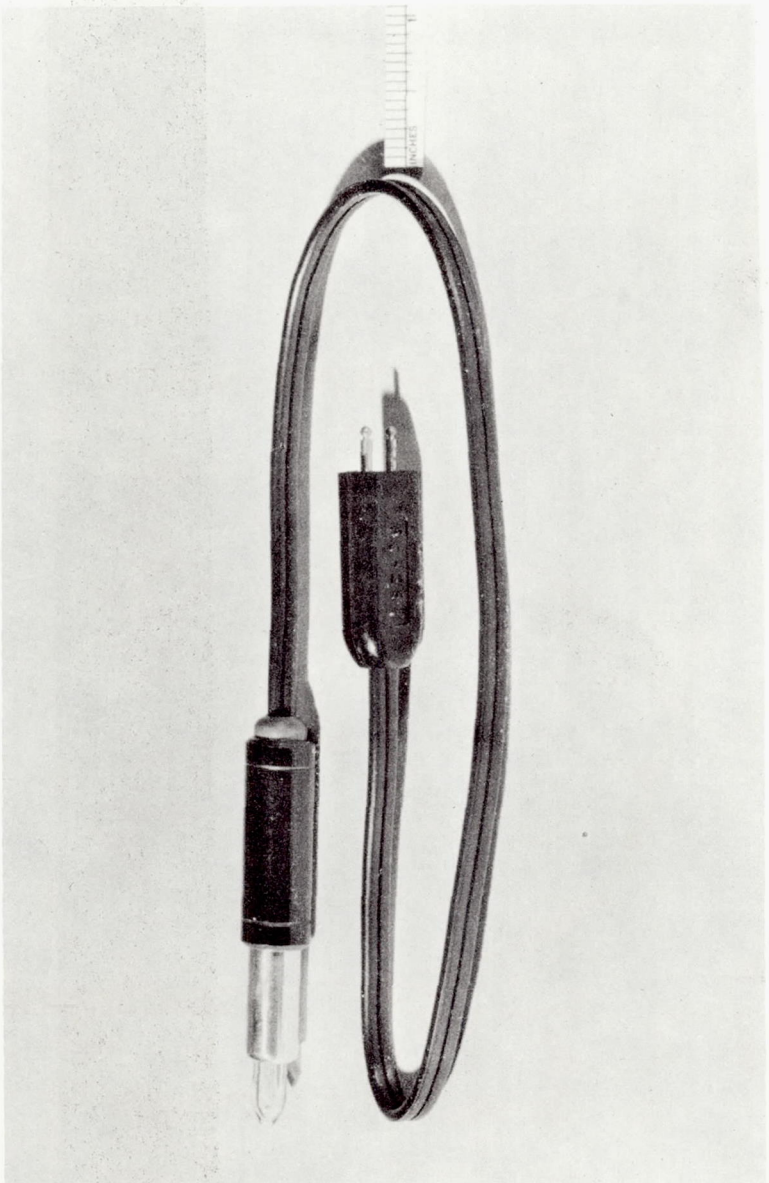

Figure 12.--Photograph of mercury - vapor calibrator lamp

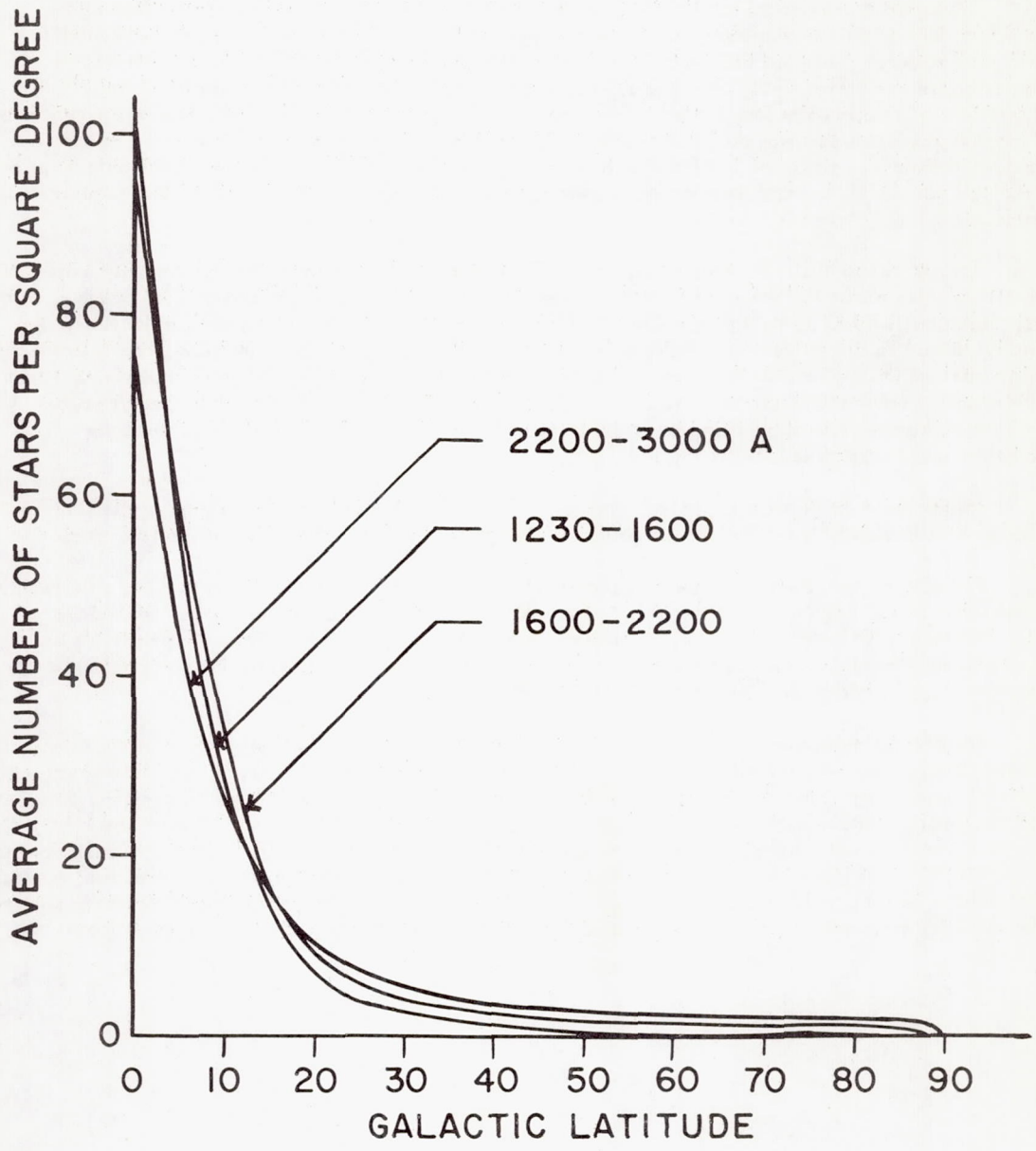

Figure 13.--Average number of stars per square degree as a function of galactic latitude and of wavelength

6. Stellar Distribution and Speed of Completion of Survey

Davis and Godfredson's (1961) study of the relationships between stellar distribution and Celescope data-handling requirements led to the results given in figure 13. This study used model stellar atmospheres published before 1958, and may therefore have overestimated the ultraviolet brightnesses of the hotter stars (See Section I.2 above). Although this study was aimed mainly at the problem of information loss caused by the presence of accidental double stars, it now appears that the most important result was that pertaining to the distribution of the ultraviolet stars. For our anticipated resolving power of 1 minute of arc, we expect only about 0.5 percent of our objects to be unresolved double stars. This percentage is very nearly proportional to the square of the angular resolution.

Two of our four all-sky broad-band ultraviolet maps will contain about 200 000 stars each, and two will contain about 100 000. Our field of view will be a circle of 2°.8 diameter (see below), so that each picture will cover 1/6700 of the sky. The average picture will therefore contain 25 stars. An average picture in the galactic plane, however, will contain about 125 stars, and the densest fields may contain 400. Figure 13 shows the expected distribution in galactic latitude of stars observed at various wavelengths. Since these numbers are by a factor of four greater than our minimum requirements, we now have some freedom in choosing our television camera tubes for characteristics other than possession of the utmost sensitivity.

In any field 60 percent of the stars are expected to be at threshold, regardless of the brightness at which that threshold is set. An average star will occupy six elemental areas of the television scan.

In order to provide a safe margin of overlap, our centers will be separated by 1°.8. We require 16 000 slews of 1°.8 each to cover the entire sky. We are allowed an average of three such slews per orbit, in addition to transfer between the University of Wisconsin and Smithsonian experiments and slewing to standard fields for calibration. At 100 percent efficiency, the time for completion of the program would therefore be 5200 orbits, or 400 days.

In order to maximize the value of the Celescope survey in the event of its premature termination, we plan first to observe a region of known special interest and high star density in the ultraviolet--the region containing the constellation Orion. The first 66 slews will be devoted to mapping the area between galactic longtitudes $\ell^{II} = 195°$ and $\ell^{II} = 215°$, and between galactic latitudes $b^{II} = -15°$ and $b^{II} = -25°$. This will require about two days. Next, we will require about 400 slews to map 22 selected areas between 8° x 8° and 18° x 4° in extent, at the locations shown in Table 2. By starting our program in Orion, and continuing it in these selected areas, we have increased the value of our early observations (as indicated schematically in figure 46) in order to reduce the effect of premature failure of the equipment.

Table 2. Selected areas for Celescope

Selected area no.	l^{II}	b^{II}	Objects of known interest in the ultraviolet	Selected area no.	l^{II}	b^{II}	Objects of known interest in the ultraviolet
1.	25°	0°	_____	12.	190	+45	_____
2.	70	0	P Cygni; NGC 6871	13.	250	+45	_____
3.	115	0	Sigma Cassiopeiae	14.	310	+45	Alpha Virginis
4.	160	0	Epsilon Persei ?	15.	55	-45	_____
5.	205	0	15 Mon; NGC 2244	16.	115	-45	Gamma Pegasi
6.	250	0	Zeta Puppis; Puppis I	17.	175	-45	Delta Ceti ?
7.	295	0	Alpha Crucis ?	18.	235	-45	_____
8.	340	0	Mu Scorpii	19.	295	-45	_____
9.	10	+45	_____	20.	355	-45	_____
10.	70	+45	Tau Herculis	21.	-	+90	_____
11.	130	+45	_____	22.	-	-90	_____

Mapping these selected areas will require about 12 days. Finally, we will fill in the remainder of the sky.

III. Experimental Instrumentation

For converting the images at the foci of our telescopes into video signals, we have had a new type of television camera tube developed. The device first evaluated was the ultraviolet-sensitive ebicon described in Special Report No. 83, and further described by Skorinko, Doughty, and Feibelman (1961). Final evaluation of the ebicon revealed inadequate sensitivity and improper target response characteristics for our intended application. The device now being tested uses a secondary-emission target. This change in the camera tube has required modification of the electronic, but not of the optical or mechanical system. It appears likely to meet our requirements. Both the old ebicon and the new secondary-emission camera tube, when fitted with ultraviolet-sensitive photocathodes, are called uvicons.

As our design of the Celescope has progressed, we have found it necessary to depart considerably from the electronic system outlined in Special Report No. 83. We have also made lesser modifications in our mechanical design. Since neither of these designs is as yet final, we can expect still further changes to be reported in a future revision to this document. The optical system and detector are probably now in their final configuration.

1. Sensory System

Figure 14 shows the spectral response curves $Q(\lambda)$ for the detectors we expect to use. The present Type A photocathodes (caesium telluride) are more sensitive by a factor of 4 than those produced before April 1962; the present Type D photocathodes (caesium iodide) are more sensitive by a factor of 10. Both in sensitivity and spectral response barium fluoride proved unsuitable as a photocathode, and the intended function of the Type C uvicon is being assumed by the Type D tube, which, when coupled with the proper optical filter, is equivalent to that previously called Type B.

The sensitivity of the uvicon tube is determined by the spectral response of the photocathode and by the minimum detectable electron image on the target. With the new transmission-secondary emission target, the minimum detectable point image (i.e., the image for which peak signal equals rms noise) contains about 1.4×10^3 photoelectrons. For the exposure times contemplated for Celescope, between 1 and 100 seconds, the number of electrons in this image is proportional to star brightness, photocathode efficiency, and exposure time; at the peak of the response curve, the minimum detectable signal after 60 seconds' exposure time corresponds to 300 photons per second in a point image for the Type A uvicon. The minimum detectable signal depends on the television camera chain, since the source of noise is the input stage of the video pre-amplifier. The value 1.4×10^3 photoelectrons stated above refers to measurements conducted at 30 frames per second, 4 mc/sec video bandwidth, with laboratory equipment. We expect to achieve comparable sensitivities with the spaceborne equipment.

Figure 15 shows the expected reflectivity $R(\lambda)$ of the telescope mirrors we plan to use with Celescope. Since each telescope uses two reflections, the $R^2(\lambda)$ curve determines the flux delivered by the telescope to the uvicon module. Figure 16 shows the transmission $T(\lambda)$ of 1.5-millimeter-thick samples of various optical filter materials we have considered using.

The Celescope will provide accurate information on all stars brighter than ten times the minimum detectable point image--i.e., all stars for which

$$\text{At} \int_0^\infty \frac{I(\lambda)\, R^2(\lambda)\, T(\lambda)\, Q(\lambda)\, d\lambda}{1.4 \times 10^3 \text{ electrons}} \geq 10 ,$$

where A is the area of the optical system, t is the exposure time, and $I(\lambda)$ is the monochromatic brightness of the star. The monochromatic stellar threshold $\Theta_s(\lambda)$ is therefore defined as

$$\Theta_s(\lambda) = \frac{1.4 \times 10^3 \text{ electrons}}{0.1 \text{ At } R^2(\lambda)\, T(\lambda)\, Q(\lambda)} .$$

Note that there is a safety factor of 10 included in this definition.

The monochromatic nebular threshold is numerically equal to the monochromatic stellar threshold, when the nebular threshold is expressed in photons per square centimeter per second per elemental area at wavelength λ. The elemental area has a diameter equal to the distance between successive scanning lines and has half the diameter of the resolution element. The conversion between these units and those more commonly used in expressing nebular brightness is

$$1 \text{ photon cm}^{-2} \text{ sec}^{-1} \text{ (e.a.)}^{-1} = \frac{2000\, A}{\lambda} (2.66 \times 10^{-4}) \text{ erg cm}^{-2} \text{ sec}^{-1} \text{ sterad}^{-1} .$$

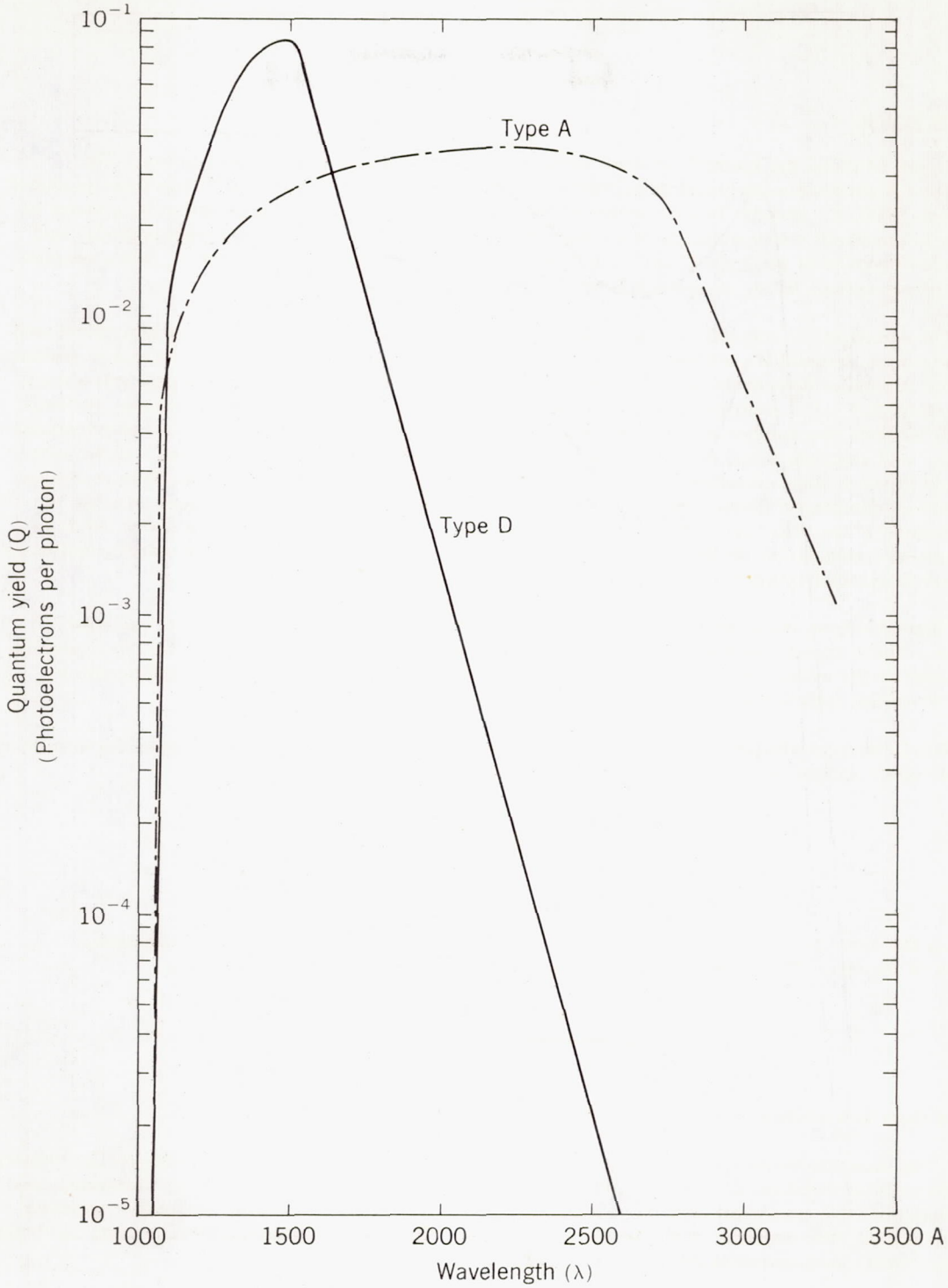

Figure 14. --Uvicon sensitivities

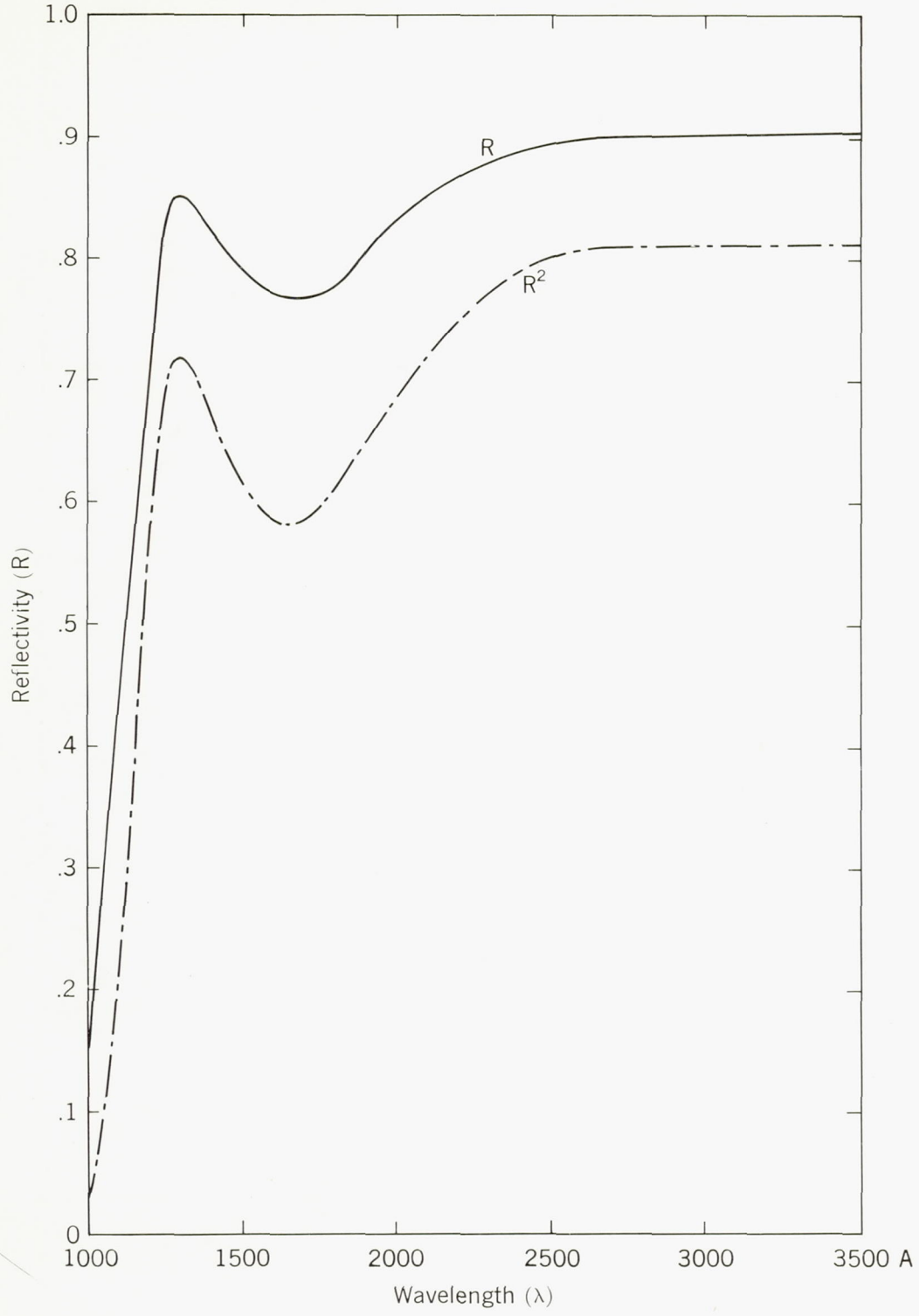

Figure 15.--Reflectivity of Celescope mirrors

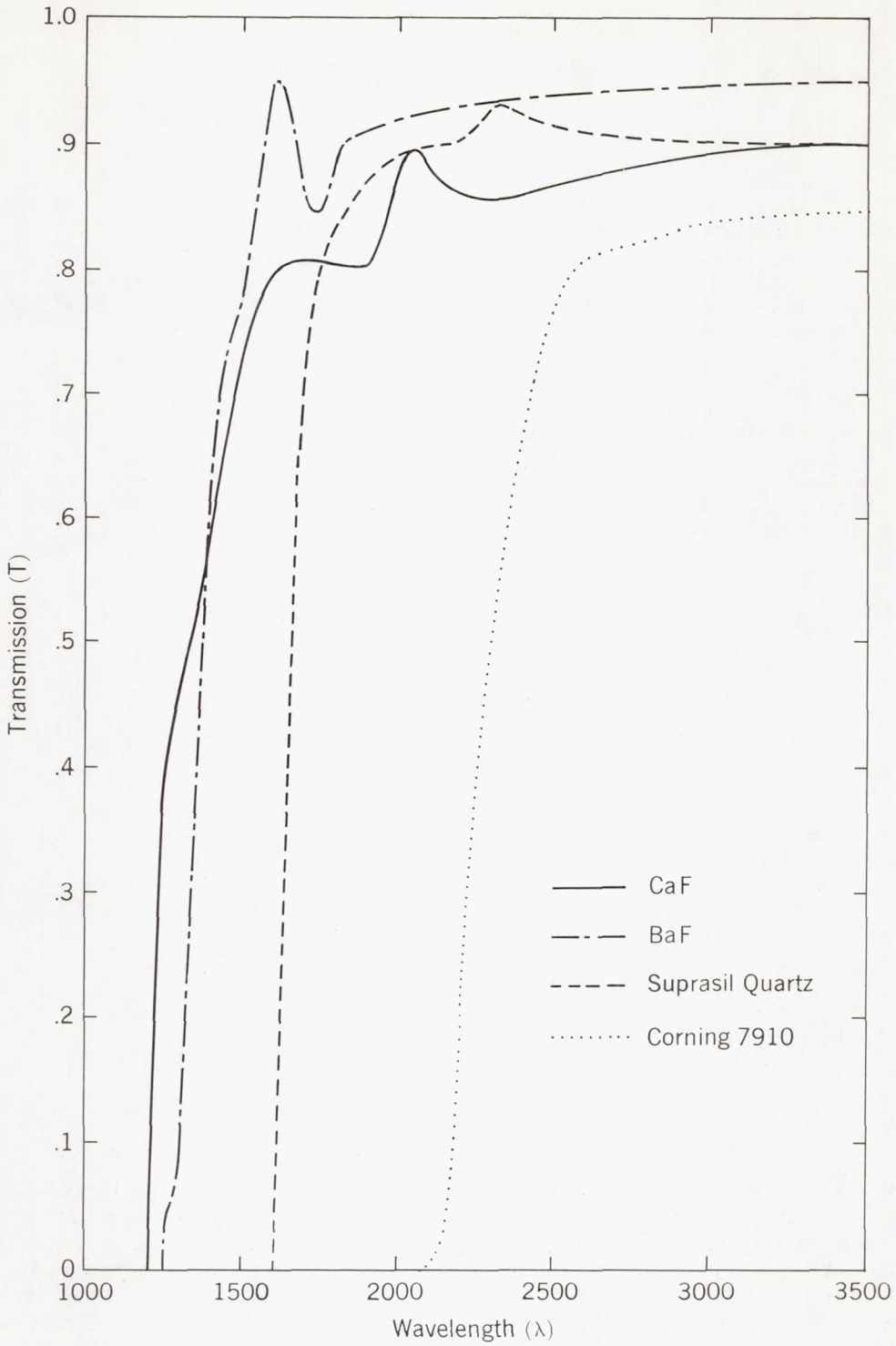

Figure 16.--Transmissivities of various optical materials

Figure 17 shows $\Theta(\lambda)$ for Celescope's four spectral regions. We have taken A = 515 cm^2, t = 60 sec.

A flat, continuous spectrum corresponds fairly well to the average stellar spectrum we expect to observe. For a flat spectrum, we define stellar spectral density threshold

$$\Theta_s'(\lambda) = \Theta_s(\lambda)/W_\lambda ,$$

where W_λ is the width of the $\Theta_s(\lambda)$ curve between half-sensitivity points.

For the nebulae, it is more probable that the spectrum will consist primarily of bright lines, and it is best to consider the threshold in terms of total flux over the bandpass of the equipment. Table 3 lists this threshold information for each of Celescope's broad-band telescopes.

Table 3. Characteristics of Celescope's four broad-band photometric regions

Spectral region	Effective Wavelength (λ_{eff})	Bandwidth (W_λ)	Stellar threshold (per unit wavelength interval) (Θ_s')	Nebular threshold (total flux) (Θ_n)
	Angstroms	Angstroms	photons cm^{-2} s^{-1} A^{-1}	ergs cm^{-2} s^{-1} $sterad^{-1}$
U_1	2600	480	0.050	2.5×10^{-3}
U_2	2300	1000	0.017	2.0×10^{-3}
U_3	1500	240	0.048	2.0×10^{-3}
U_4	1400	320	0.025	1.6×10^{-3}

Zeta Puppis is expected to be the brightest ultraviolet star in the sky, with $I(\lambda)$ = 380 photons cm^{-2} sec^{-1} A^{-1} at 1500 A, and 780 photons cm^{-2} s^{-1} A^{-1} at 2500 A. This value is a factor of 2×10^5 above the minimum detectable signal for the U_2 spectral region. In our preliminary determination at Electro-Mechanical Research of the uvicon's transfer function, we were able to obtain a point image only up to a brightness level 10^4 times the minimum detectable signal. However, as shown in figure 18, the transfer function of the system over this range was linear at least to within $\pm$ 35 percent. Although we expect fewer than 1 percent of our stars to be brighter than 10^4 times the minimum detectable signal, we now have reason to hope that even for these brightest starswe will be able to measure intensity with reasonable accuracy.

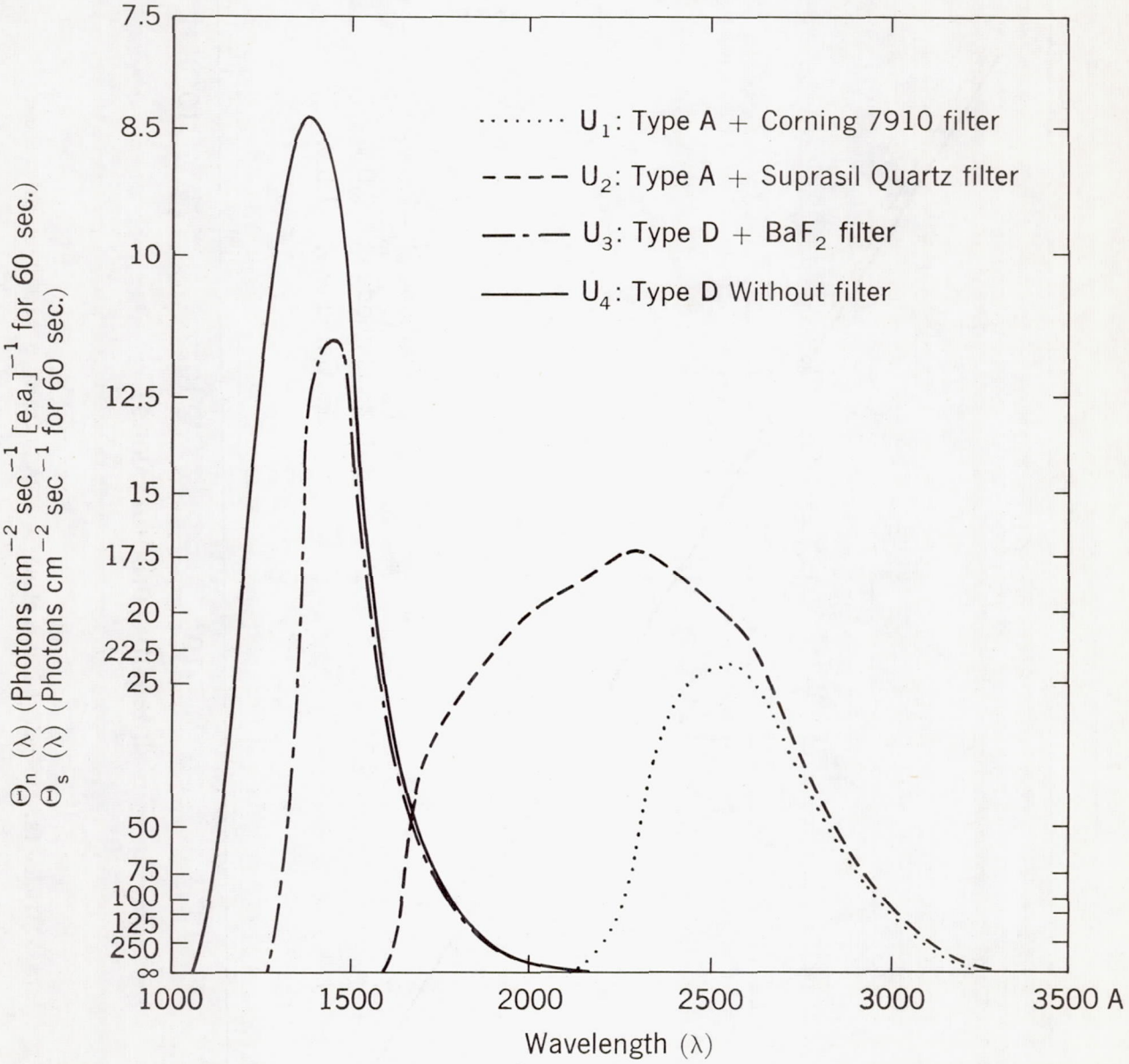

Figure 17.--Spectral response curves for Celescope

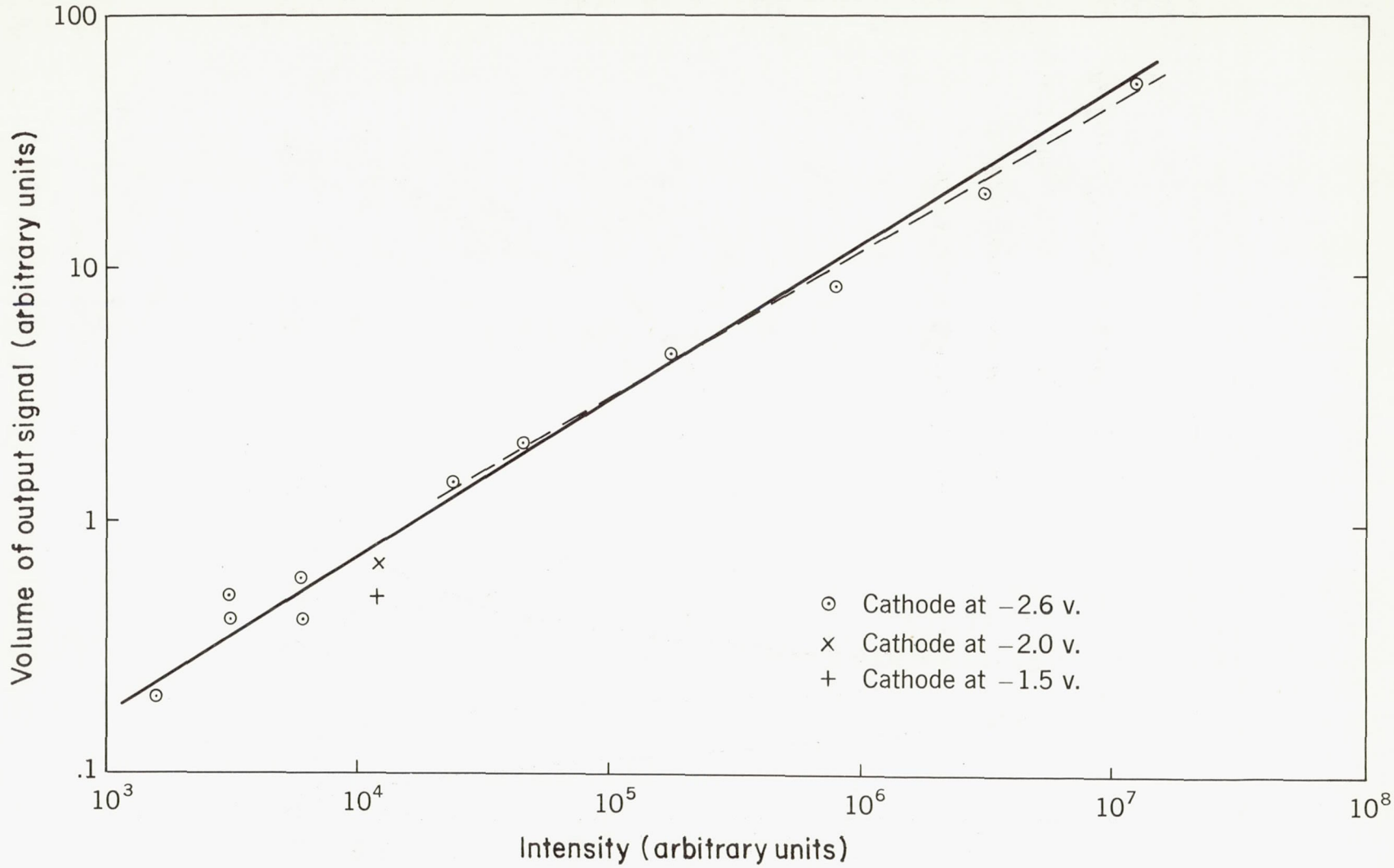

Figure 18.--Transfer function of uvicon S32A in Celescope digital television chain

The nebular threshold corresponds to about 0.002 erg cm^{-2} sec^{-1} $sterad^{-1}$. The brightest nebula observed by Kupperian, Bogges, and Milligan (1958) is 0.003 of these units at about 1300 A; their Spica nebulosity is about 0.002 of these units. We therefore require special extended exposures to study these ultraviolet nebulosities.

Although the present uvicon does not operate on the ebic principle, we have not had to change the external dimensions of the tube, which can be depicted by figures 19 and 20.

The front section of the uvicon is an electron-imaging section. Photoelectrons from the photocathode are accelerated through 12 kilovolts and focused onto the target, the resulting electron image being one-half the size of the initial optical image. The photocathode manufacturing process has recently been improved as a result of a concerted effort by the Westinghouse Research Laboratories; the improvement in photoelectric yield is responsible for most of the recent improvement in sensitivity demonstrated by the uvicon.

The new target operates by transmission secondary emission. It exhibits approximately the same gain as did the old ebic target -- 250 electrons in the image for each impinging photoelectron -- but the gain remains high even when the target voltage is reduced to a point where target defects cannot be seen. For most tubes, optimum target voltage is between 0 and +5 volts. At optimum beam current, even the most intense images can be erased completely and permanently in less than twenty microseconds. This target is further described in Electronic Preview and Sciences Review (1962).

The back section of the tube is an electron gun used for reading the target in exactly the same manner as for a vidicon. We now plan to overscan the uvicon, since we can still achieve the full resolution of the best electrostatic tubes when operating them at a resolution of 256 television lines over the sensitive area of the photocathode (1.2 inches in diameter). The scanned area will thus be a square somewhat more than 1.2 inches on a side.

Experience indicates that point sources of moderate intensity appear to be spread over a number of adjacent elements on readout. Quantitative intensity data are achieved by summing on the ground of the peak amplitudes of the individual elements. Present system planning is to use the same readout technique for both the digital-direct and the digital-store mode of operation. Experiments indicate that the uvicon performs best at high readout speed. Since high average readout speed is incompatible with our limited communication bandwidth, we are experimenting with various specialized scanning techniques for obtaining high instantaneous readout rates and low average readout rates.

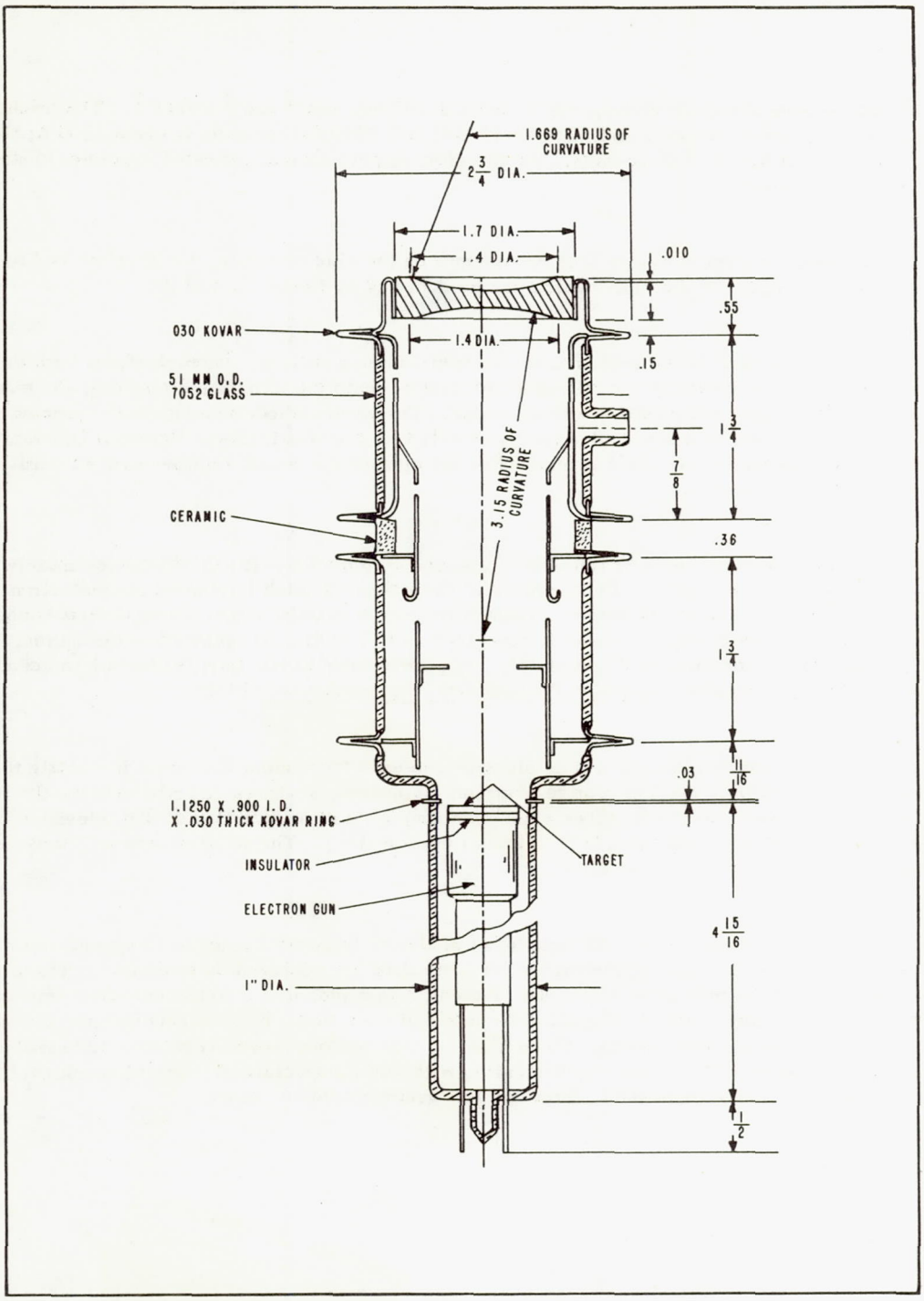

Figure 19.--Diagram of uvicon

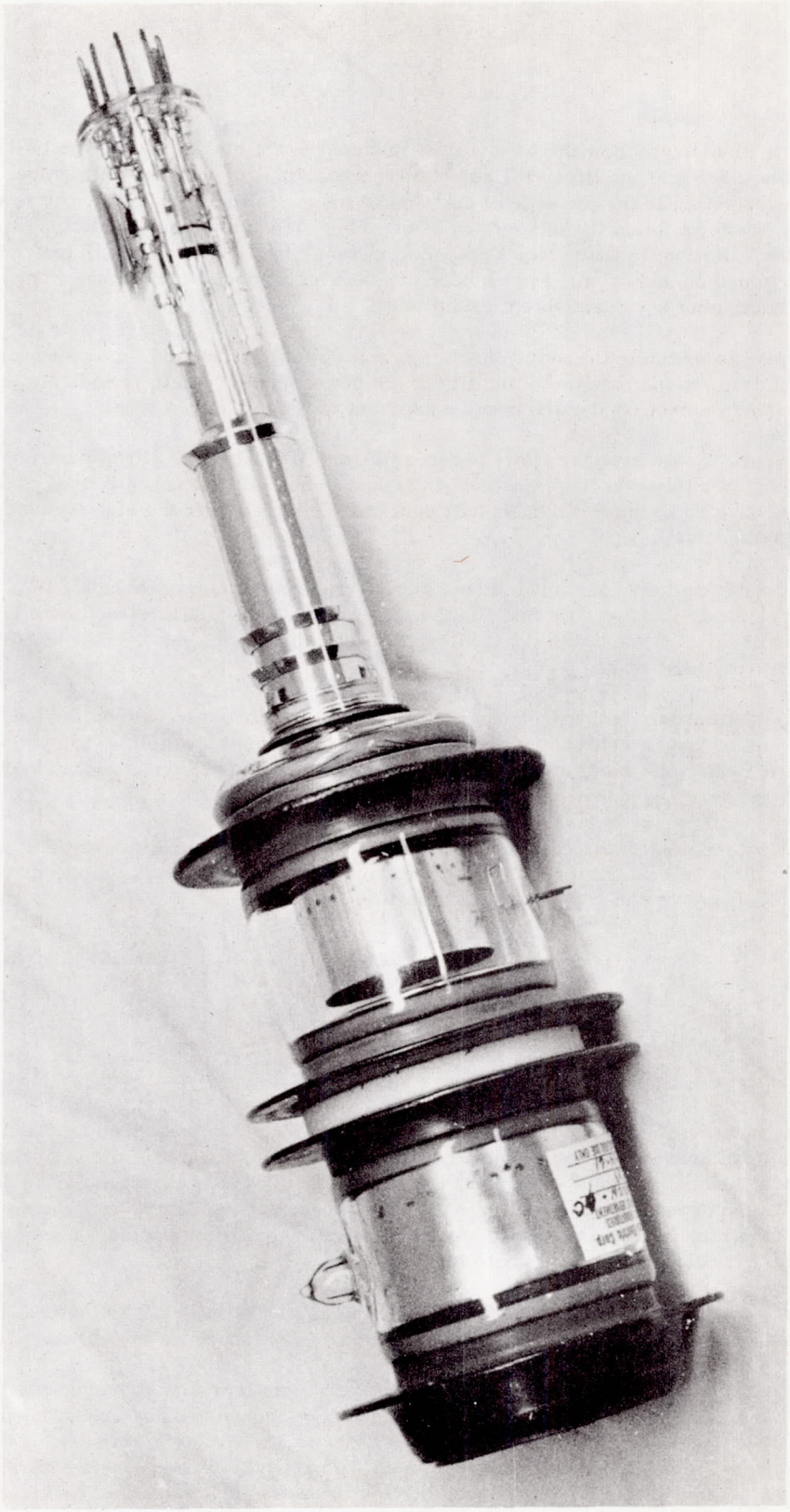

Figure 20.--Photograph of uvicon

Figure 21 indicates how the tube will be mounted in the uvicon case. The 12-kilovolt power supply and the video pre-amplifier will be potted in this case near the base of the tube. In order to assure proper operation in the presence of anticipated magnetic fields (primarily the earth's field) of up to 0.5 gauss, we must shield the gun section of the tube. We are now just initiating a program for measuring the variations in the uvicon's operating characteristics with change in temperature. We have successfully turned on and operated one uvicon over the entire temperature range from +20° C to -90° C, and we are continuing low-temperature experiments.

We plan to maintain the uvicon heaters at full power continuously, in order to increase uvicon operating lifetime, to increase the reliability of the power supply, and to provide a more suitable temperature environment for the electronic equipment inside the uvicon case.

We expect to use exposure times between 0.1 and 100 seconds. Since these tubes can integrate the signal from an ultraviolet image only when high voltage (-12 000 volts) is applied to their photocathodes, we have no need for a mechanical shutter. We merely turn the high voltage on and off to regulate exposure time.

For good focus, the electron-imaging section requires voltage ratios stable to 0.1 percent. The over-all accelerating voltage, however, can vary between 8 and 20 kilovolts without disturbing the focus. The nominal imaging voltages are -12.0 kilovolts, -11.5 kilovolts, -11.2 kilovolts, and ground. The target is nominally at +5 volts.

The electron-gun section is identical to that of an electrostatic vidicon. We have chosen electrostatic rather than electromagnetic focusing and deflection to enable us to reduce power and weight requirements, eliminate high magnetic fields, and use simpler electronics in our digital scanning mode. Heater power is one watt.

A major problem in the construction of this tube is proper ruggedization. The program will succeed only if the tubes are capable of surviving launch and of operating in orbit, and will be completed only if the tubes survive one year of orbital operation.

2. Optical System

The linear resolution and field of view of the Celescope are prescribed by the detector. In turn, these set limits of between 16 and 40 inches on the first basic parameter of the optical system, the effective focal length. For a 40-inch focal length, the field of view becomes 1°.7 in diameter, and we require 25 000 pictures to cover the sky. We do not expect to have time during the useful life of this satellite to take more pictures than this. And it becomes very difficult to design a system of adequate aperture with a focal length as short as 16 inches.

The second basic parameter of the optical system, the aperture, is set by the physical dimensions of the spacecraft that NASA is supplying. This aperture is 12 inches for each of our four instruments.

Within this framework, we require the simplest system that will give adequately small aberrations throughout our field of view. Complex instruments cannot adequately survive the launch environment. We cannot allow large lenses in our system, since they are not available in materials that are useful in the far ultraviolet. We studied the properties of one-mirror systems, and found none that could meet our requirements. In two-mirror systems the Schwarzschild camera is the simplest that can fit our needs.

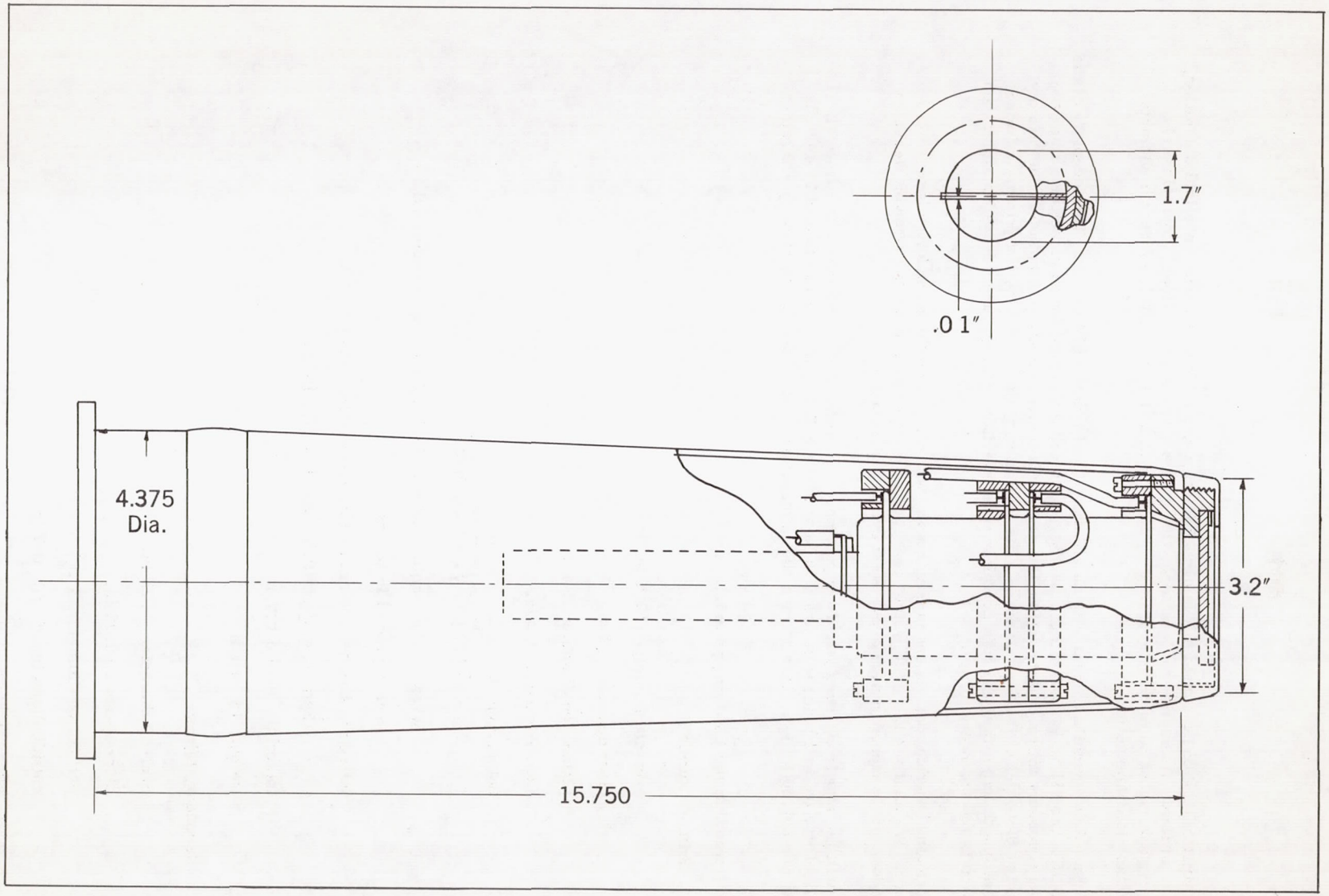

Figure 21.--Mounting case for uvicon

Schwarzschild (1905) designed this family of telescopes to be free of coma, spherical aberration, and curvature of field. As applied to Celescope, this system gives nearly uniform, approximately circular star images about 50 microns in diameter, throughout a field of view 1.4 inches in diameter. Figure 23 shows the configuration.

We use a Schwarzschild camera with an effective focal length of 24 inches. The faceplate of the detector modifies the EFL to 24.893 inches. We have designed the system for no vignetting, since the shadow of the secondary mirror and its cell on the primary is larger than the perforation in the primary, even for stars at the edges of the field of view. The reflection of this shadow by the primary mirror is over its entire length larger than the case containing the television camera tube. It is also larger than the perforation in the secondary mirror.

By grinding spherical depressions in their backs, we will lighten the secondary mirrors to 1.5 pounds apiece. We must use the light-weight construction in order to increase the resonant frequency of the secondary mirror support system above 2000 cycles per second.

We will use four broad-band television photometers, mechanically and optically identical. To increase reliability, we will place split filters in front of the uvicons, as shown in figures 21 and 22. Thus, if any one uvicon fails, we can recover the information it was supplying by slewing 0°.9 rather than 1°.8.

The system has the following parameters:

Primary Mirror :

over-all diameter, 12.5 in.

clear aperture, 12 in.

perforation diameter, 5 in.

edge thickness, 2.2 in.

shape, hyperbolidal,

$$z = h^2 / 72 \left(1 + \sqrt{1 + 0.000700h^2}\right),$$

where z is the sagitta and h is the height above the optic axis,

both expressed in inches.

reflecting surface, aluminum plus magnesium fluoride

(Berning et al., 1960; Angel et al., 1961).

material, fused quartz

weight, 18 pounds

Secondary Mirror:

over-all diameter, 6.25 in.

clear aperture, 6.05 in.

perforation diameter, 1 in.

outside diameter of cell, 6.7 in.

edge thickness, 1 in.

shape, oblate ellipsoidal

$$z = h^2 / 57.6 \left(1 + \sqrt{1 - 0.012043h^2}\right),$$

where z is the sagitta and h is the height above the optic axis, both expressed in inches.

material, fused quartz

reflecting surface, aluminum plus magnesium fluoride

weight, 1.5 pounds

System: effective focal length, 24.893 in.

total length between mirror vertices, 21.6 in.

distance between secondary mirror vertex and focal plane, 9.6 in.

field of view, 1.2 in. circle = 2.8 circle

effective focal ratio ("transmission ratio"), T/3.7, assuming 75% reflectivity

sensory system: see above

image quality, 95% of light within 100-micron circle under all conditions of decentration less than .01 in. from optimum focus, throughout the field of view, for collimated input beam.

focal surface, plane except as modified by detector faceplate. See above.

weight, 58.5 pounds, including optics, detector, and telescope structure, but omitting integrating structure.

Although Schwarzschild's work was published in 1905, no Schwarzschild camera has ever been used successfully in astronomical research. Two such instruments, one at Brown University and one at Indiana University, proved ineffective because of the difficulty of figuring the optics, and because of the inconvenient location of the focal plane. For ground-based astronomy, the Schmidt camera gives much better performance. In space, however, the Schwarzschild system is far preferable. First, the Schmidt corrector plate poses great difficulties for work in the ultraviolet because of the small choice and sizes of transmission optical materials that are available. Second, the field of view and the resolution of our television system are too poor to enable us to take advantage of the superior resolving power and field of view provided by a Schmidt system. And third, to withstand the rugged environment of launch, it is easier to mount small thick mirrors than large, thin corrector plates. It is true that Schmidt systems have been designed with reflective corrector plates, but such systems must be built off-axis with consequent difficulties in figuring and mounting them.

The calibration optical system is shown in figure 23. An array of pinholes varying in diameter between 7 and 50 microns is placed near each calibrator lamp. The diagonal plane mirror allows this array to be focused by a lithium-fluoride lens onto the uvicon photocathode. The resulting artificial stars have diameters of less than 60 microns. The lens has a focusing adjustment of $\pm$ 0.125 inch, allowing motion of the artificial star images by $\pm$ 0.075 inch relative to the uvicon photocathode to achieve optimum focus. To insure that the focus of the lens will lie within this range, the index of refraction of the lithium-fluoride blanks need be measured only to $\pm$ 1 percent. The lithium-fluoride lenses to be used with the 1470-A calibrator lamps will be double convex, with equal radii of curvature approximately 4.0 inches. Those to be used with the 2537-A calibrator lamps will also be double convex, with radii of curvature approximately 3.0 inches.

3. Mechanical System and Thermal Requirements

The Celescope mechanical system can be considered in two sections: telescope modules and integrating structure.

The purpose of the structure for the telescope modules is to hold the various elements of the optical system in correct alignment. One of the primary considerations in our design of the Schwarzschild system was the allowable decentration error. Decentration is the departure, in any dimension, of an optical element from its position for optimum focus. Our system as designed will allow a decentration of any component parallel to the optic axis, up to 0.010 inch. Perpendicular to the optic axis, it will allow decentration of the primary mirror by 0.050 inch, of the secondary mirror by 0.025 inch, and of the faceplate of the television camera tube by 0.015 inch. No component may be tilted by more than 3 minutes of arc. Longitudinal decentration of the secondary up to 0.1 inch can be adequately compensated by focusing motion of the uvicon faceplate. Within these limits, image size throughout the field of view is less than the detector's resolution limit of 100 microns.

The temperature at which the Celescope must operate is $-30° \pm 15°$ C. The laboratory in which it must be adjusted prior to launch will, however, have a temperature of $+20° \pm 10°$ C. Since we require that the Celescope have no moving parts, we must choose structural materials that will preserve the proper dimensional relationships between the optical components over a temperature range of up to 75° C.

We have two alternatives for solving the problem of thermal expansion. The first is to build our optical components and structure from materials with the same coefficient of expansion. Unless this coefficient is negligible, this method requires that all structural elements be at the same temperature. In addition, mechanical considerations point toward a choice of structural materials with a medium or high coefficient of expansion, whereas optical considerations point toward optical materials of negligible coefficient of expansion.

Although we are investigating the use of novel techniques for obtaining dimensional stability from such low-expansion materials as Pyroceram, our primary effort is now directed toward the second method, that of passive compensation. The usual method of compensation makes use of two concentric cylinders, the shorter of which has a higher coefficient of expansion. These two cylinders are joined at one end. The distance between the free ends then remains constant regardless of temperature.

We plan to make use of the optical properties of the Schwarzschild system to simplify our compensation network.

Figure 23 shows our preliminary design of the telescope modules. The main structural tube between the primary and secondary mirrors will be titanium alloy 6Al-4V, having a coefficient of expansion 8.1×10^{-6} per degree centigrade. This material determines the distance between the backs of the mirrors, approximately 24.8 inches. The faceplate of the uvicon is held in a position approximately 14.2 inches from the back of the primary mirror, and 16.0 inches from the rear of the titanium structure, by a case made from aluminum alloy 2014 having a coefficient of expansion 21.4×10^{-6} per degree centigrade. With this combination, any defocusing caused by thermal contraction of the titanium structure will be compensated by the even greater total contraction of the aluminum case. Our optical system will thus remain in satisfactory focus over a temperature range exceeding that contemplated in going from laboratory to space conditions (+30° to -50° C.) Our compensating structure will operate satisfactorily so long as thermal gradients and departures from design conditions do not exceed $\pm 15°$ C.

Figure 24 shows how our telescope modules will be mounted in the experiment container, with emphasis on the thermal design. Figure 25 is a photograph of this experiment container. The container is supported by the spacecraft structure at four mounting points, and maintained at the same temperature as the spacecraft structure by radiative heat transfer between two cylinders of about 90 percent emissivity The equilibrium temperature of this structure will be $-30° \pm 15°$ C. Longitudinal and lateral temperature variations as great as 20° C are possible over the 50-inch span of the experiment container.

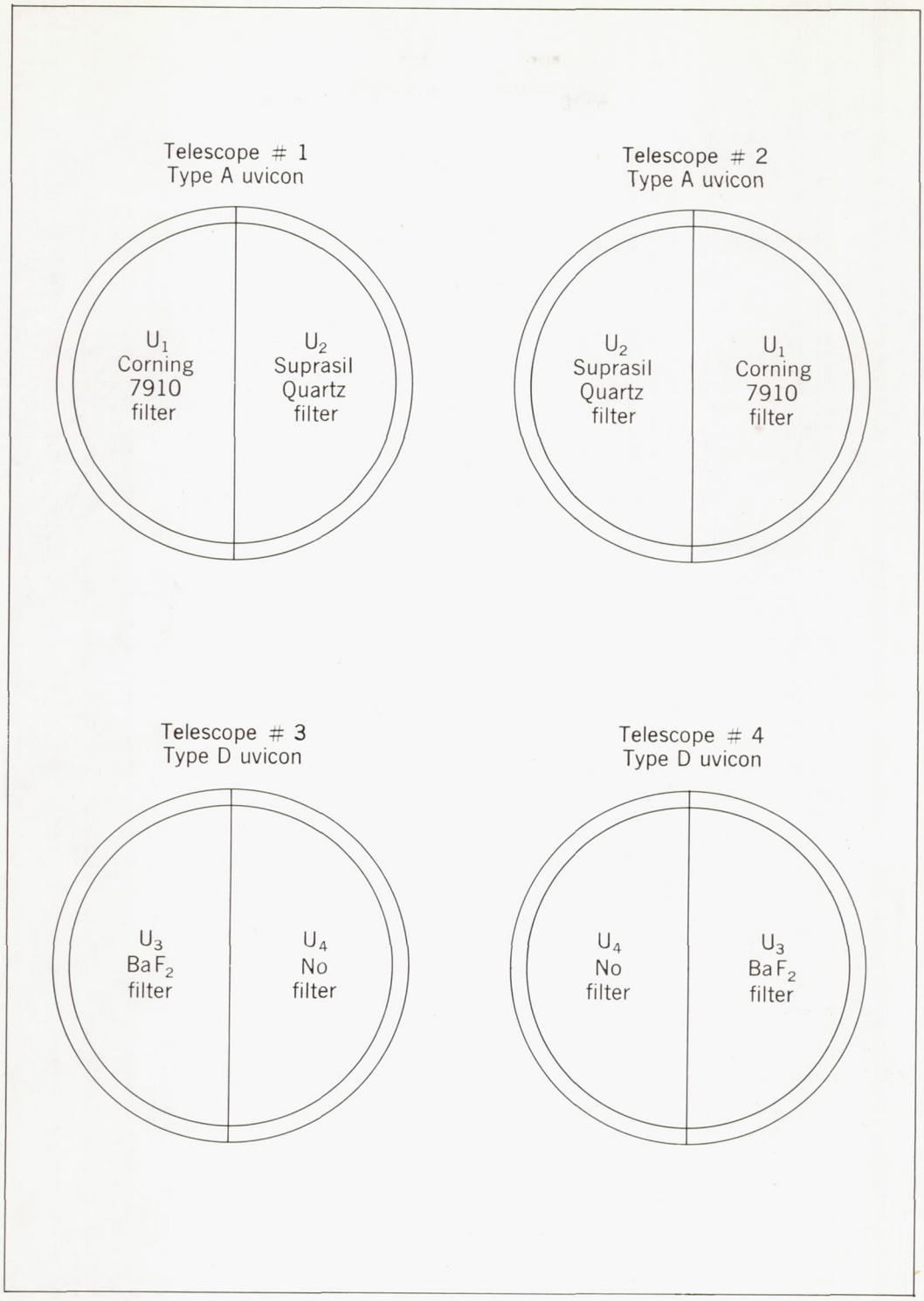

Figure 22. --Filter arrangement for Celescope

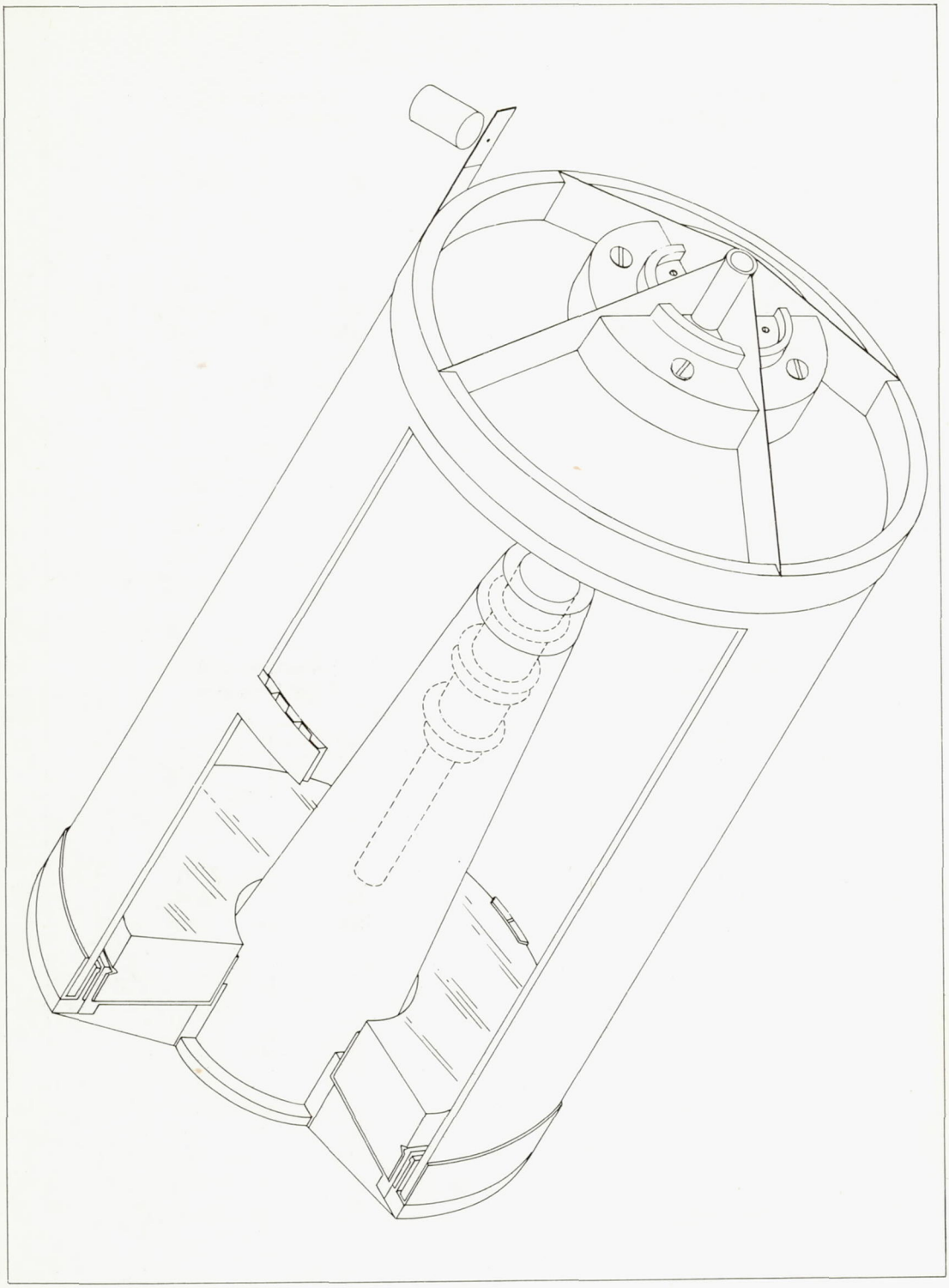

Figure 23A. --Individual telescope module showing optical system

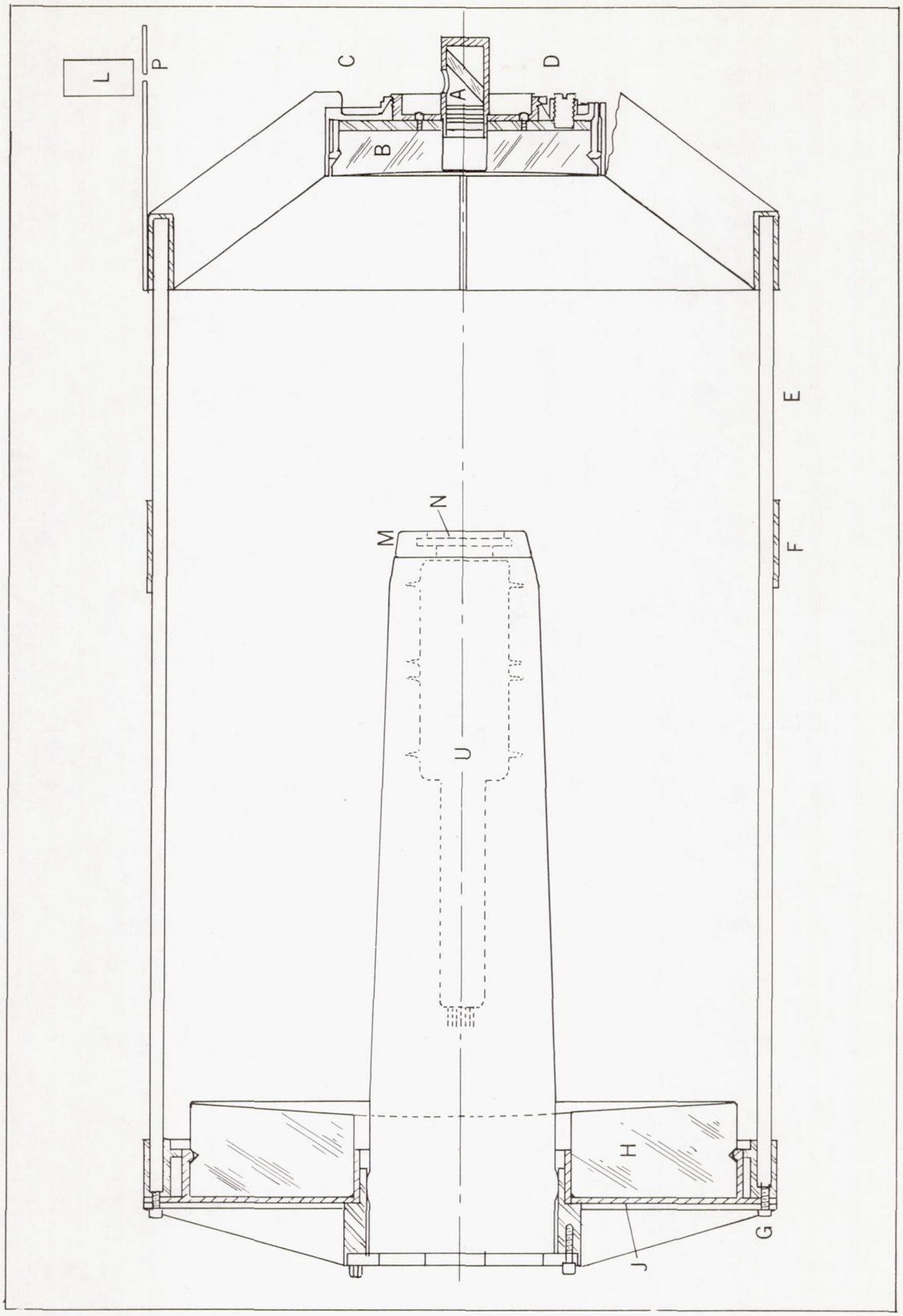

Figure 23B.

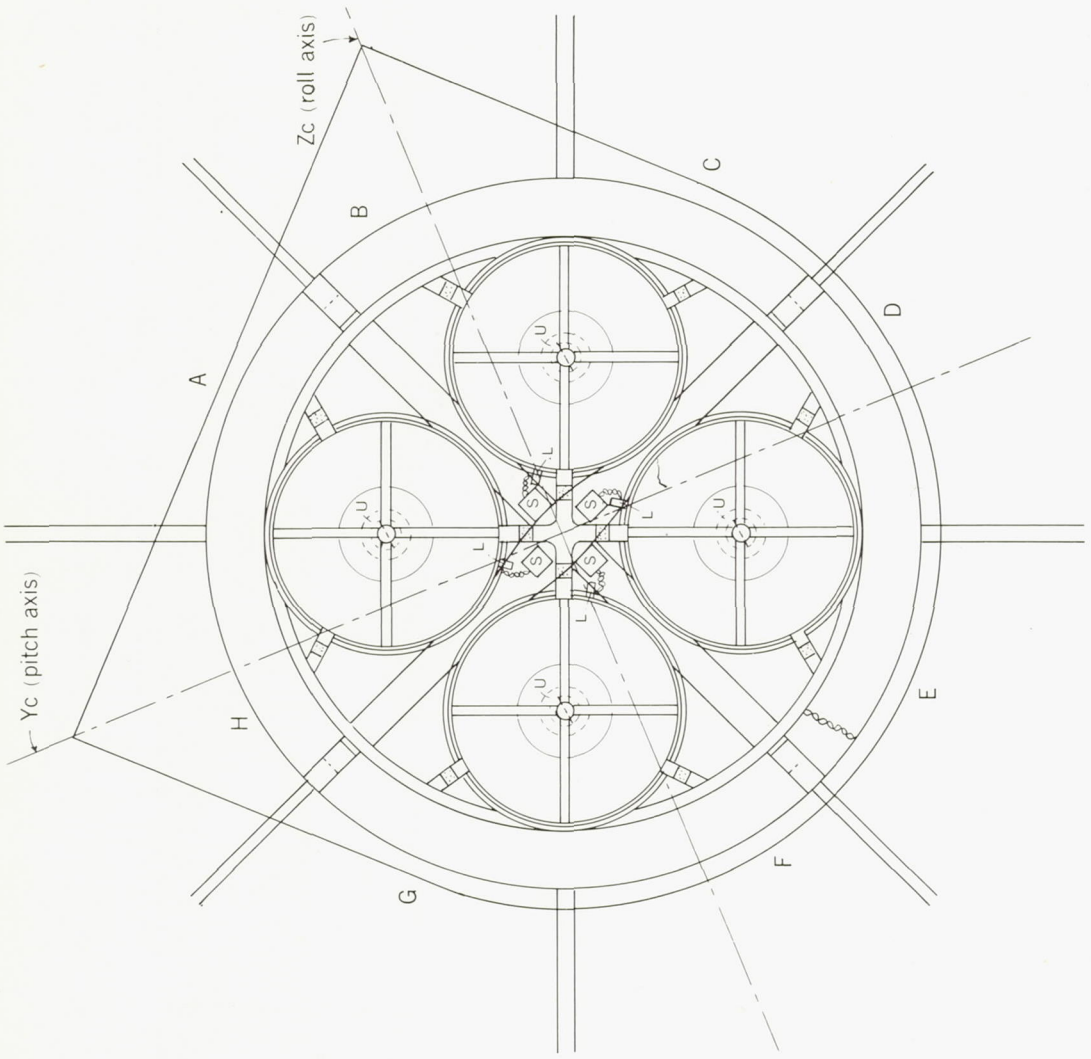

Figure 24A. --Celescope in relation to the spacecraft

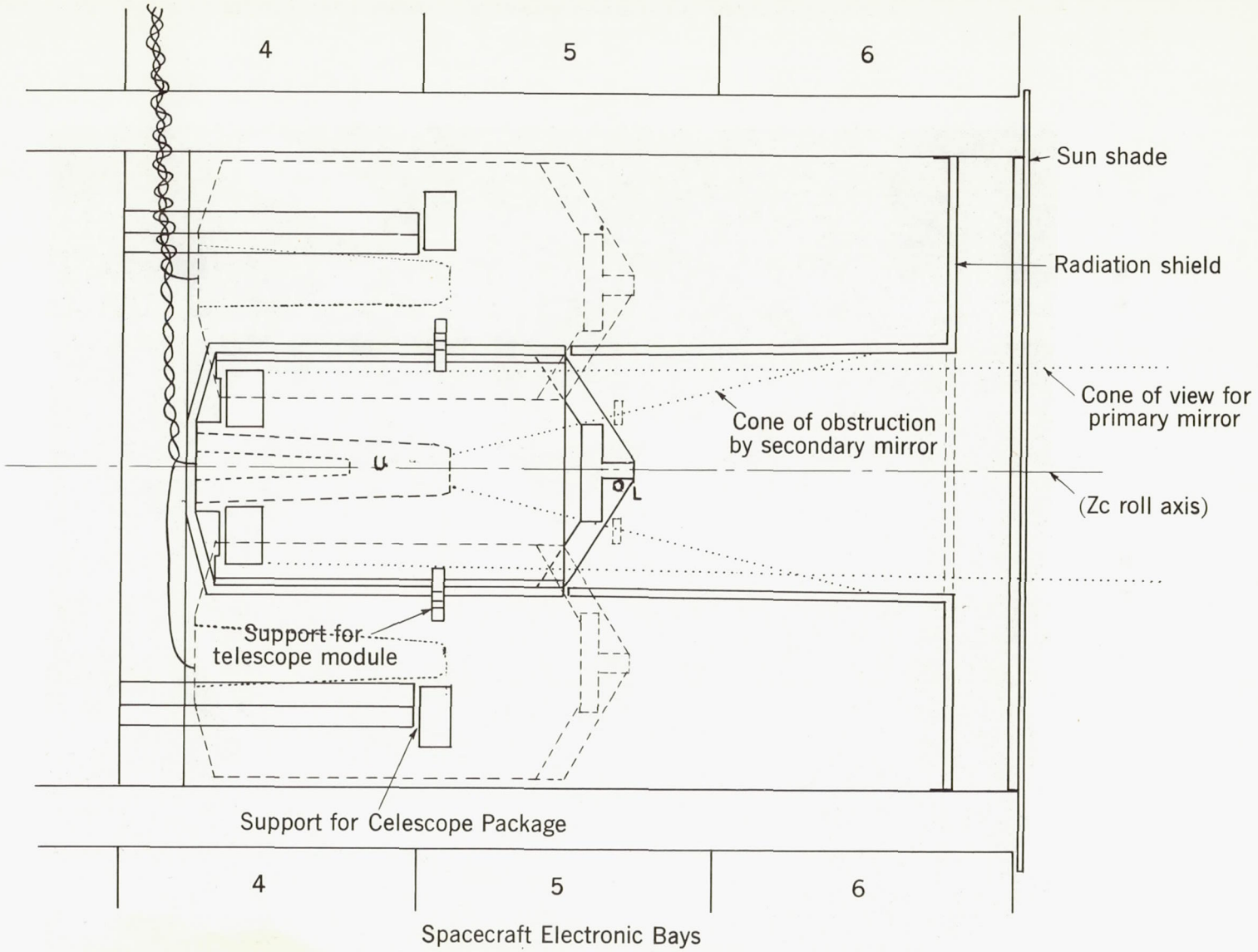
4
5
6
Sun shade
Radiation shield
Cone of view for primary mirror
Cone of obstruction by secondary mirror
(Zc roll axis)
Support for telescope module
Support for Celescope Package
4
5
6
Spacecraft Electronic Bays

Figure 24B.

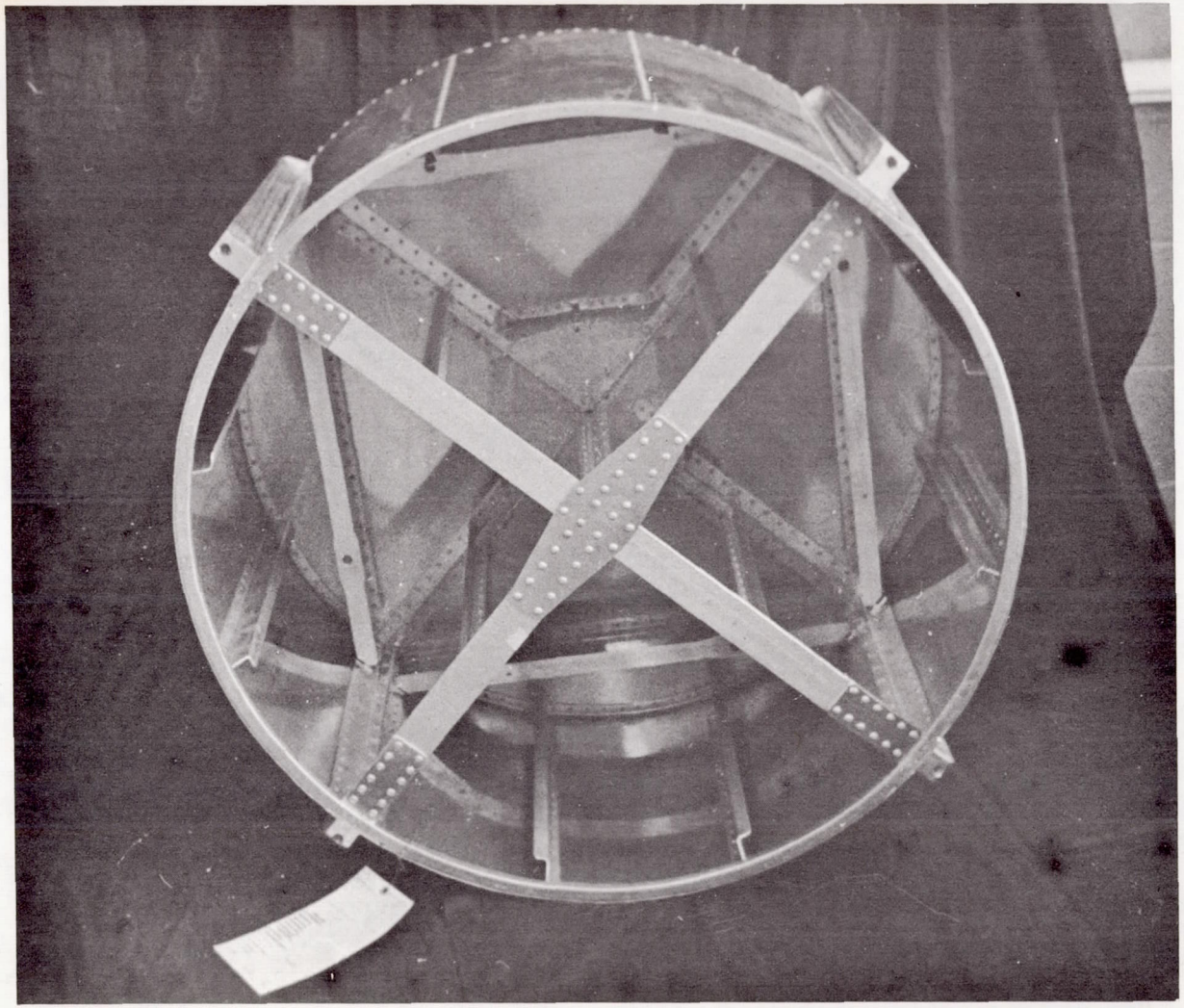

Figure 25.--Photograph of spacecraft experiment container for Celescope

The telescope modules are thermally isolated from the experiment container by means of insulation having a low-emissivity coating. By reflection, this coating tends to reduce the temperature gradients in the spacecraft structure. The thermal barrier completely surrounds each telescope module, being continued beyond the end of the telescope structure by the radiation shield. The cathode of an electrostatic ion trap is incorporated into each radiation shield, with the anode supported above the secondary mirror support, to prevent incoming positive ions from being attracted to the -12 kilovolt potential of the photocathode. The interior surfaces of the telescope modules and the heat shield are chosen for their optical properties: they must be dull black in the ultraviolet. We expect to use a material similar to Grumman black epoxy #604, having a reflectance in the ultraviolet of about 5 percent, and an emissivity in the infrared of about 85 percent.

An average power of 1.3 watt is dissipated in each of the four uvicon cases, marked U in figure 24; 1.15 watts is continuously on, being accounted for primarily by the 1-watt uvicon heater. Each high-voltage power supply, dissipating 3.8 watts, is on for an average of 3 minutes per orbit.

The average power dissipated in the calibrator lamps and power supplies is about 35 milliwatts for each lamp and for each supply. Each lamp and each supply dissipates about 0.5 watt when it is on (an average of 7 minutes per orbit).

The thermal properties of the potting material used in the detector cases, calibrator lamps, and power supplies are of the kind to render negligible any temperature fluctuations of structural members arising from fluctuations in power dissipation. Approximately 5 BTU per hour (corresponding to 1.5 watts, or 0.4 watt per telescope module) are transmitted into the telescope modules along the electrical cables from the Celescope electronics in Bay E-4, the temperature of which can vary between +35° F and +155° F.

Each telescope module is supported near its center of gravity at three mounting points. To minimize thermal conduction through them, each will incorporate approximately a one-inch cube of insulating material.

Table 4 gives our present weight estimate for each of the four telescope modules.

Table 4. Weight breakdown for an individual telescope module

Primary cell	3.82 lbs.
Primary finger ring	3.44
Primary stiffener	3.59
Structural tube	11.04
Secondary structure	2.48
Secondary finger ring	.45
Secondary cell	.62
Calibrator cell	.13
Retainers	.06
Calibrator mirror and lens	.02
Support ring	2.73
Calibrator lamp support and lamp (tentative)	.43
Subtotal (structure)	28.81 lbs.
Primary mirror (unmodified)	18.19
Secondary mirror (lightened)	1.50
Uvicon case	3.00
Uvicon, electronics and potting	7.00
Total for 1 module	58.50 lbs.

Weight estimates of the integrating structure are not yet as accurate as those for the individual modules. However, the over-all weight breakdown is given in Table 5.

Table 5. Weight breakdown for the Celescope system

Four telescope modules @ 58.50 lbs.	234.0 lbs.
Radiation shield	3.0
Experiment container (includes 10 lbs. integrating structure added to container supplied by spacecraft manufacturer)	57.2
Electronics in Bay E-4 (includes 3.4 lbs. for mounting shelf supplied by spacecraft manufacturer)	33.4
Cabling	5.0
Total (includes 294.2 lbs. in optical area)	332.6 lbs.

The total moment of inertia for the four telescope assemblies as they will be located in the OAO is as follows:

About the spacecraft roll axis (x-y axis): 9.04 slug ft^2.

About the pitch or yaw axis (y-y or z-z): 12.20 slug ft^2.

These quantities are for the four telescopes alone and do not include the integrating structure.

The center of gravity of each telescope module is 12.0 inches from the roll axis of the spacecraft and at Station 113.55. This point is 7.8 inches from the back of the module, and 3.5 inches from the front surface of the primary mirror.

4. Electronic System

The design of the Celescope electronic system is now nearing completion at Electro-Mechanical Research, Inc., Sarasota, Florida. Although the function of this system is still to operate the uvicons so as to obtain the most reliable and accurate information feasible on both stars and nebulosities, the design details vary considerably from those described in Special Report No. 83. These changes have arisen from our improved understanding of the uvicon, from requirements imposed by considerations of reliability, and from the need for compatibility with the spacecraft.

Figure 26 illustrates our most likely sequence of operations for Celescope in orbit. This sequence commences with a series of stored commands to slew the OAO into the first Celescope orientation and turn on all calibrator lamps 5 minutes or more prior to commencement of a ground-station pass. The calibration exposures are made during the first 3 minutes of the pass and stored on the uvicon targets as electrical charge patterns until the full facilities of the spacecraft are turned over to the Celescope. The first 2 to 3 minutes of each pass are otherwise reserved for the spacecraft and for the University of Wisconsin.

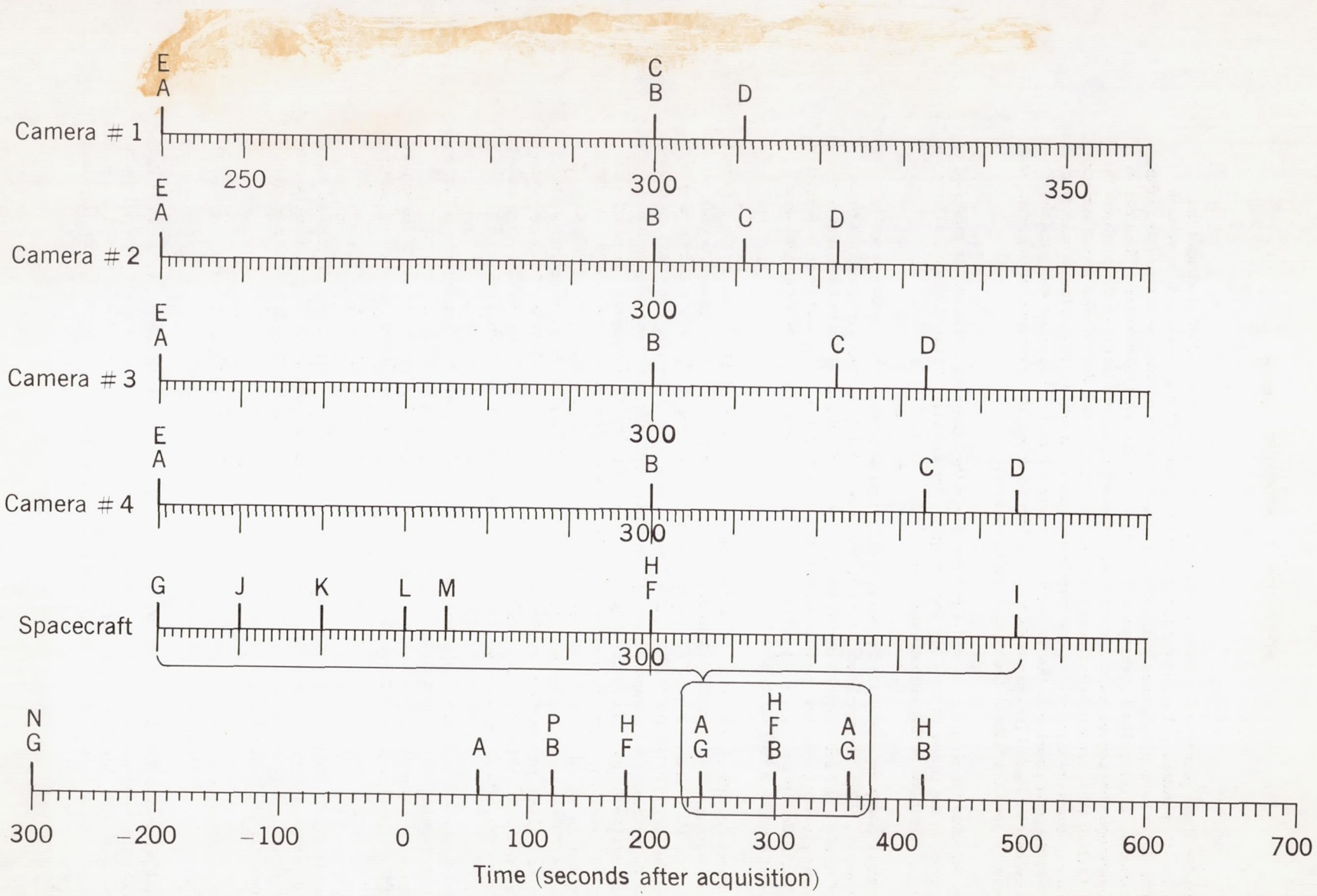

Figure 26.--Sequence of operations for Celescope in orbit

The remainder of the pass is utilized to send real-time commands to the OAO to control the Celescope sequence of operations. Each operation indicated in figure 26 requires one or more such commands. First, the uvicons are scanned in the digital-direct mode, and the first picture, including calibration information, is transmitted to the ground through the wide-band transmitter. Then one or more standard Celescope data sequences are commanded, depending on the length of the pass over the ground station. Each of these sequences includes a 60-second exposure and digital-direct scan for each camera. The four exposures are commenced and terminated nearly simultaneously; after termination, we begin a 1°8 slew to the next position. In the 60-second exposure interval in each data sequence the command memory may be loaded for operations to be performed during the remainder of the orbit, and the status data may be read out through the wide-band transmitter.

Merely by changing the sequence of real-time commands, the above sequences can be modified to fit experience gained in the course of the Celescope program, for example, to allow longer, shorter, or multiple exposures, variations in the calibration program, etc.

There are three operating modes for Celescope's television cameras. The primary mode is digital-direct scanning. Here the amplitude of the signal at each image element is converted to an 8-bit word (PCM format) and transmitted directly to the wide-band transmitter for transmission to the ground. This mode gives accurate information about both stars and nebulosities, and since it generates more than half a million bits per picture, it cannot be used in conjunction with the spacecraft data storage system, but must be a real-time operation.

A PCM frame consists of 260 words. The first four words form the PCM synchronization. Word 5 gives the TV line number. The next 255 words give TV intensity data to 7-bit accuracy; the 8th bit is for parity check. One TV frame consists of 256 PCM frames. The 4-word PCM sync code consists of the sequence 11100010010000111011010001110110; this is the same as the 32-bit sync code used for readout of the spacecraft data storage. Each transmission will be started with alternate 1-0 for a period of not less than 128 milliseconds (6400 bits). In addition, any dead time between TV frames will be filled with alternate 1-0. The switchover from alternate 1-0 to PCM frames will always be followed by the PCM sync code and will maintain bit phase. Word phase may not be maintained during the switchover. The dead times between TV frames will be no less than 128 milliseconds, and in the worst case could be as long as 10 seconds. A large part of the television picture will be black. To prevent a large percentage of zeros in the transmission and the resulting problem for bit detection, the Celescope will complement every other bit from the A-to-D converter so that zero and full-scale read alternate 1-0.

The second mode is digital store. In this mode the position and amplitude are determined for each resolution element for which the amplitude exceeds an adjustable threshold. This information is digitized and transmitted as a 25-bit word to the experimenters' data handling equipment of the spacecraft for storage in the data memory. On the average, there will be six such words for each star in the picture.

As figure 18 shows, the sum of the signal amplitudes from all elemental areas affected by a star can be used to determine the brightness of that star. Either the digital-store or the digital-direct mode provides this information with full accuracy. The digital-store mode, however, gives no information about nebulosities. It will be used only as a back-up mode.

The third mode is analog direct. Here the video signal is transmitted directly to the wide-band transmitter. This mode will be used only upon failure of the digital-direct mode.

The digital processing unit is the basic television digital data processing system, as shown in figure 27. It consists of (1) a video amplitude analog-to-digital converter; (2) horizontal and vertical digital sweep generators to provide the digital raster; (3) a PCM system for generation of a 50 kilobit/sec serial PCM signal; and (4) an over-all digital television programmer for general timing in both the digital-direct and digital-store modes.

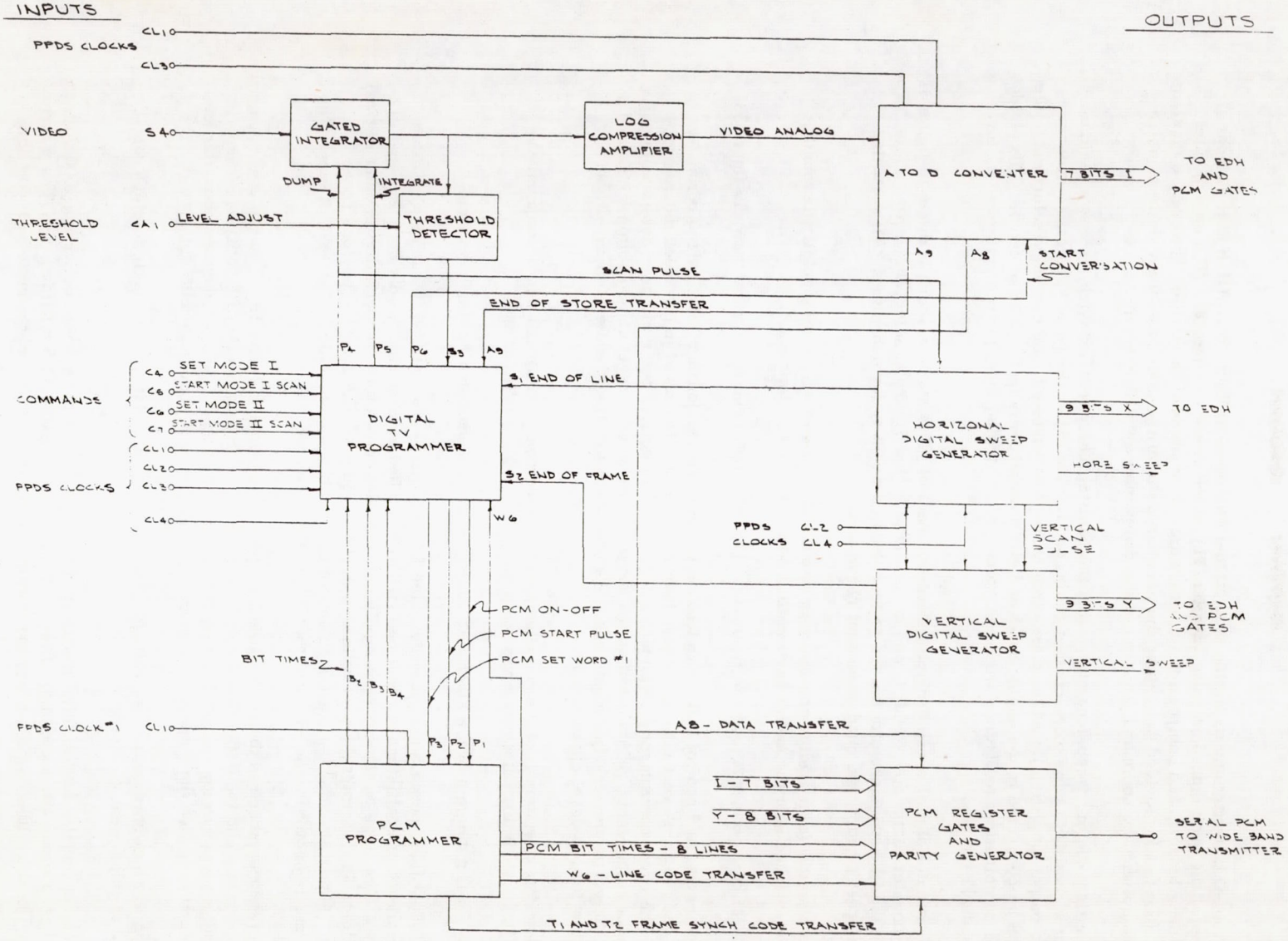

Figure 27.--Digital processing unit

The A-to-D converter and its timing programmer are shown in figure 28. All digital portions of this unit employ the quad-redundant pulse-inverter (PI) switch shown in figure 29. The analog gates (AG), resistance ladders, and comparator amplifiers are all nonredundant circuits; however, a duplicate set of these elements is provided to achieve the necessary reliability. Selection of the desired analog chain is accomplished by command selection of the comparator amplifier outputs.

The vertical digital sweep generator, using the parallel sub-system approach, is shown in figure 30. Each generator consists of two binary-counter chains and two analog chains (analog gates, resistance ladders, and output amplifiers). All of these circuits are nonredundant. By command selection, either BC chain can be connected to the analog gates, and either amplifier output can be selected. This yields four possible combinations to obtain a working system. All switching functions are performed by the quad-redundant PI circuits.

The horizontal digital sweep generator using the parallel sub-system approach is shown in figure 31. Two binary counter chains are provided, and command selection is used to select the desired chain. The outputs from the line sync generator are fed to four nonredundant sweep generators. All switching functions are performed by the quad-redundant PI circuits.

The circuitry for providing and inserting into the deflection circuits the specialized scanning techniques mentioned near the end of Section III.1 is still under development.

The PCM programmer is shown in figure 32. The PCM gates and register are shown in figure 33.

The command and control unit for Celescope performs two major functions: uvicon parameter adjustment and program event control. These two functions are illustrated in the block diagram of figure 34. The event controls may be either an on-off type of control or simply an event-execute pulse. The parameter adjustments, as indicated on the diagram, are sixteen-level analog voltages obtained by decoding a digital parameter adjustment code. We are also evaluating the use of motor-driven potentiometers for 100-level adjustment.

A relay control system is also under study, since the uvicon controls will only infrequently be adjusted. This system dissipates minimum power in the stand-by condition.

Figure 35 is a diagram of the electronic analog adjustment unit that has been developed.

The low-voltage power supply provides three DC voltages: +18 volts $\pm$ 0.1% at 25° C with a negative temperature coefficient of about one millivolt per degree centigrade; +6 volts $\pm$ 2%; and -12 volts $\pm$ 0.1%. The slope on the +18-volt supply will provide temperature compensation in other critical circuits. Figure 36 illustrates the low-voltage concept. Figure 37 illustrates the payload power distribution. Figure 38 shows the basic elements of a switching pre-regulator. The +6-volt supply, as well as the pre-regulator for the +18-volt supply, uses this concept.

The present approach to the uvicon power supply is illustrated in figure 39. The target is operated at ground potential, and the deflection amplifiers are operated from a floating 70-volt power supply. Separate heater supplies with current-limiting provisions will be used. A new redundant converter has been developed to reduce the number of transformer windings, thus increasing reliability.

Switchover networks for the low-voltage system have been designed. Magnetic latching relays will be used to implement the design.

The power supplies for the calibrator lamps are current-regulated supplies delivering 3000 volts in the no-load condition. When the lamps fires, the current is limited to 0.5 milliampere. The mercury-vapor lamps operate with 270 volts across the lamp, whereas the xenon lamps operate with 400 volts across the lamp.

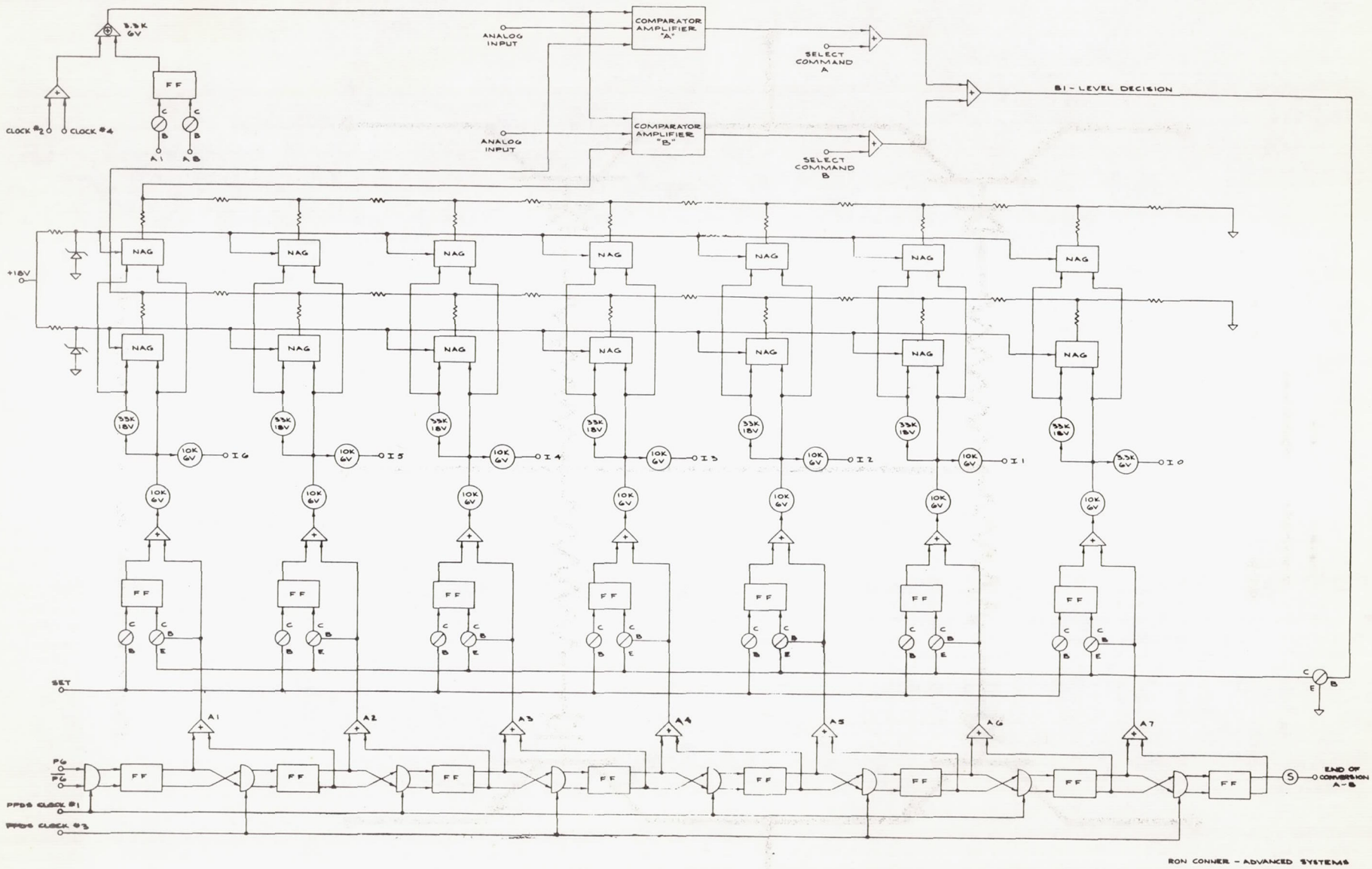

Figure 28.--Analog-to-digital converter and timing programmer

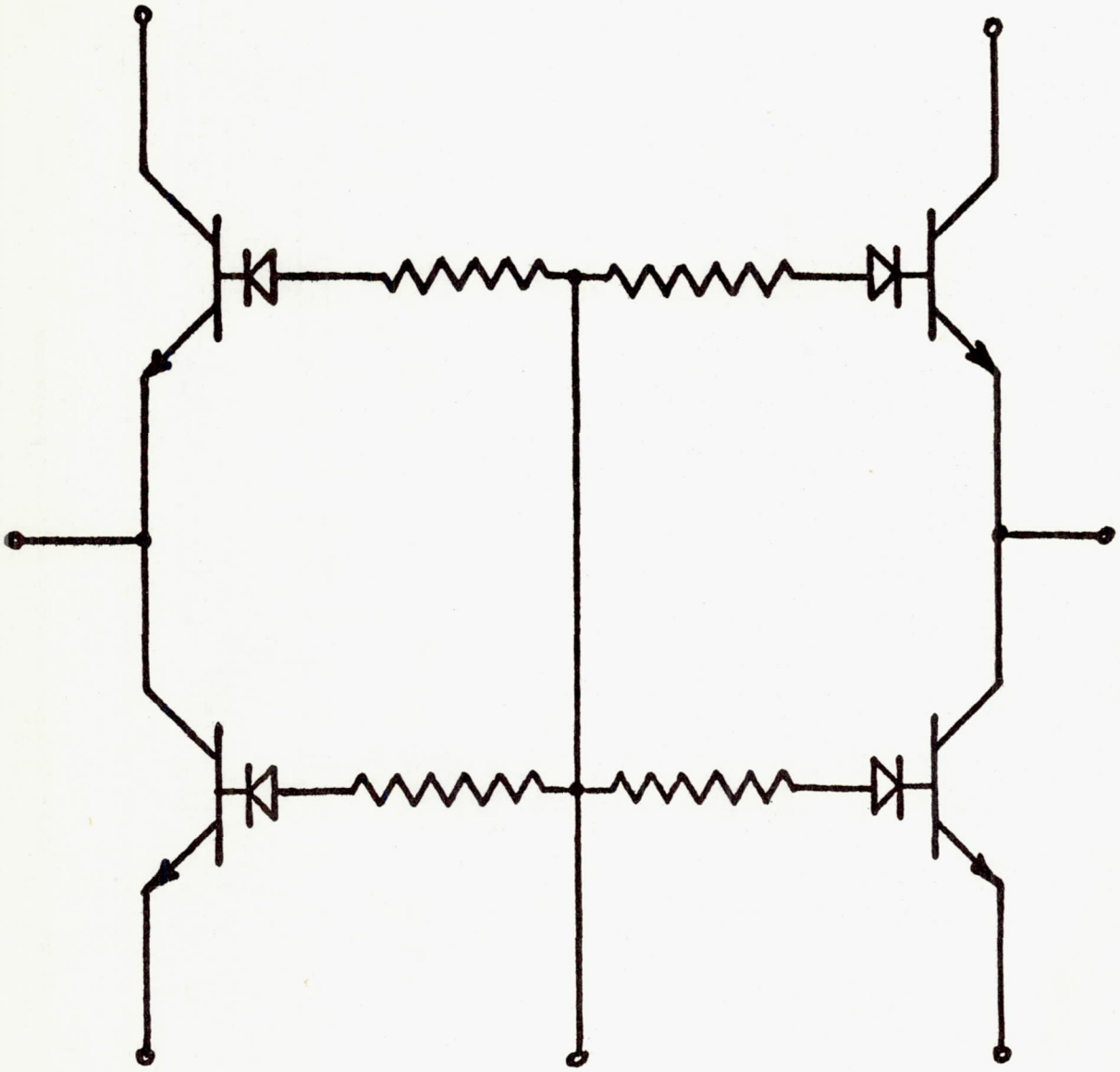

Figure 29.-- Quad-redundant pulse inverter sub-module

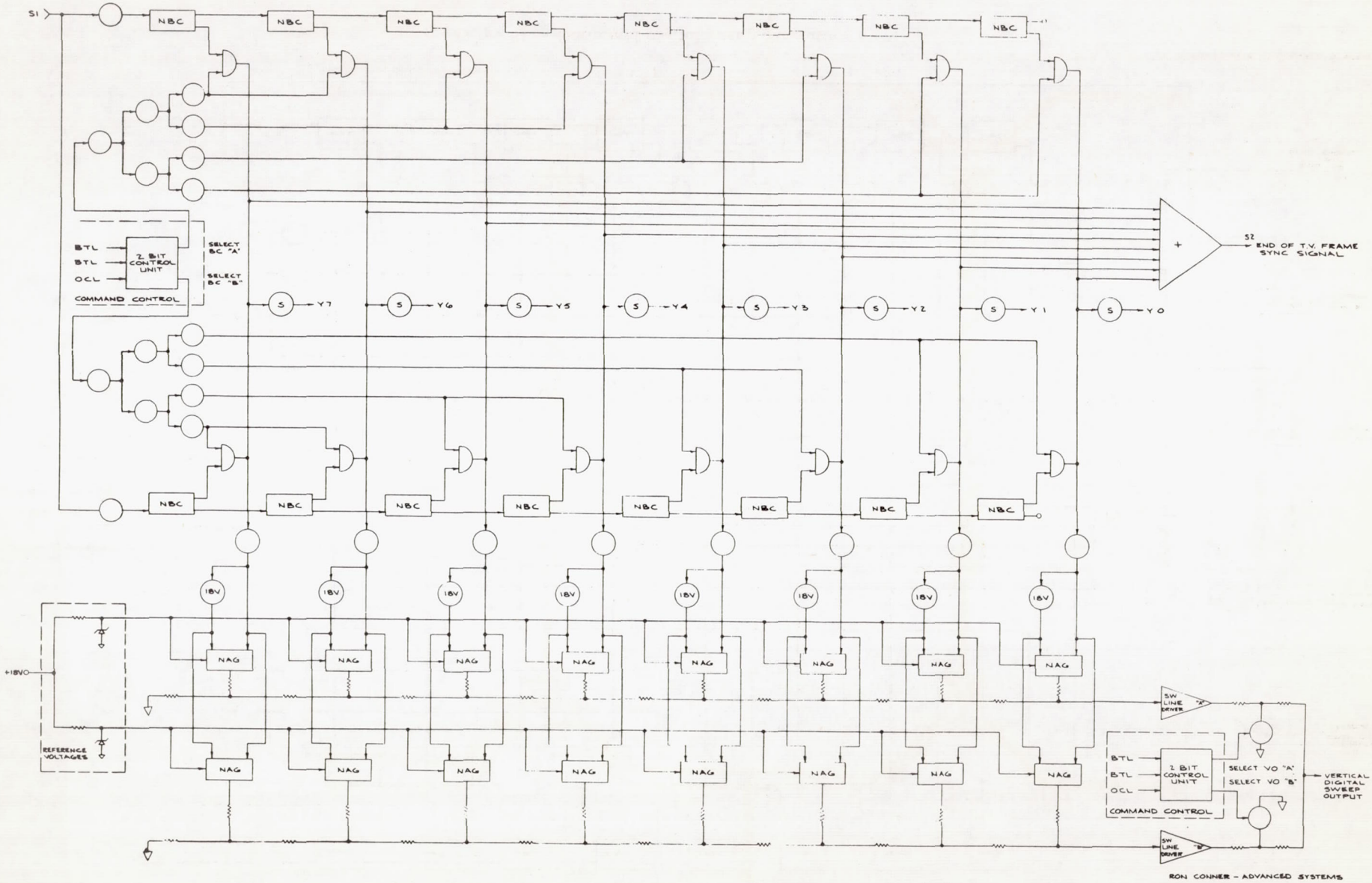

Figure 30.--Vertical digital sweep generator

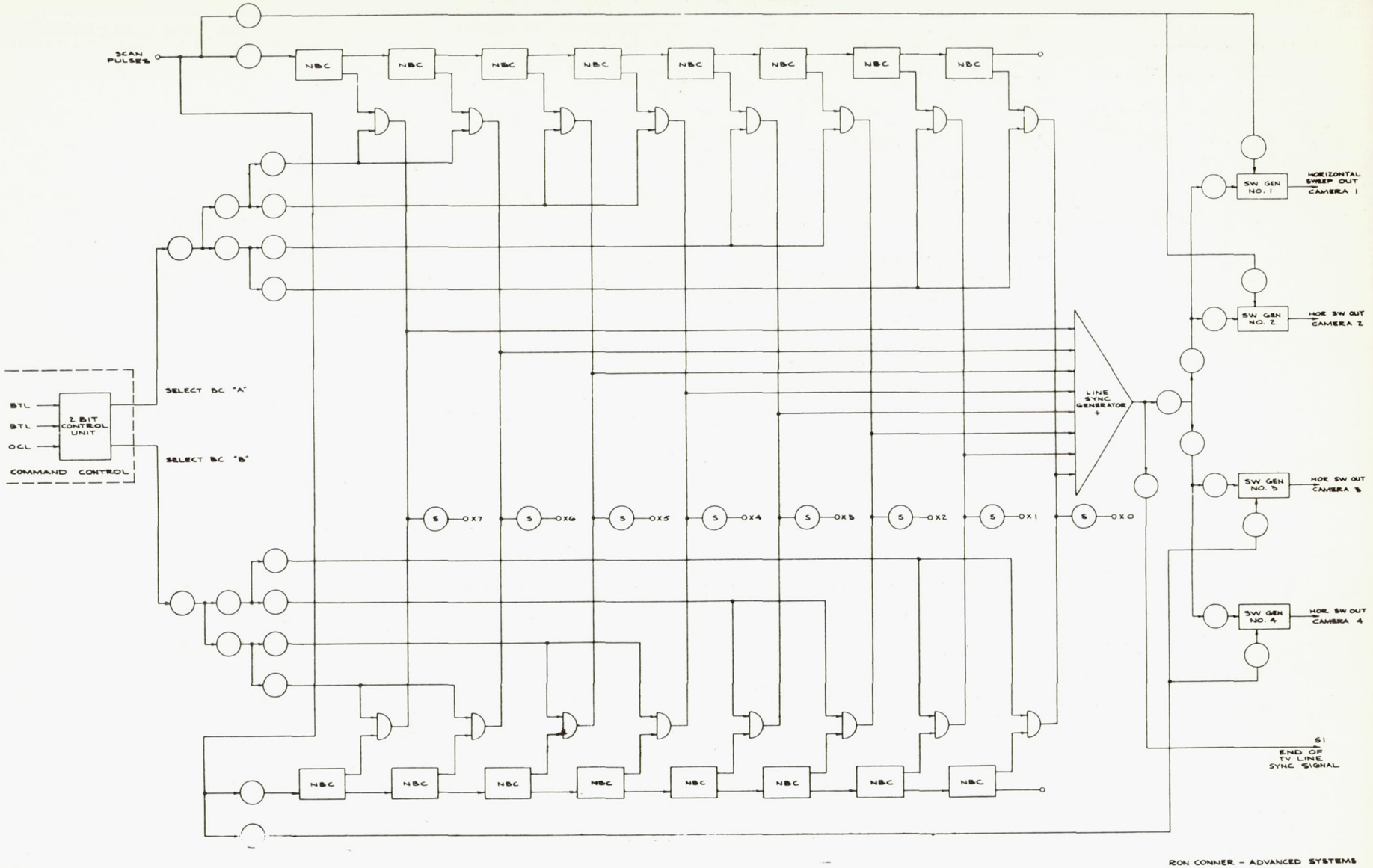

Figure 31. --Horizontal digital sweep generator

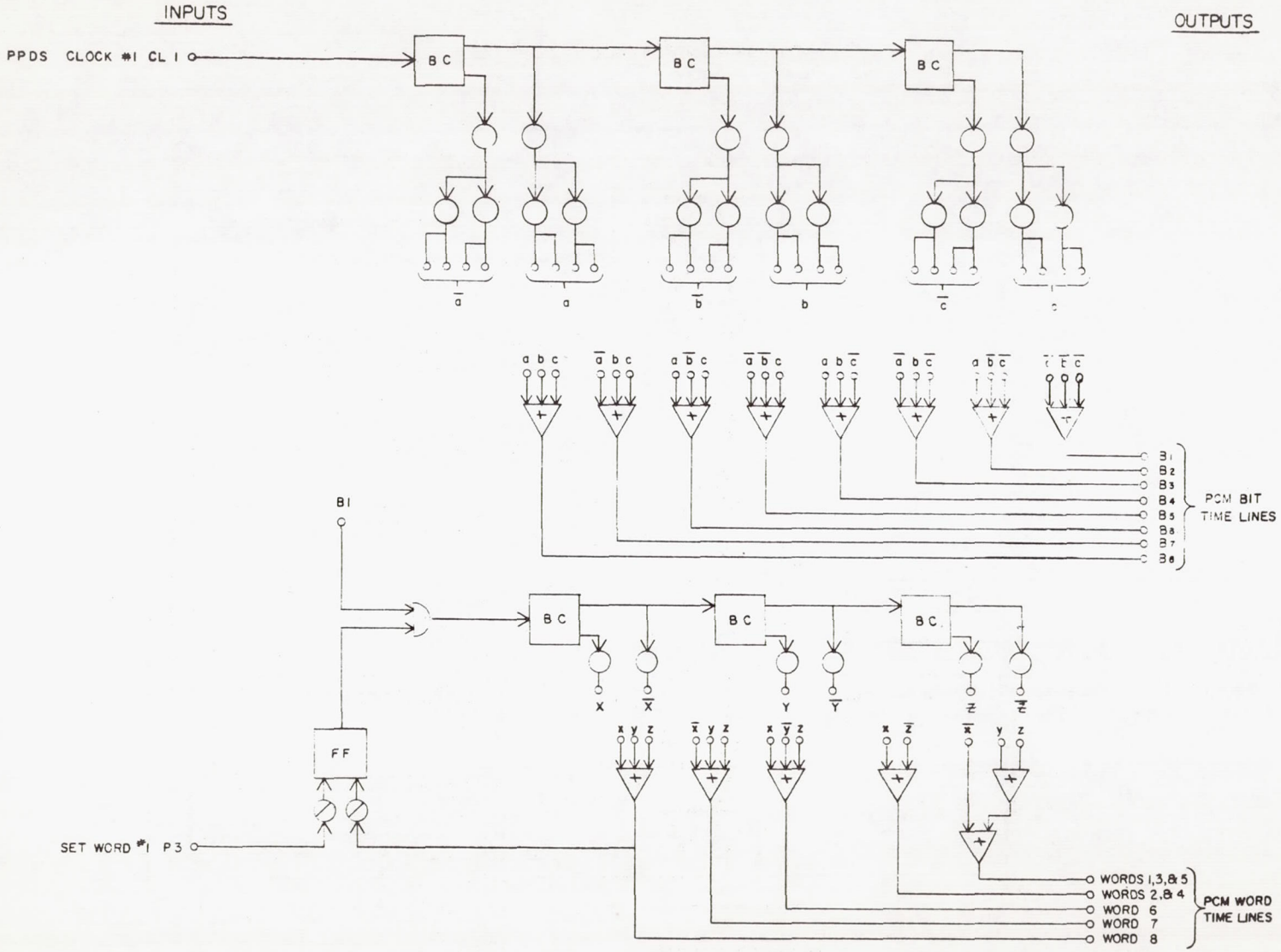

Figure 32. --PCM programmer

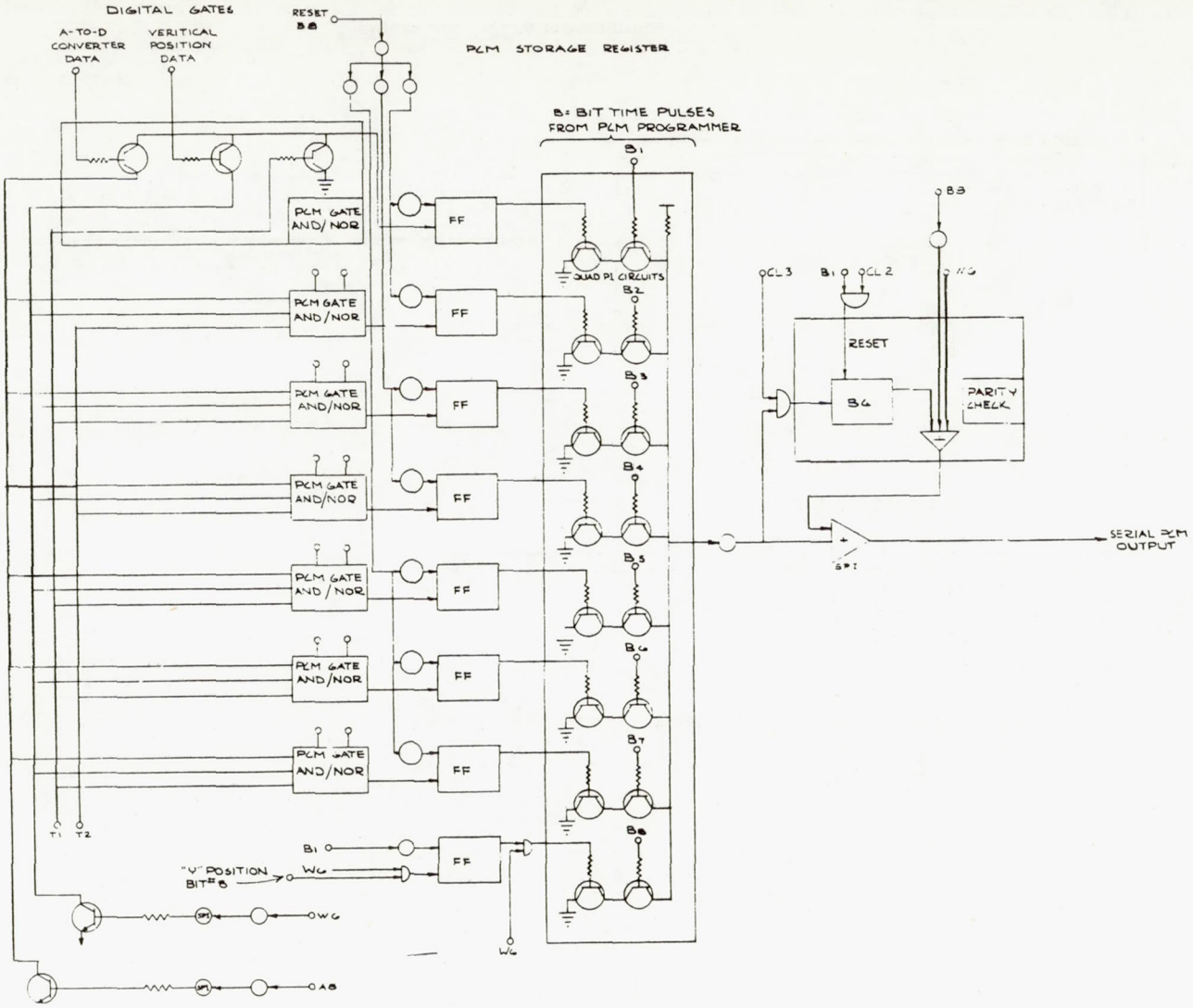

Figure 33.--PCM register and gates

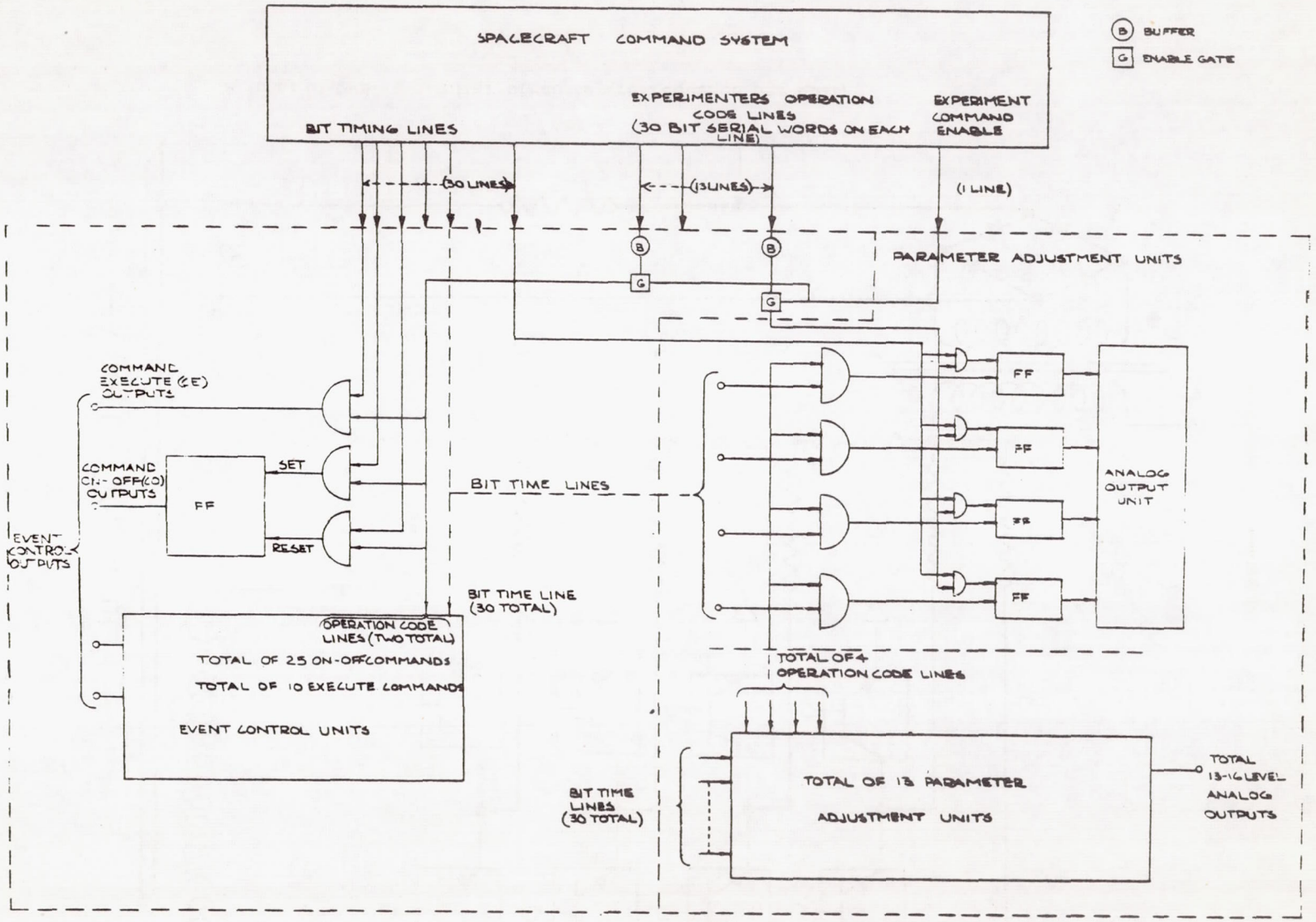

Figure 34.--Command and control unit

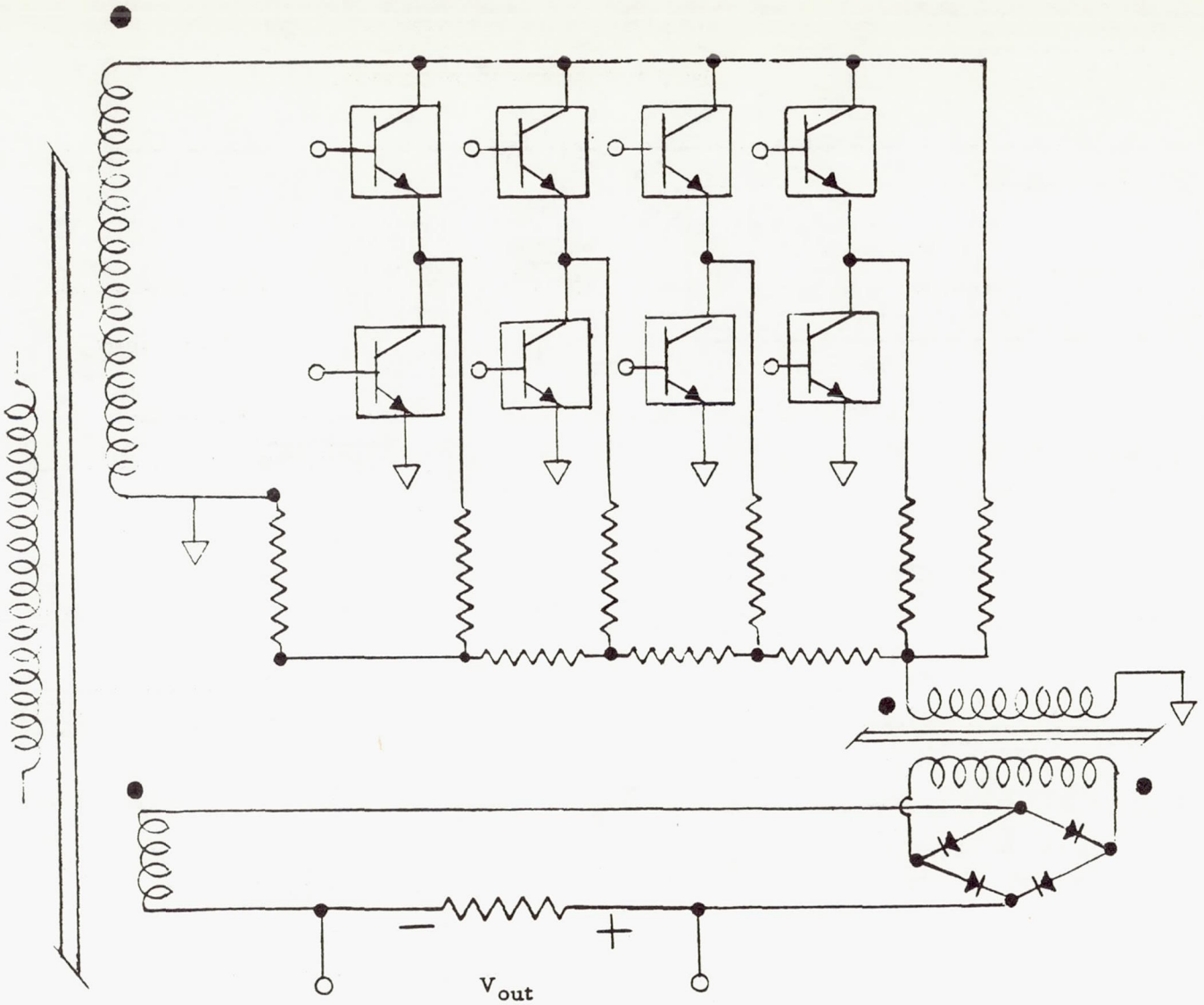

A total of twelve similar circuits are required per unit.

Figure 35.--Electronic analog adjustment unit

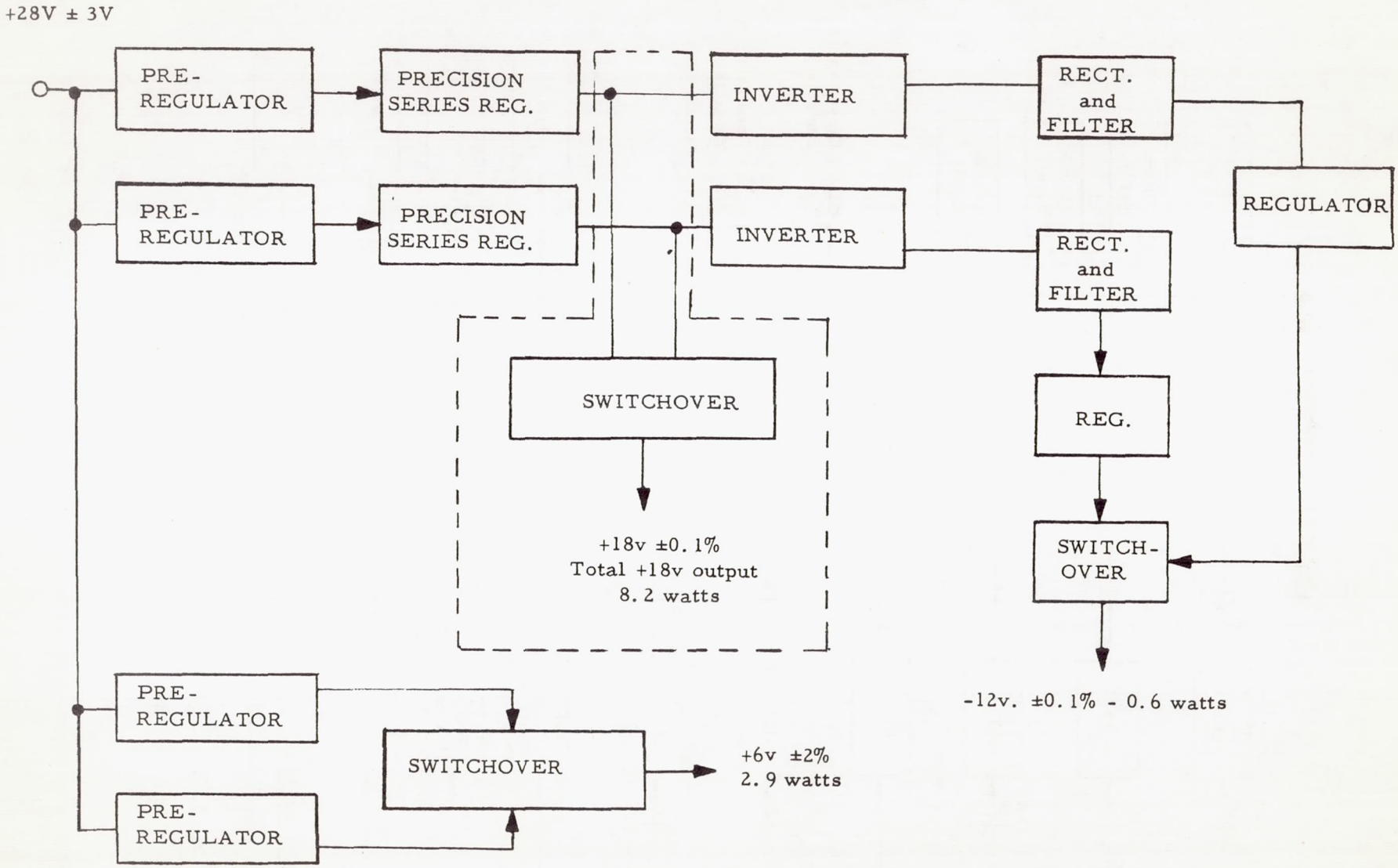

Figure 36.--Low-voltage power supplies

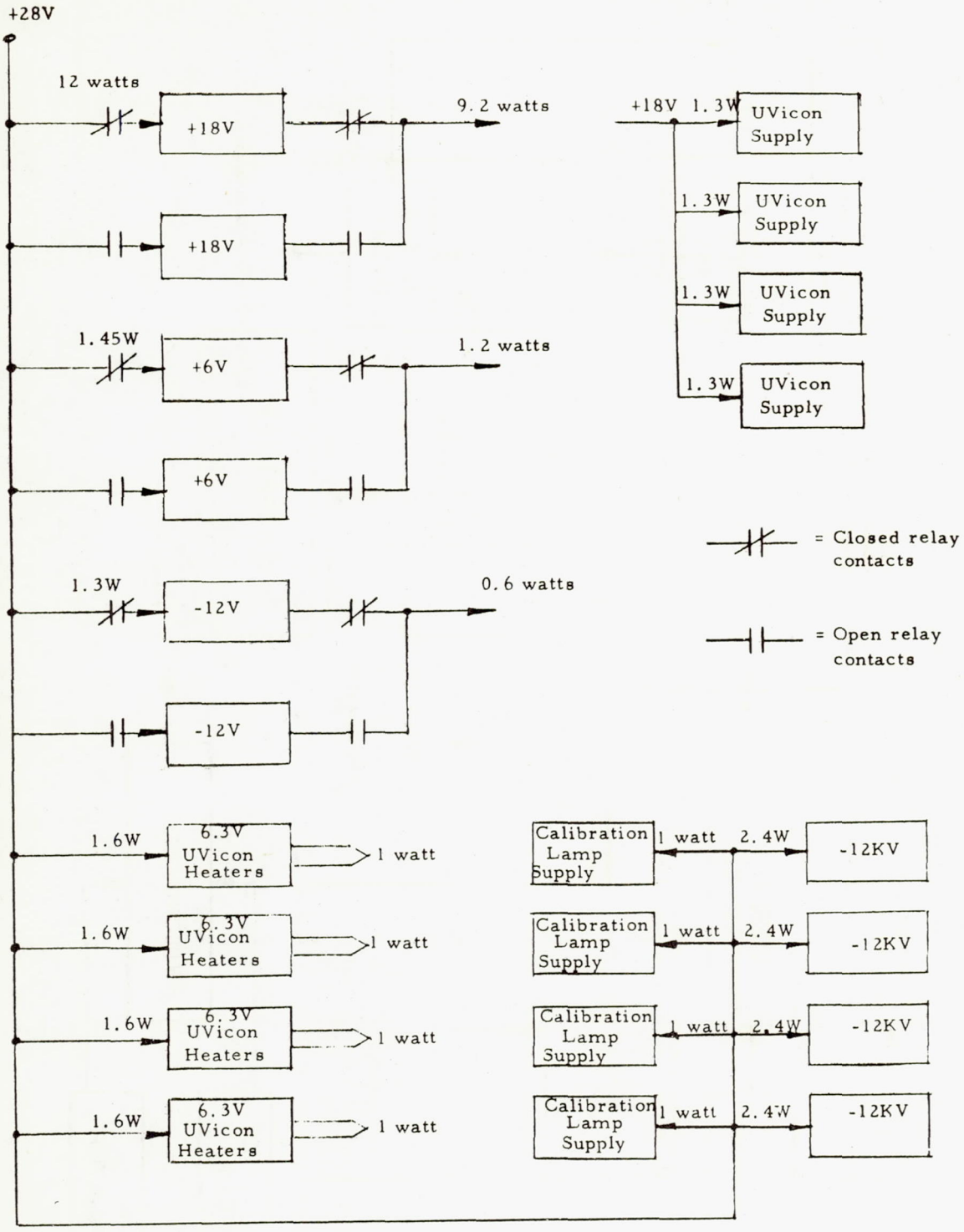

Figure 37.--Celescope power distribution

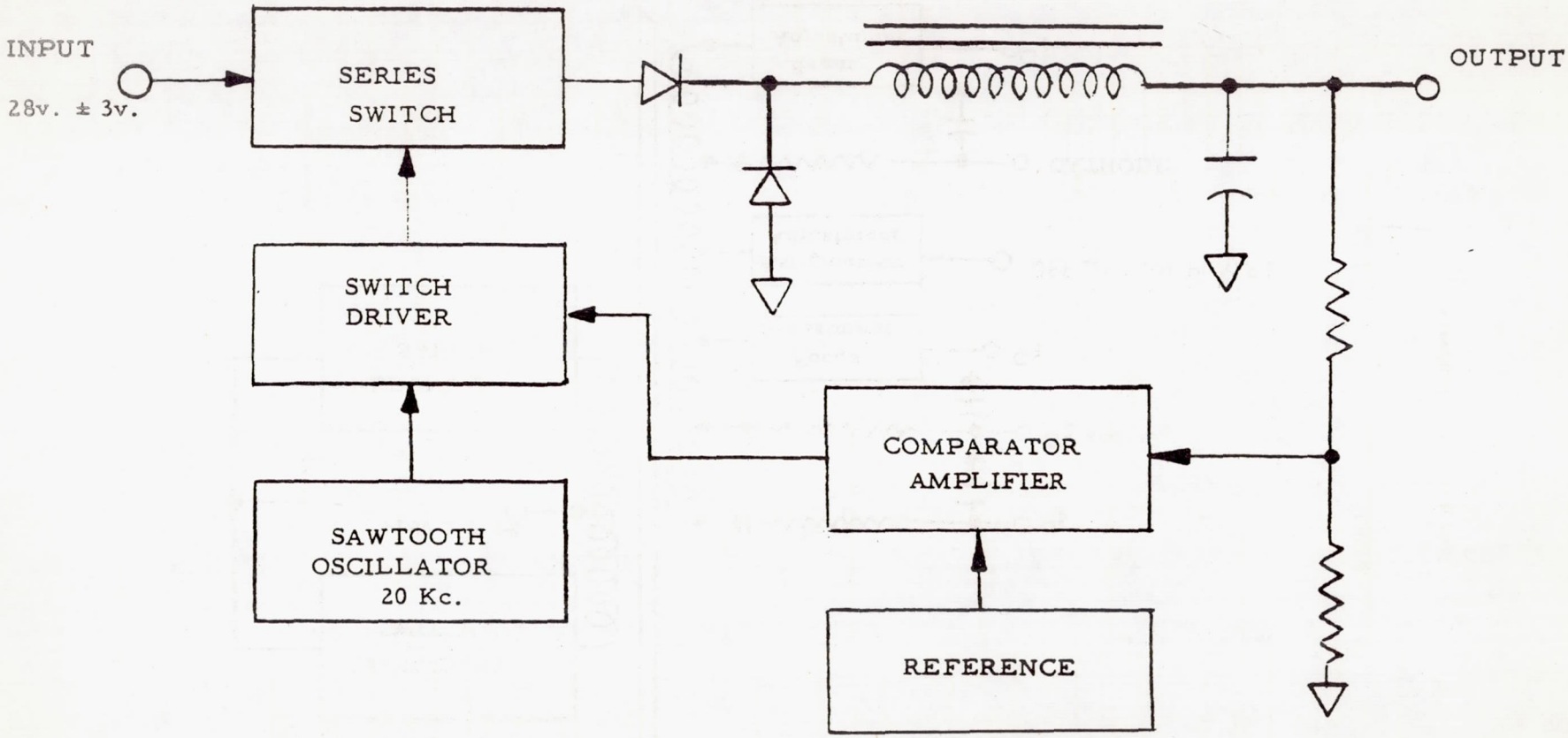

Figure 38.--Switching pre-regulator

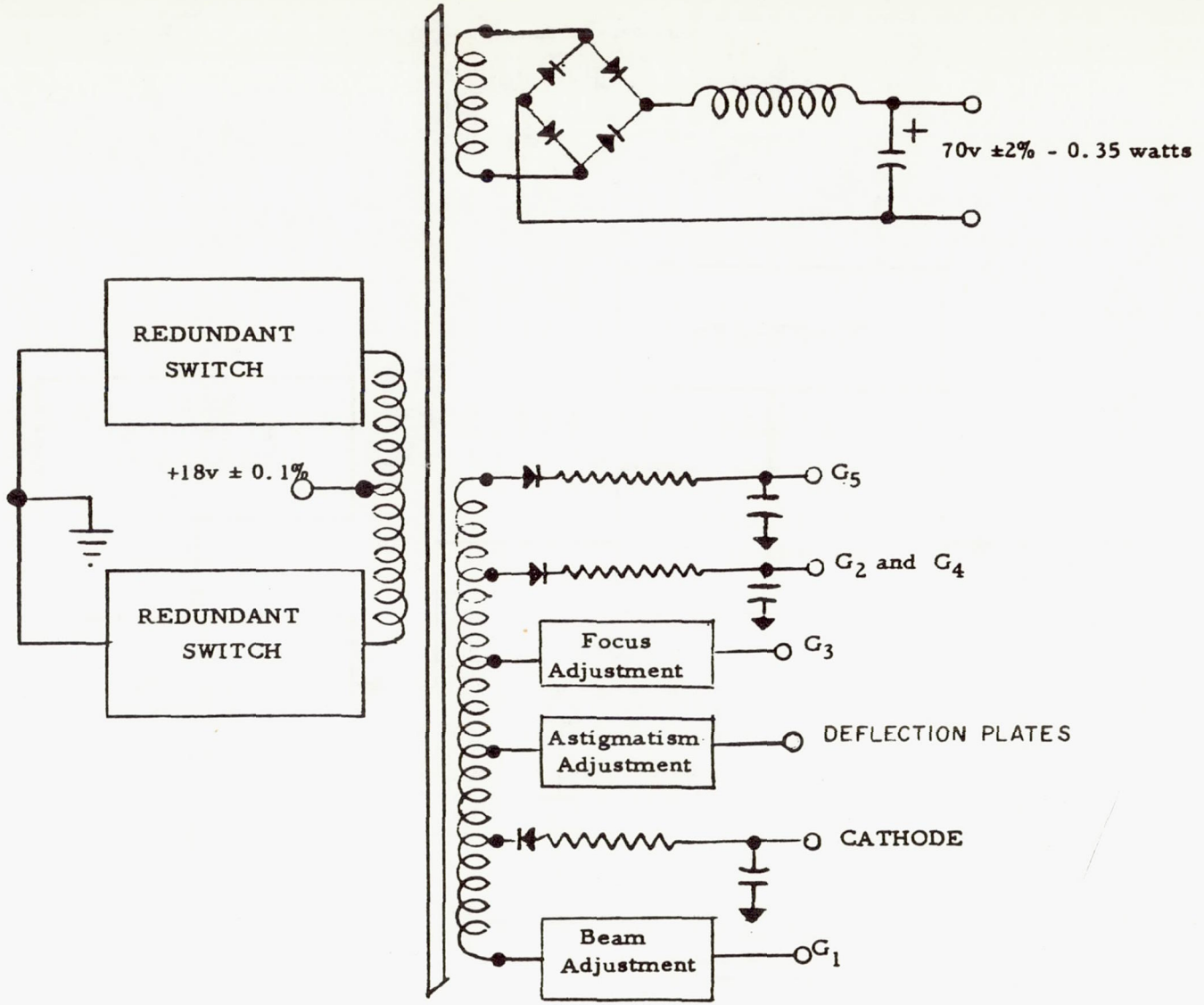

Figure 39.--Uvicon power supply

Circuit development work is continuing in order to achieve an optimum video pre-amplifier with good DC stability over the temperature range.

Several circuits have been investigated for the characteristics of (1) low noise; (2) gain; (3) bandwidth; and (4) bias stability. The most successful consists of a double stage followed by a triple. These two, in series, give a transconductance of about 10^{-7} mhos. The gain-bandwidth product is about 4×10^{12} cycle ohms sec^{-1}. The amplifier requires DC power supplies of +12 volts and -12 volts. Total power is about 50 milliwatts. The unit is designed for a maximum output voltage of about 10 volts and output bias of 0 volt.

Figure 40 is a schematic diagram of the double stage now being used as the pre-amplifier input. The triple stage is still in process of development.

The noise was estimated to be 6.6×10^{-10} amperes (10 c/s to 100 kc/s). We hope to improve this noise figure considerably.

The requirements of the video selector circuit are determined almost entirely by the output characteristics of the pre-amplifiers; therefore, no actual design work will be done in this area until the pre-amplifier design is relatively firm. At this time, however, we expect the selector circuit to be of the form illustrated in figure 41. The circuit consists of four parallel, common-base stages operating as gated current-amplifiers; this configuration was chosen to accommodate the large required dynamic range while minimizing the effects of base-emitter voltage variations.

The function of the analog horizontal sweep generator is to generate, in accordance with the control signals from the command control unit, a linear sweep voltage waveform with a period of 2 milliseconds. The important output parameters are sweep linearity and voltage stability, both of which have a tolerance of $\pm$ 1 percent of full scale. This unit includes switching circuitry for the purpose of selecting either the analog or digital horizontal sweep as input to the horizontal deflection amplifier, on command. A separate unit is used in conjunction with each uvicon camera to enhance system reliability. The circuit diagram is shown in figure 42.

The function of the analog vertical sweep generator is to generate a linear sweep voltage waveform with period of approximately 0.5 second. The operation of this unit, the schematic diagram of which appears in figure 43, is similar to the operation of the horizontal sweep generator. In the analog scan mode, the bistable circuit composed of Q7 and Q8 returns the sweep generator to its quiescent state after exactly one sweep, by driving PI3 into saturation. An output from the bistable circuit is routed to the horizontal generator for the same purpose.

During the uvicon polarization mode, the polarize command inhibits the action of the bistable circuit so that the sweeps are continuously generated until the polarize command is removed.

The Schmidt trigger circuit, composed of Q5 and Q6, is included to reset the bistable circuit on reception of each sweep start command.

The deflection amplifier is basically a differential amplifier having sufficient negative feedback to insure adequate stability; provisions have been made for centering, gain, and astigmatism adjustments by selection of bias resistors in accordance with the requirements of the particular uvicon used. Figure 44 is a preliminary schematic diagram of the deflection amplifier.

We will use a Cockroff-Walton type supply to generate the 12 000 volts required by the uvicon imaging section. Reliability and size were the main factors influencing this decision. In this supply a transistor inverter delivers a 2000-volt peak-to-peak square wave to an 8-stage Cockroff-Walton circuit. Because of the high efficiency of this circuit, we can use a 100-megohm divider accross this supply to deliver the correct voltages to the intermediate high-voltage electrodes of the uvicon. Use of a resistance near or below 100 megohms gives increased stability and reliability to the system.

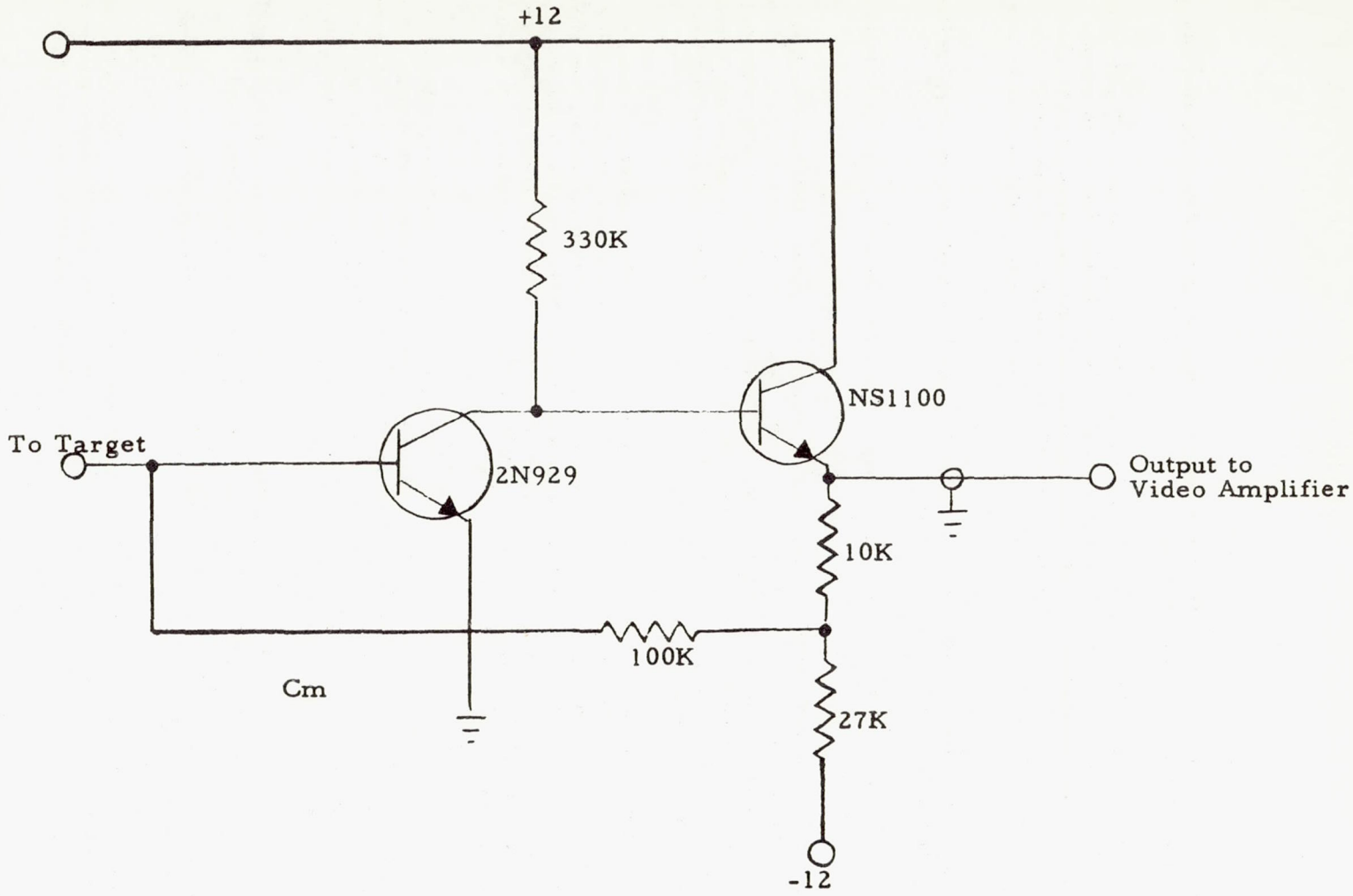

Figure 40.--Video pre-amplifier

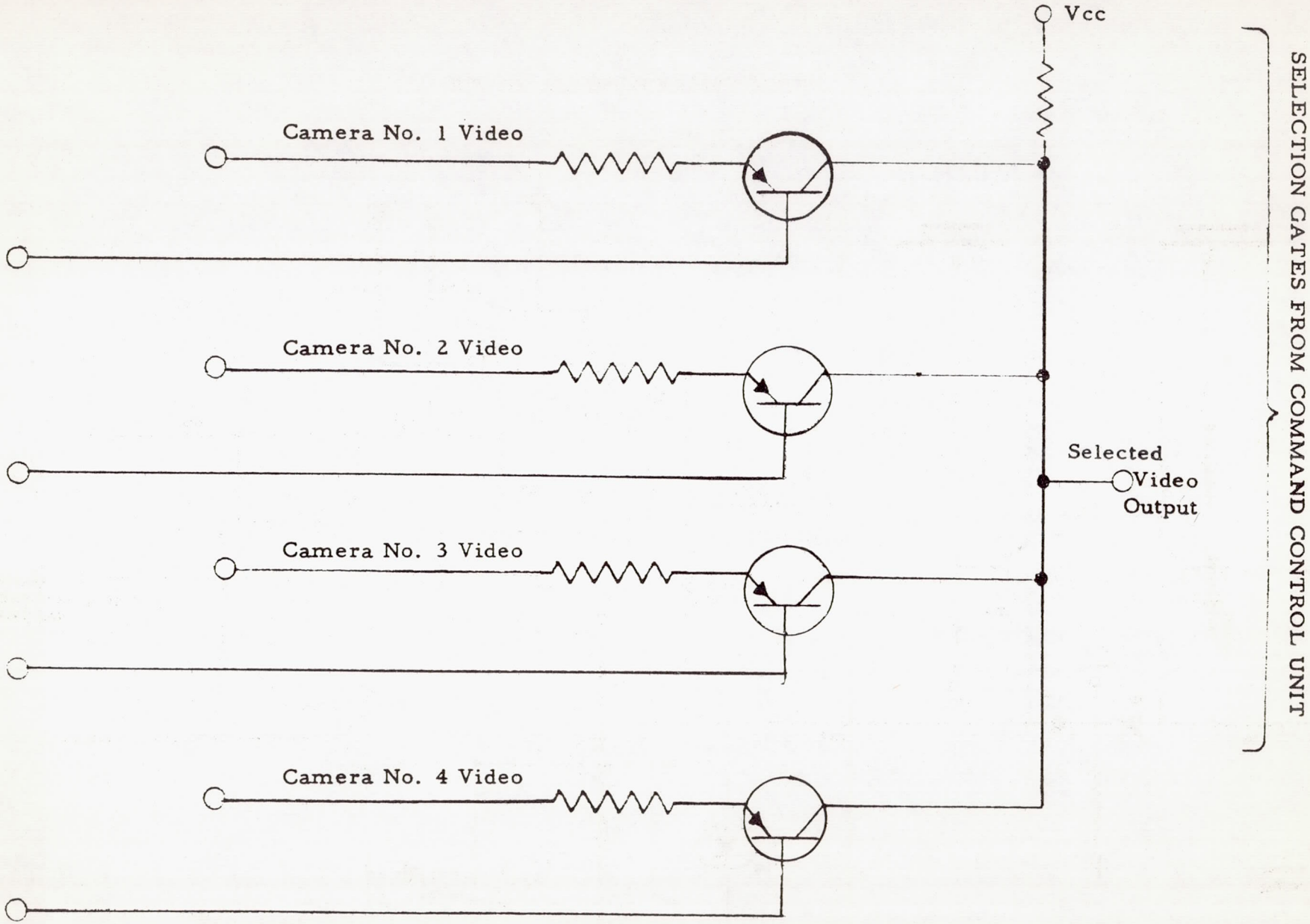

Figure 41.--Selector circuit

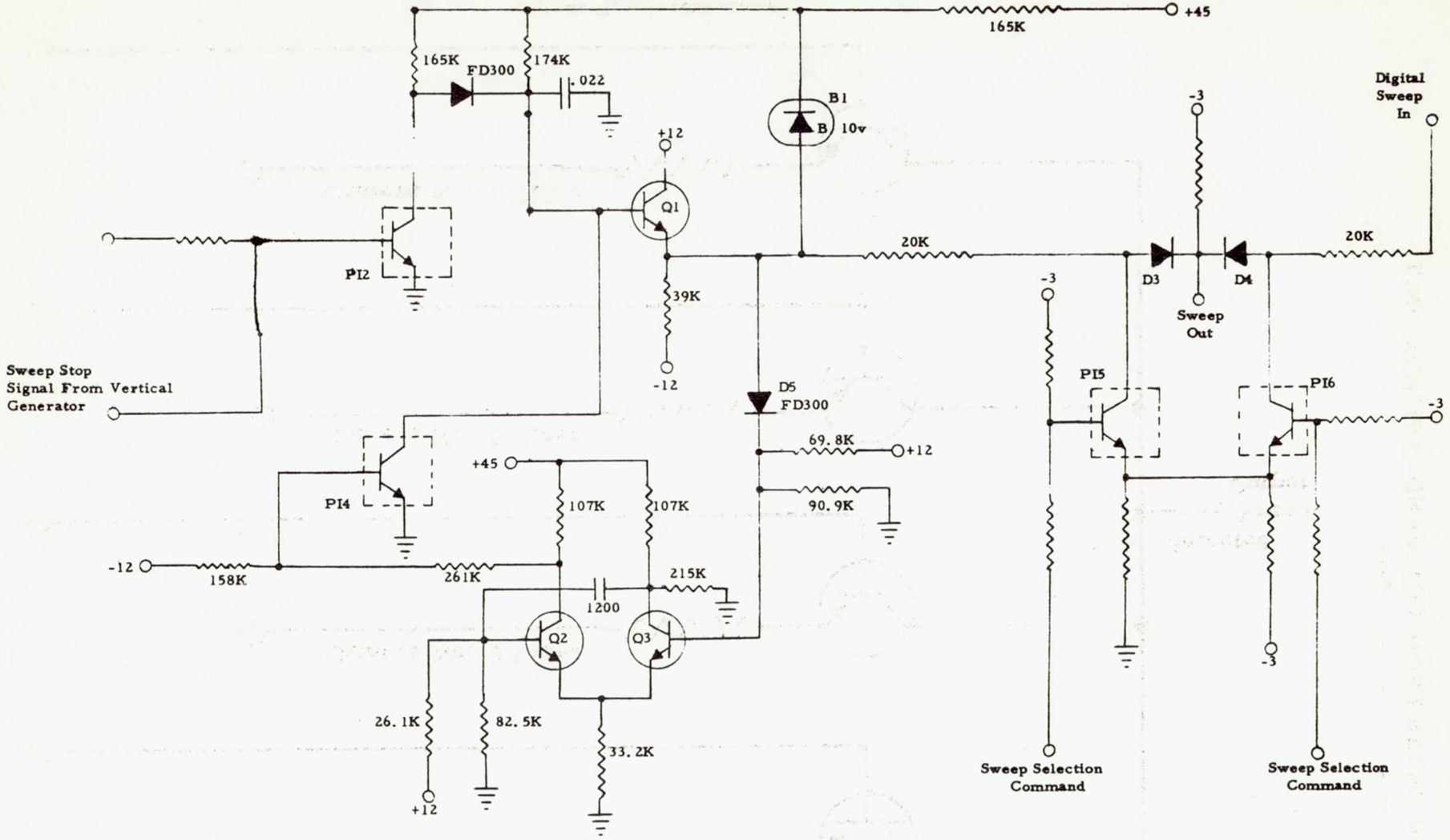

Figure 42.--Horizontal analog sweep generator

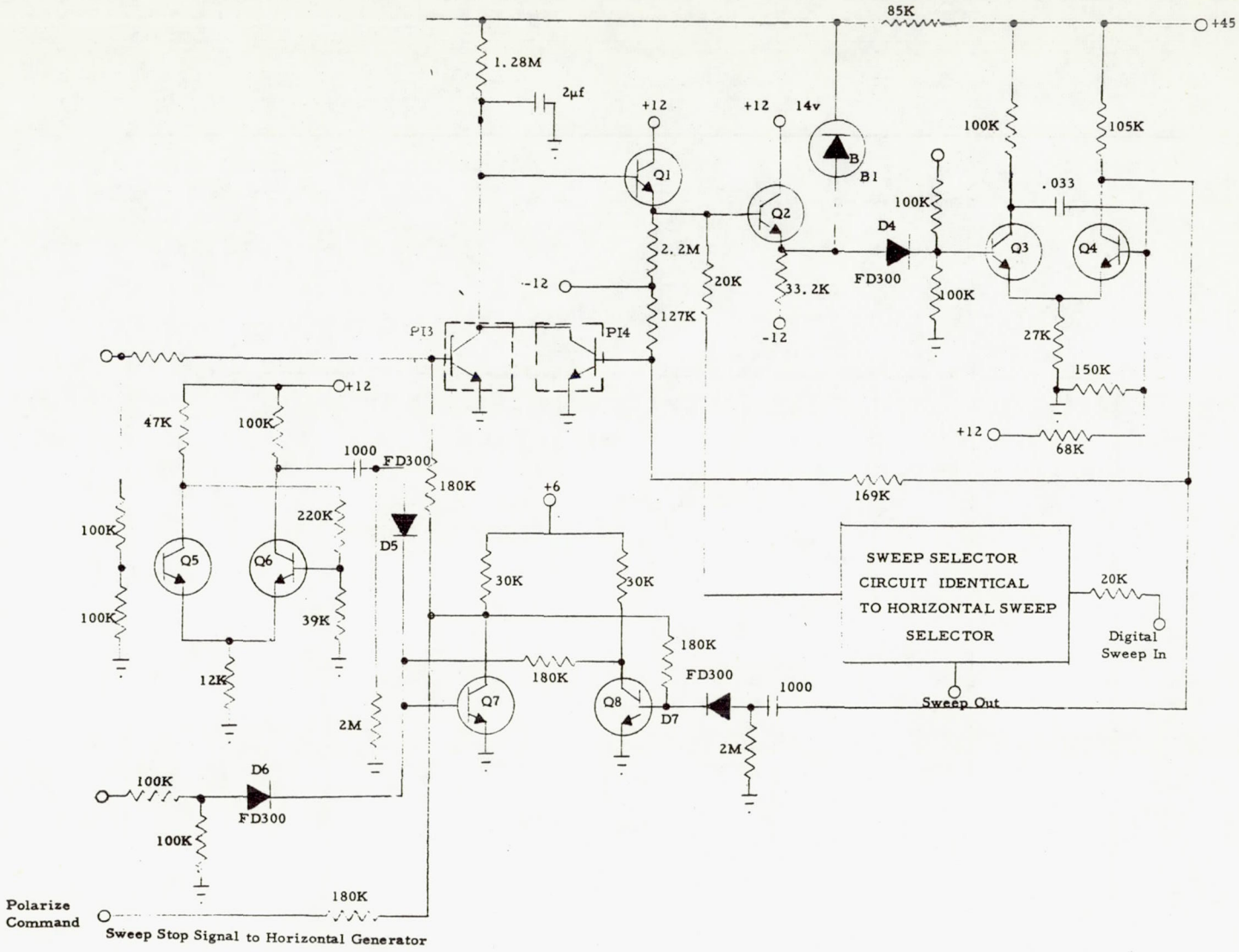

Figure 43. --Vertical analog sweep generator

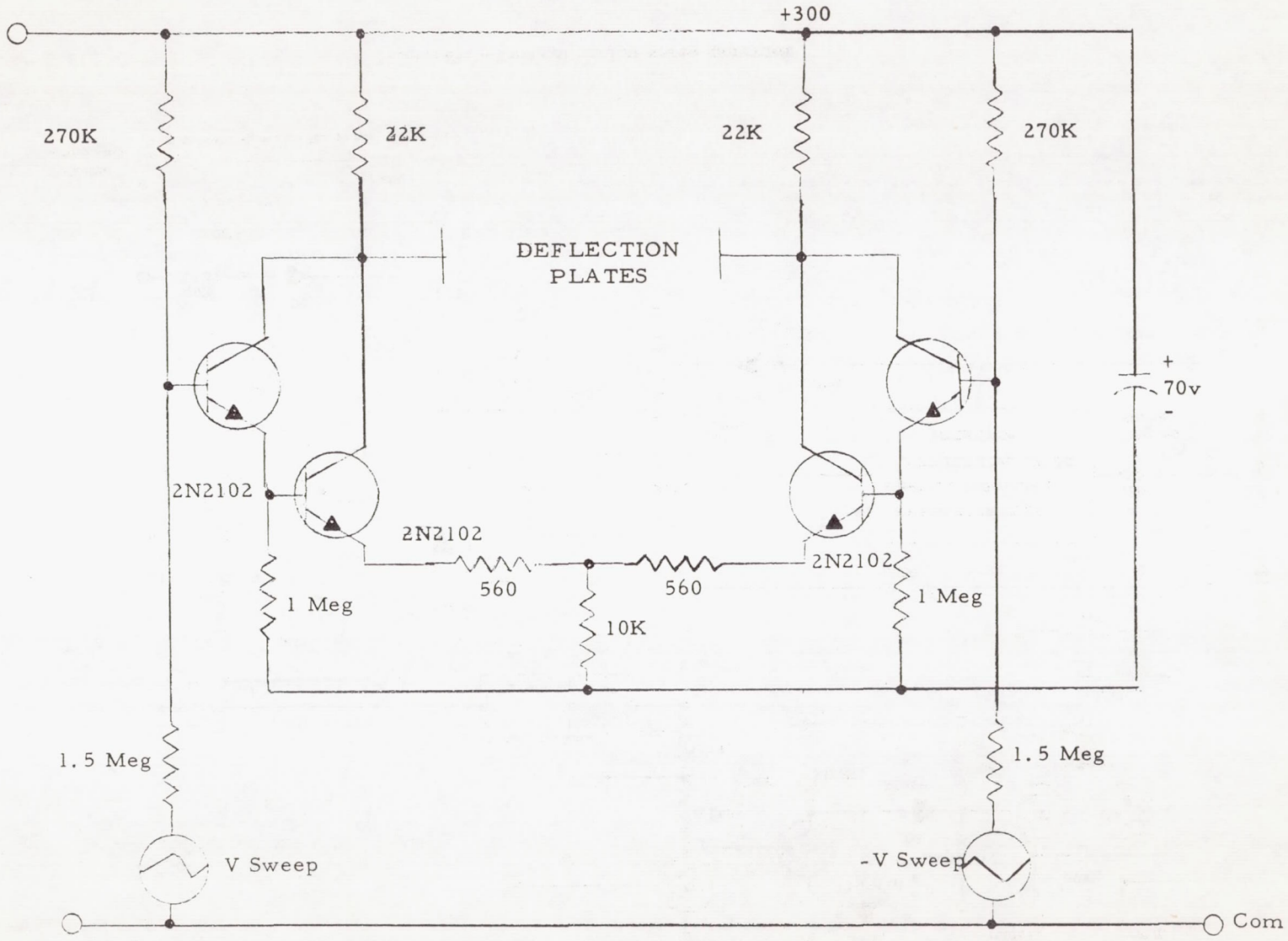

Figure 44. --Deflection amplifier

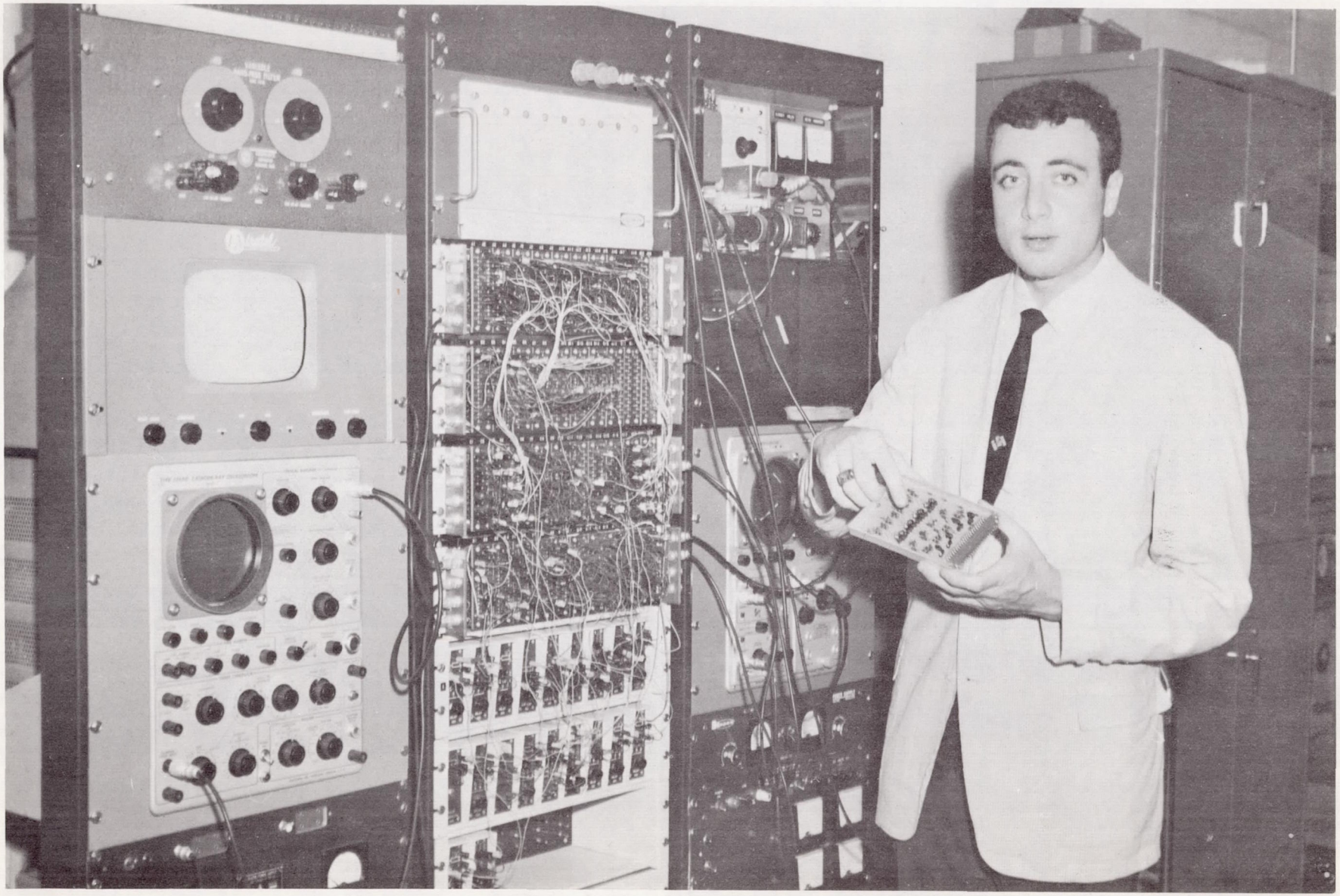

Figure 45.--Breadboard digital television system

In our electronics laboratory we have built a breadboard version of the digital television system. This model has demonstrated the feasibility of such a method. The input is an electrostatically scanned vidicon that can observe an artificial star field. It is scanned by the digital store mode. Figure 45 shows this breadboard equipment.

5. Reliability

Probably the most severe requirement that we have placed on the Celescope is that of reliability. Even with rather optimistic assumptions about the efficiency of our mapping operation, we will need about fourteen months to complete the survey. To give us a reasonable chance of fulfilling our objective, we require an expectation of 70 percent successful completion of our planned all-sky mapping.

We are attacking the problem of reliability on four fronts:

A. First comes the problem of redundant circuit design. The basic block for the digital portion of the system is the redundant pulse-inverter sub-module, shown in figure 29. A resistor sub-module, consisting of four resistors in parallel, is used in conjunction with the PI sub-module. The question of analog circuit redundancy was solved by designing redundant systems rather than redundant sub-modules. This problem of system redundance affects even the optical design of the Celescope: we are using split filters in front of each uvicon to insure that failure of one camera or telescope system will not prevent acquisition of any portion of the data.

B. Second is the problem of procuring high-quality components having small, predictable failure rates. For example, Electro-Mechanical Research is testing incoming semi-conductors for poor hermetic seals by additional detergent or helium leak tests in conjunction with temperature cycling tests. Foreign particles are detected by vibration test with the transistor operating. A burn-in test with readings of critical parameters before and after burn-in detects units that exhibit abnormal parameter drifts and helps eliminate infant mortality failures. Optimum burn-in time varies with the particular device and ranges from 10 to 500 hours. Similar techniques are being used in the procurement of other components. The failure rates of the basic electronic components to be used in Celescope are given in Table 6.

For these components the failure rate is independent of whether the system is on or off, since our reliability engineering requires that every component be operated far below its rated capacity. The probability of failure of a component after time t is

$$p = 1 - e^{-\lambda t},$$

where λ is the failure rate.

For the PI sub-module, a "component" is considered to be a transistor with a series resistor and diode in its base lead. For this configuration the failure rate of the "component" is

Quantity	Part type	Failure rate
1	Transistor, small signal	17×10^{-8} hr^{-1}
1	Resistor, metal film	5×10^{-8}
1	Diode, logic application	10×10^{-8}
		$\lambda = 32 \times 10^{-8}$ hr^{-1}

Table 6. Failure rates for Celescope components

Part type	Failure Rate (λ)	λt for 18 000 hours *
Capacitor, glass	1×10^{-8}	18×10^{-5}
Capacitor, paper	1×10^{-8}	18×10^{-5}
Capacitor-solid tantalum	2×10^{-8} **	30×10^{-5}
Capacitor-ceramic, feed-thru	5×10^{-8}	90×10^{-5}
Resistor, metal film	5×10^{-8}	90×10^{-5}
Resistor, carbon film	8×10^{-8}	144×10^{-5}
Transistor, silicon, small signal, NPN	17×10^{-8}	306×10^{-5}
Transistor, silicon, small signal, PNP	17×10^{-8}	306×10^{-5}
Transistor, power, NPN	29×10^{-8}	522×10^{-5}
Transistor, unijunction	10×10^{-8} **	180×10^{-5}
Diode, logic application	10×10^{-8}	180×10^{-5}
Diode, general purpose	22×10^{-8}	396×10^{-5}
Diode, zener reference	25×10^{-8}	450×10^{-5}
Diode, fast switching	0.2×10^{-8} **	3.6×10^{-5}
Inductor	100×10^{-8}	1200×10^{-5}
Transformer, power	100×10^{-8}	1200×10^{-5}
Transformer, pulse	60×10^{-8}	1080×10^{-5}
Resistor, wirewound	100×10^{-8}	1800×10^{-5}

* λt and probability of failure for 18 000 hours do not differ significantly for these magnitudes of λt. However, in calculating the probability of failure for the entire system, larger values of λt are encountered, and the difference does become significant (i.e., for values of λt greater than 0.01). For this reason λt will be used in the subsystem analyses.

** Minuteman Part Type

In the redundant quad configuration the probability of failure of the PI sub-module is

$$p_{PI} = 2p^2$$

For an 18 000-hour lifetime, $p_{PI} = 4.41 \times 10^{-5}$. Similarly, the probability of failure of a resistor sub-module is found to be $p_R = 0.33 \times 10^{-5}$. Since the failure of either a resistor sub-module or a PI sub-module constitutes circuit failure, the probability of failure of the basic building block of the digital portion of the system is $P = p_{PI} + p_R = 4.8 \times 10^{-5}$.

There are, unfortunately, a number of key components for which we as yet have no information concerning failure rate. The situation is further complicated because these components are subject to gradual deterioration as well as to catastrophic failure. They include the uvicons, the calibration lamps, and the structural and optical components.

Westinghouse has been pursuing an accelerated life-test program for the uvicon. To date no uvicon has failed in life test, although some of the tubes have been subjected to the equivalent of more than one year in orbit. It is, however, too new a device to permit applying the statistical results of such tests toward determination of the failure rate. Lacking a really firm figure on the reliability of this component, we must therefore rely instead on careful inspection and test of the tubes to be installed in the flight-model Celescope. We face a similar situation with the ASCOP calibrator lamps.

The deterioration rate of the nonelectronic components will be determined from the environmental test program and from available information on the behavior of materials in space. NASA is paying special attention to ultraviolet-reflective optical coatings.

C. Third, we compute the probability of success of the experiment from the failure rates of its various components, and from the criteria for success given in figure 46. The slewing order, the operating program, and the Celescope design have interacting effects on the probability of success, and have been chosen with the purpose of maximizing this probability. The results of the reliability computation are fed back into the design and planning of the Celescope equipment.

Table 7 gives the present reliability assignment to the various units required for proper operation of the Celescope as a percent probability of failure for 18 000 hours (i.e., one year of test and one year in orbit).

Table 7. Reliability assignment for Celescope units

Circuit		Percent probability of failure for 18 000 hours
a)	Camera unit	74.0 %
b)	Low-voltage power supply	14.0
c)	Threshold circuit	4.06
d)	Digital sweeps	12.8
e)	PCM register and gates	0.45
f)	PCM programmer	0.51
g)	Digital TV programmer	0.33
h)	Analog-to-digital converter	11.3
i)	Command and control unit	1.98
j)	Sync code generator	0.03
k)	Video selector	2.97

Our present assessment of the reliability of the Celescope under the primary and various failure modes of operation is given in Table 8.

Table 8. Probability of success of Celescope for 18 000 hours' lifetime

Operating Mode	Number of cameras operating				
	1 or more	2 or more	3 or more	4	1 or more of each type
Digital-direct	.48	.25	.05	.00	.16
Digital-store	.47	.24	.05	.00	.16
Analog-direct	.67	.32	.08	.00	.24
1 or more mode	.67	.32	.08	.00	.24
1 or more digital mode	.48	.25	.05	.00	.16
All 3 modes	.46	.24	.05	.00	.16

D. Fourth, we maintain a strong quality-control program of inspection and test to guard against failures in junctions, etc., caused by faulty workmanship.

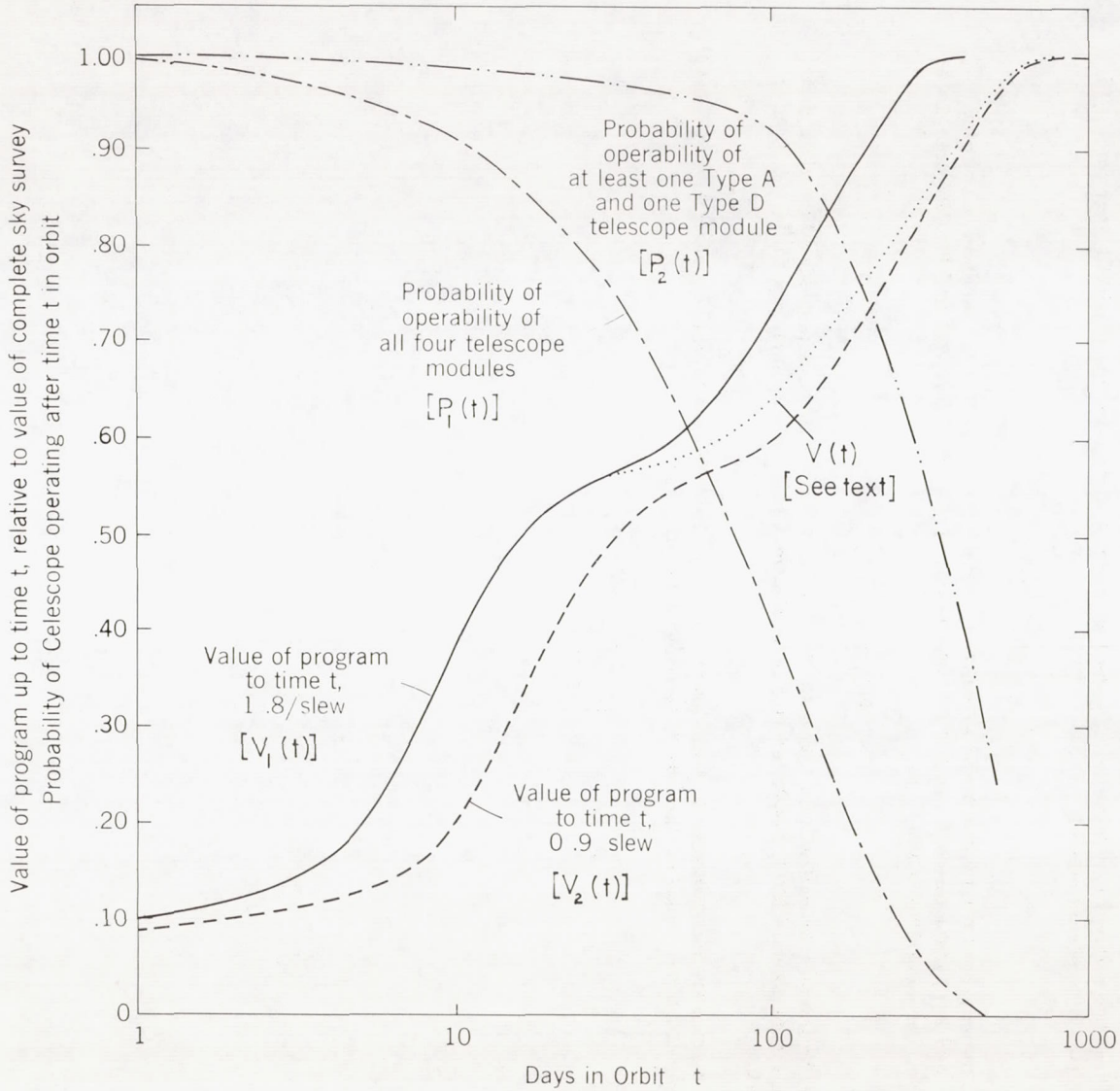

Figure 46. --Criteria for success of Celescope

Figure 46 denotes, as well as is possible in firm mathematical form, our subjective evaluation of the relationship between the value of the experiment and the fraction of the sky mapped. The fraction of the sky mapped before the first telescope module fails is, of course, proportional to the length of time before that failure. After that time the sky is mapped at half this rate until two telescopes of the same type have failed. For mathematical purposes, the experiment is then considered to be terminated.

The two stages of operation as defined above are characterized by two distinct probabilistic survival curves. These two survival curves are related and together they determine the expected final value. The basic definition of expected value is

$$\bar{V} = \int_0^{\infty} V(t)dP(t) .$$

Here, $\bar{V}$ is the expected final value of the experiment, $V(t)$ is the value that the program has attained by time t, and $P(t)$ is the survival curve of the equipment. Figure 46 shows $V(t)$ and $P(t)$ for both stages of operation. As mentioned above,

$$P(t) = 1 - e^{-t}.$$

As is indicated schematically in figure 46, the $V(t)$ curve has a shape dependent on the time that the first telescope module fails; the dotted line indicates the $V(t)$ curve for such first failure at 30 days after launch.

After extensive manipulation to formulate the exact probabilistic connection between the two stages in mathematical terms, final evaluation of the above integral gives

$$\boxed{\bar{V} = 87\%.}$$

IV. Requirements on Spacecraft

1. Optical System

The aperture stop of the optical system -- 12 inches -- is at the primary mirror, near station 100 at the center of the spacecraft. To keep the system free from vignetting, the clear aperture must increase by 6 inches for each 100 inches of distance from the stop. At the secondary, the aperture must be 13.5 inches, and at station 158.25 -- the end of the optical "can" -- it must be 15.5 inches. The aperture at the radiation shield, 40 inches from the primary mirror, must be 14.5 inches. These openings must be centered over each primary mirror. The configuration of the radiation shield is shown in figure 24.

The nominal resolving power of the detector, operating at 128 line-pairs per 1.2 inches, is about 1!.5 of arc. Each of the other sources of blurring -- optical aberrations, decentration of the optical components, and image motion -- should individually be kept to 30" of arc or less. Since the maximum anticipated exposure is one minute, our requirement for spacecraft stability is $\pm$ 15" of arc for one minute of time. Since Celescope will not generate an error signal, this degree of stability must be maintained by the coarse control system of the spacecraft. (See below.)

2. Mechanical System

See the discussion in Section III.3., and figure 24.

The center of gravity lies on the roll axis, near station 110.

The electronic equipment in Bay E-4 will occupy a space approximately 21.5 x 12.75 x 6 inches.

3. Thermal Requirements

Each uvicon case will radiate approximately 1.5 watts with little fluctuation due to thermal damping inside the case. The spacecraft structure is insulated from this heat source by insulation around each telescope module and by the radiation shield. About 1.25 BTU per hour are transmitted from Electronic Bay E-4 into each telescope module along the shielded electronic cabling.

We expect the temperature of the experiment container to be the same as that of the spacecraft structure, -30° $\pm$ 15° C. The telescope modules are isolated from this structure, and by radiation to space will be about 10° cooler. The uvicon cases, containing a 1.3-watt heat source, will be about the same temperature as the spacecraft structure. The temperature within Electronic Bay E-4 is expected to be between +35° F and +135° F.

The electronic equipment in Bay E-4 will dissipate a nearly constant power of 16.5 watts.

4. Control Requirements

As mentioned above, the coarse control system of the spacecraft must be able to maintain stability of the optic axis of $\pm$15" of arc for one minute of time.

The 256 x 256-element raster we plan to use in the Celescope corresponds to a resolution of 1!.5 of arc. No other source of blurring should exceed one-third of this value, or 30" of arc. As is indicated in figure 26, we plan to use 60-second exposures, and therefore require spacecraft stability of $\pm$15" of arc for 60^s of time. Even longer times of stable control would be desirable, to allow us long exposures on objects of special interest.

The basic Celescope experiment has no absolute a priori requirement for accurate knowledge of the position of the optic axis. We do require that adjacent positions be separated by 1°.8 ± 0°.1 about one of the two major axes perpendicular to the optic axis. The experiment can become nearly 90 percent efficient if we know the starting position to within 1°, and approaches 50 percent or somewhat lower efficiency if our control of the starting position is in error by more than 10°.

In most parts of the sky, a map 1°.8 x 7°.2 should be sufficient to determine unambiguously the direction, but the reduction would be extremely difficult. The finder television to be installed as part of the spacecraft will make this a posteriori positional reduction much faster and easier, should the positional control system aboard the spacecraft fail.

The Celescope will not provide an error signal to the spacecraft's fine control system. Should the control system fail, but we still have manual ground control over the inertia wheels and inertia dumping mechanism, we could complete our mapping by stabilizing the television picture at the beginning of each pass and slewing a controlled number of coarse-wheel turns between positions.

5. Power Requirements

Unless we are to reduce our reliability and thermal stability by routine use of the main power switch to Celescope, we require an average power of 22.5 watts. Our peak power occurs during the calibration exposures and amounts to 35 watts.

Figure 47 shows the routine cycle of power consumption.

6. Slewing Requirements

We are now planning on an average of three 1°.8-slews per orbit. If the spacecraft control system requires more than 60 seconds to slew and restabilize, we cannot meet this average. Nor can we meet it if we cannot slew four times during passes longer than eight minutes, since some passes will be long enough for only two slews.

7. Data-handling Capability

Section I.4 gave the number of stars we expect to observe. In the digital-store mode, each of these stars will be displayed as a number of 25-bit words -- on the average, six words for each star. In the event of failure of Celescope's digital-direct mode or of the wide-band transmitter, we would plan to store all information obtained during a single slew operation for later readout and transmission to the ground. The maximum expected number of words to be stored during such an operation is 1700 words per telescope, for a total of 6800 words, or 170 000 bits. Only for about 6 percent of the slews, however, do we expect the need for storing more than 100 000 bits. We know in advance those few regions where this will be necessary; we will be able to modify the program for those regions to include an additional read-out between scanning the second and third camera. The maximum number of unloadings required for Celescope will be eight per orbit.

Each digital-direct scan will contain 65 536 eight-bit words. To fit the 62-kilocycle/second band-width of the wide-band transmitter, the scan will require 10.5 seconds per telescope.

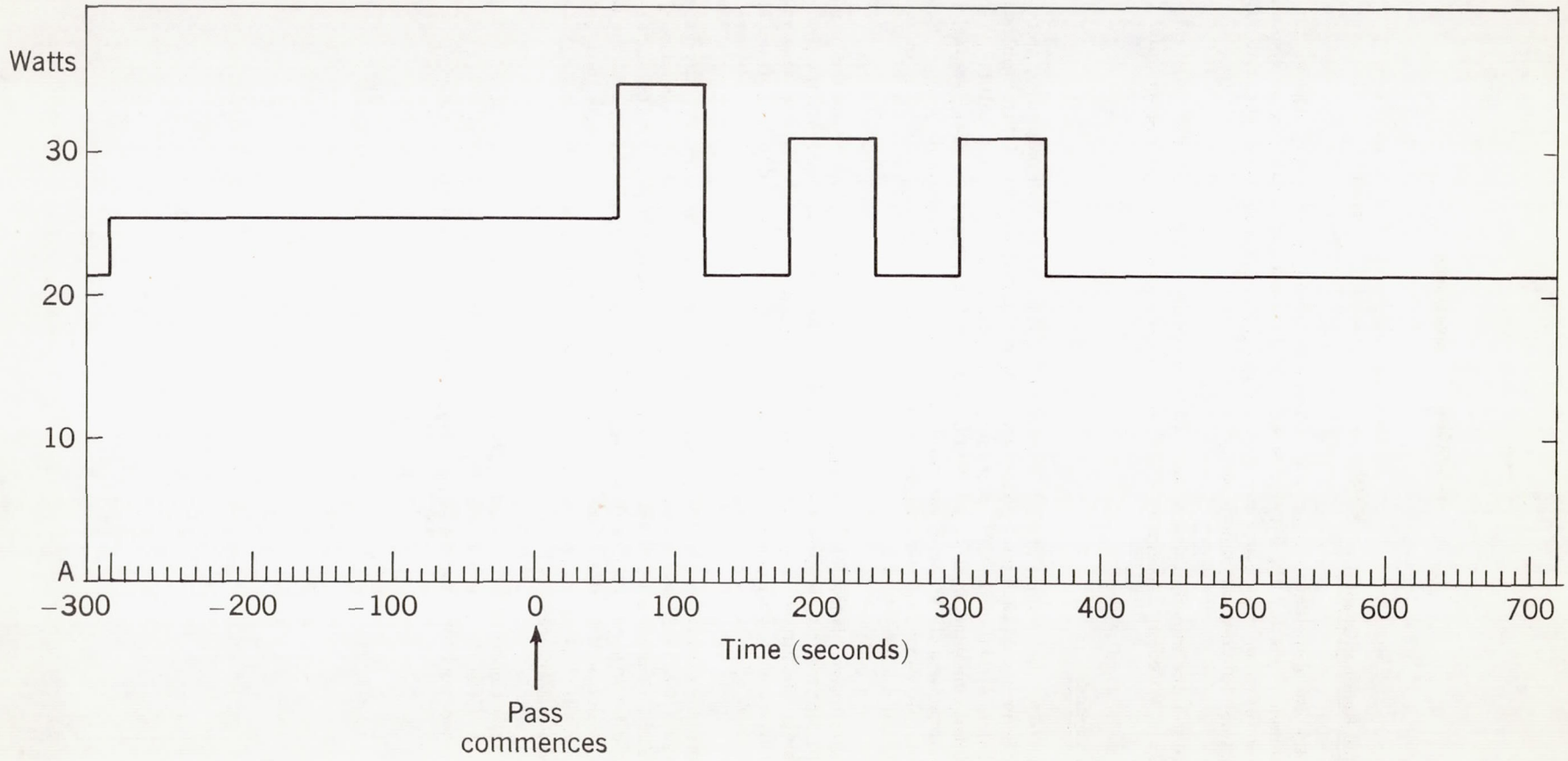

Figure 47.--Schedule of power fluctuations

8. Data Storage and Readout Capability

We require the use of the data storage as a buffer in the digital-store mode. Our maximum anticipated requirement is the full 100 000-bit capacity of the spacecraft's data storage system. This information will usually be unloaded once per slew, for an average of three times per orbit. Celescope will require a maximum of eight unloadings per orbit.

The first two to three minutes of each pass will be devoted to reading out the stored information from the University of Wisconsin experiment and to checking the operation of the spacecraft.

9. Experiment Commands

We now plan to use the command storage capabilities of the spacecraft only to set up the OAO for our initial slewing sequence of each pass. After completion of the University of Wisconsin's data-acquisition program, and before arrival of the OAO over the ground station, the spacecraft will be slewed to our first position by stored command, and the calibration lamps will be turned on. The 3-axis slew will require fifteen commands, and the lamps one command. There will normally be no need to adjust the operating voltage levels, but if changes are planned these should be accomplished by up to eight stored commands executed at the same time.

Sixty seconds after acquisition of the satellite by the ground station, we require that a series of eight commands be sent to the Celescope to end the polarization scan and commence the first exposure. The calibration lamps will already have been turned on prior to acquisition. Sixty seconds later we require a series of five commands to end the first exposure on all cameras and to turn off the calibration lamps.

One command for each telescope, transmitted at the appropriate time, is necessary for operations A and B of figure 26. Two or three commands are necessary for each telescope for operation C, depending on the final assignment of command coding. One command is necessary for each telescope for operations D and E; however, no more than two commands will be required for simultaneous operation of more than one camera in the polarization mode. Five commands are necessary for initiating the single-axis slew (operation F); none are required for its termination (operation G). One command each is required for operations H through K.

Table 9 lists the commands to be used by the Celescope. Where the number listed is four, one command is required for each telescope module. Operation code lines and bit-time lines have been selected for these commands such that loss of any single line will not in itself completely disable the Celescope.

Table 9. Celescope command code

Command	No. of commands	Bits per command	Total bits
1. Adjustments	(17)		(102)
1.1. Focus	4	6	24
1.2. Astigmatism	4	6	24
1.3. Beam	4	6	24
1.4. Target	4	6	24
1.5. Threshold	1	6	6
2. On-off operational commands	(18)		(42)
2.1. High voltage	4	2	8
2.2. Calibration	4	2	8
2.3. Polarization	4	2	8
2.4. Sweep mode-duration	4	3	12
2.5. Video selector	1	3	3
2.6. Digital mode	1	3	3
3. Execute operational commands	(12)		(12)
3.1. Start analog scan	4	1	4
3.2. Start digital scan	1	1	1
3.3. Repeat sequence start	1	1	1
3.4. Digital data store	4	1	4
3.5. Analog data store	1	1	1
3.6. Repeat command	1	1	1
4. Emergency sub-system select commands	(12)		(24)
4.1. A-to-D converter	1	2	2
4.2. Horizontal binary counters	1	2	2
4.3. Vertical binary counters	1	2	2
4.4. Horizontal output	1	2	2
4.5. Vertical output	1	2	2
4.6. +18-volt power supply	1	2	2
4.7. +6-volt power supply	1	2	2
4.8. -12-volt power supply	1	2	2
4.9. Camera power	4	2	8
Total	59		180

10. Experimenter's Status Data

Table 10 lists the parameters that will be included in the experimenter's status data. The 75 digital status data lines will give the settings of various control flip-flops in the Celescope equipment. The 15 analog status data lines will give information concerning various key voltage levels in the television cameras. The analog data will be more important in analyzing malfunctions of the equipment.

The complete sequence of status data, consisting of four frames, will be read out once per slew. One of these frames includes both the Celescope and the University of Wisconsin's status data -- 15 analog and 75 binary channels apiece. The other three frames give spacecraft status data that will be used in the Celescope data reduction program.

Table 10. Status data tabulation

I. Analog Group 2

Channel	Parameter
1	+6V
2	+18V
3	-12V
4	Honey Comb Panel Temp.
5	Uvicon No. 1 Support Tube Temp.
6	Uvicon No. 3 Support Tube Temp.
7	Calibrator Power Supply Temp.
8	Target Voltage - Camera No. 1
9	Target Voltage - Camera No. 2
10	Target Voltage - Camera No. 3
11	Target Voltage - Camera No. 4
12	Beam Current - Camera No. 1
13	Beam Current - Camera No. 2
14	Beam Current - Camera No. 3
15	Beam Current - Camera No. 4

II. Digital Word 5

Bit	Parameter
1	A to D Converter Select
2	Horz. BC's Select
3	Vert. BC's Select
4	Horz. Output Select
5	Vert. Output Select
6	+6V Select
7	+18V Select
8	-12V Select
9	Video Selector Bit 1
10	Video Selector Bit 2
11	Direct-Digital Mode on-off
12	Store-Digital Mode on-off
13	Camera No. 1 Sweep Mode (D or A)
14	Camera No. 2 Sweep Mode (D or A)
15	Camera No. 3 Sweep Mode (D or A)
16	Camera No. 4 Sweep Mode (D or A)
17	Camera No. 1 Polarization on-off
18	Camera No. 2 Polarization on-off
19	Camera No. 3 Polarization on-off
20	Camera No. 4 Polarization on-off
21	Spare
22	Spare
23	Spare
24	Spare
25	Spare

Table 10. Status data tabulation (continued)

III. Digital Word 6

Bit	Parameter
1	Video Threshold Bit 1
2	Video Threshold Bit 2
3	Video Threshold Bit 3
4	Video Threshold Bit 4
5	Spare
6	Spare
7	Spare
8	Spare
9	Spare
10	Spare
11	Spare
12	Spare
13	Spare
14	Spare
15	Spare
16	Spare
17	Spare
18	Spare
19	Spare
20	Spare
21	Spare
22	Spare
23	Spare
24	Spare
25	Spare

IV. Digital Word 7

All Spare *

* Table 10 assumes the use of the stepper-motor potentiometer for focus and astigmatism adjustments. If solid-state adjustment units are used instead, then these spare channels will be used to monitor the flip-flop settings in those units.

V. Ground-Support Equipment

The Celescope ground-support equipment has three functions: to test and calibrate the Celescope during production, testing, and countdown; to perform c prompt and accurate reduction of the data; and to assist in necessary adjustment of the Celescope in orbit.

Fortunately, the NASA ground station contains a General Mills computer and an IBM digital tape recorder that includes an IBM-729 tape transport. This equipment will be able to translate the information on the raw data-tape into a format suitable for input to an IBM-7090 computer. The Celescope ground-support equipment will therefore not need to incorporate this translation circuitry into its digital signal-conditioning unit.

Under normal conditions the General Mills computer and the IBM-729 tape transport will be used to convert the output from the raw data-tape into more useful form. The computer will be programmed to recognize the various types of information contained on the raw data-tape.

Our analog picture, of 62 kc/sec bandwidth, will be converted to digital form by pulse-code modulation. In this type of modulation the computer must sample the amplitude of the waveform at a rate of 124 kilosamples per second, numerically equal to twice the highest frequency of the video signal. Since we require at least 20 shades of gray, these samples must be digitized to 5-bit accuracy. The PCM data-rate must be 620 kilobits per second to accommodate 5 bits at a rate of 124 kilosamples per second. The General Mills computer together with the raw data-tape has this data-rate capability for PCM conversion. However, we must either store temporarily each picture while the IBM-729 digital tape recorder reads out the information at the slower rate of 300 kilobits per second, or we must reduce to one-half the playback speed of the tape recorder to be used at the input to the chain.

Our digital pictures and status information will be converted and recorded in correct format for later input to an IBM-7090 computer. Irrelevant information will be omitted from the converted tape. The General Mills computer will assign a serial number to each picture as it is converted into correct IBM format.

The Celescope ground-support equipment will consist of portable equipment and a fixed installation. Figure 48 is a block diagram of the portable equipment, which can be transported by two men and a station wagon. It will be used as necessary to analyze the performance of the Celescope during manufacture, testing, pre-launch count-down, and orbital operations. It will also allow an accurate check of the correctness of the format conversion performed by NASA's General Mills computer. Figure 49 is a block diagram of the fixed installation, to be used in Cambridge for final data analysis and for preparation of the observational results for publication.

Figure 50 illustrates the analog mode of operation for the portable ground-support equipment. In this mode no inputs are required from the PCM ground equipment. The composite video signal is taken directly from the ground station receiver. It is inserted into a sync separator which subsequently feeds the video information to the intensity channel of the display and the sync signal to the sweep circuits. The sync pulse is used to trigger the re trace of a free-running analog horizontal sweep generator. The same pulse is counted, and the outputs from the counters are used to drive a digital-to-analog converter. The output of the D-to-A converter is the vertical sweep signal.

The ground-command system must provide the "start" command for the analog scan to reset the vertical sweep counter to zero. Prior to recording new information on the storage-tube display, it is necessary to erase all previous information. Therefore, a signal must be provided at least one second ahead of any new information to be displayed on the storage tube to allow for erasure. This is required in all modes. Provision for manual erasure will also be provided.

The block diagram of figure 51 illustrates the digital-store mode. A 25-bit digital word is received from the PCM ground station describing position and intensity of each signal to be displayed. Seven bits are used to describe intensity, eight bits for vertical position, and eight bits for horizontal position. The remaining two bits are dummies. After the 25-bit word is complete, a transfer pulse will be provided which will permit the transfer of binary data to the buffer stores in each of the three channels. The display equipment is in a blanked condition until the D-to-A converters have had sufficient time to arrive at their proper status. The technique for accomplishing this is omitted from the simplified block diagrams but is illustrated in figure 49 and is discussed in more detail below.

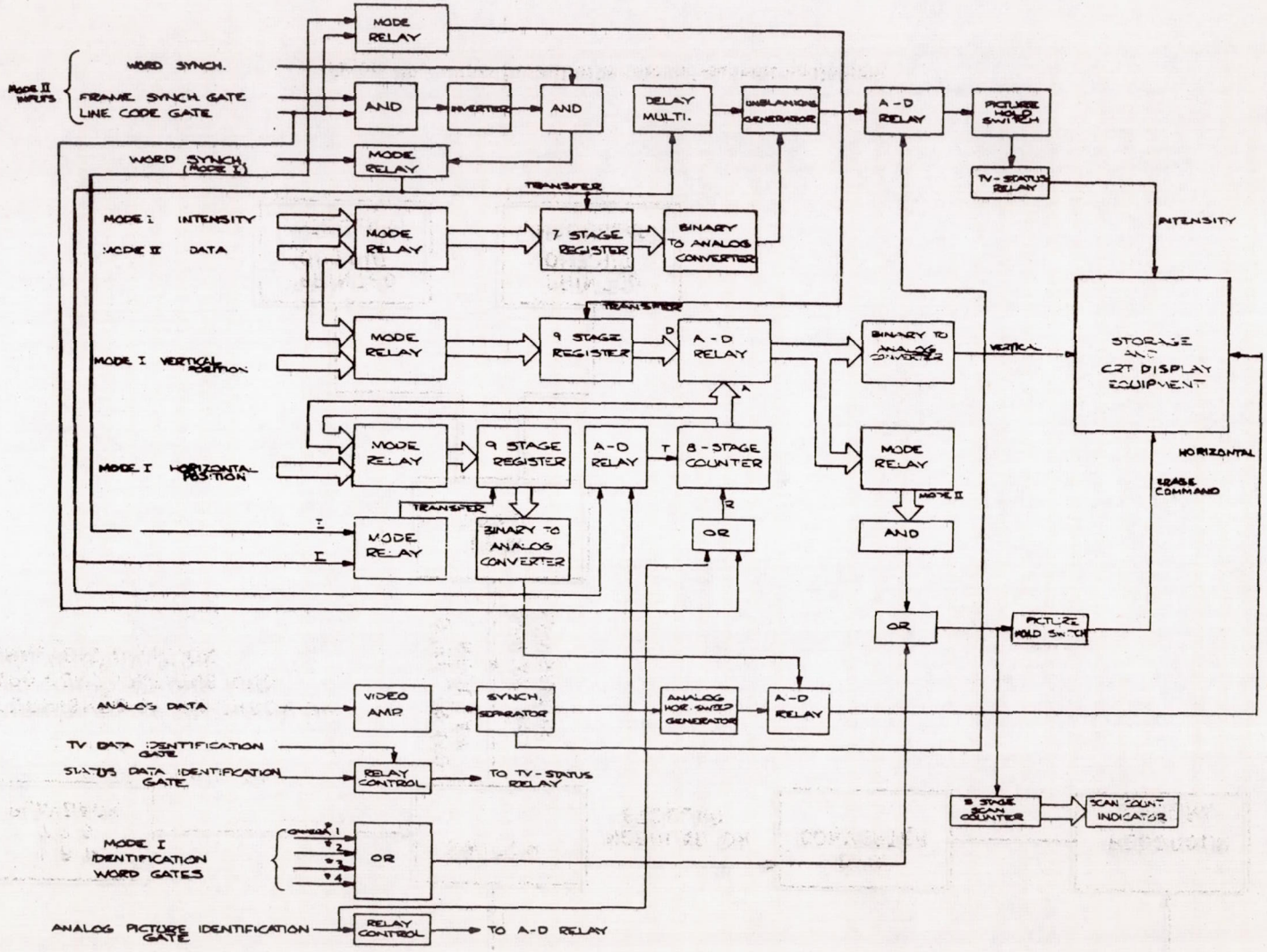

Figure 48.--Portable ground-support equipment

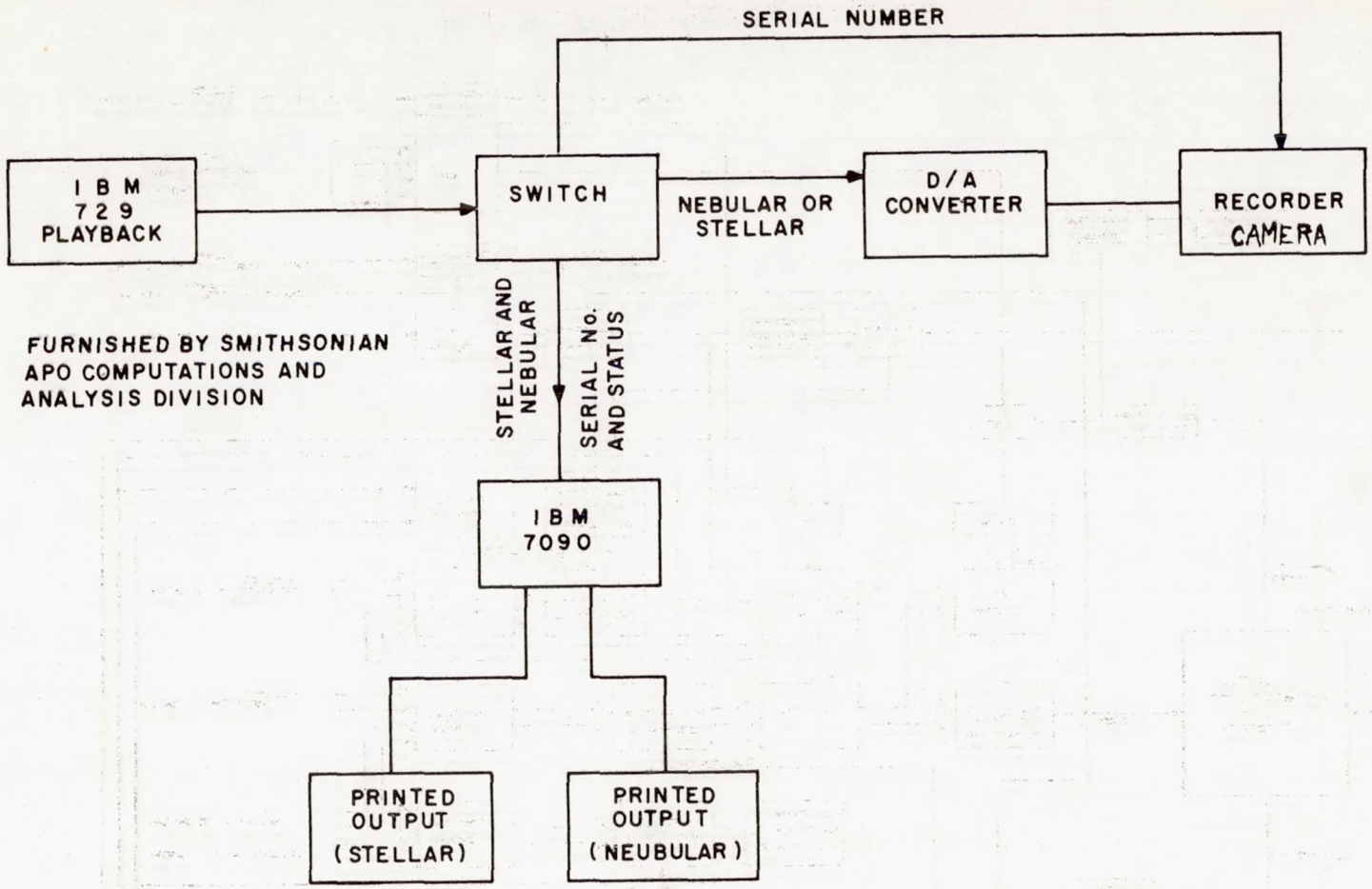

Figure 49.--Fixed installation ground-support equipment

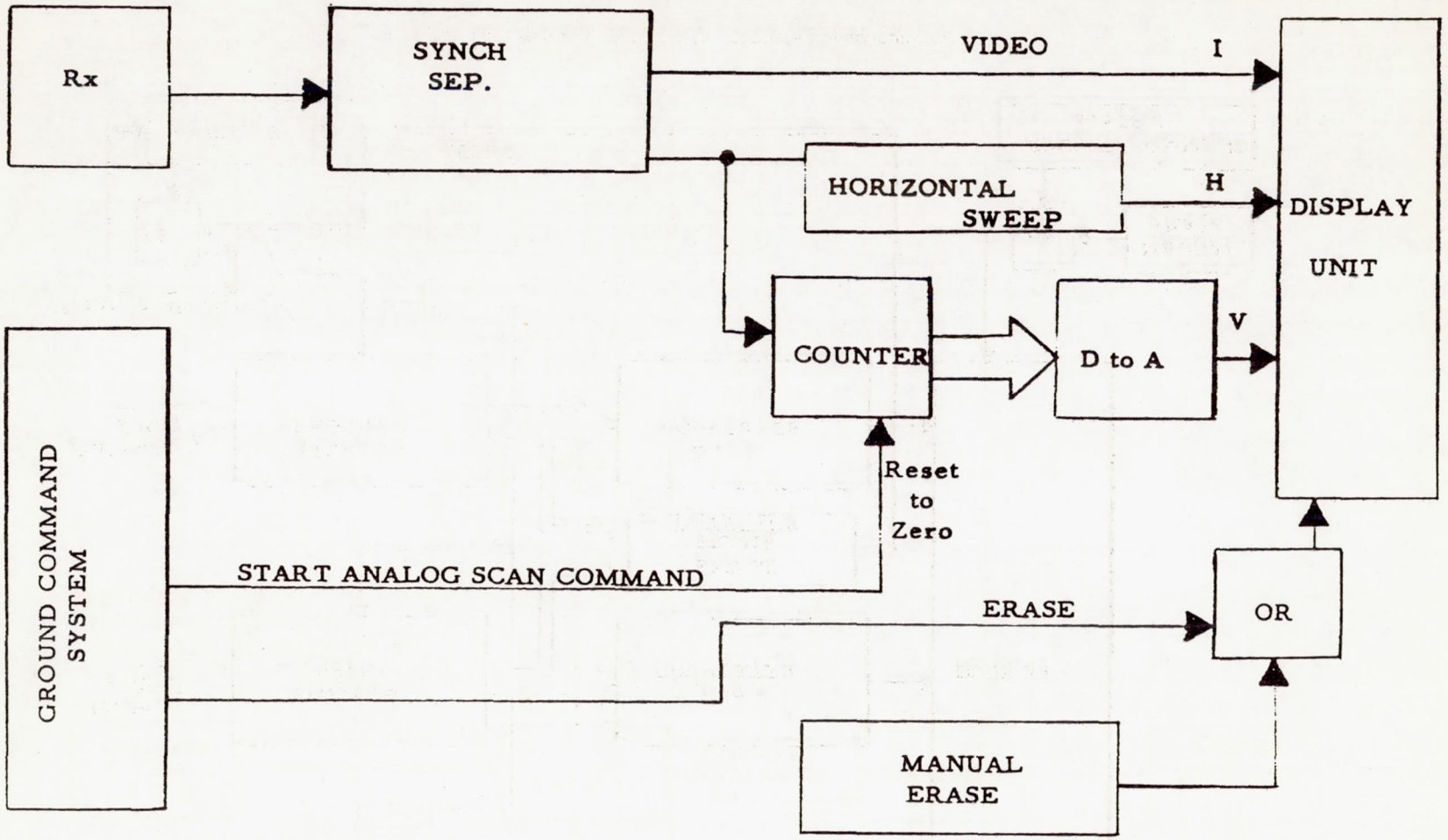

Figure 50.--Analog mode, ground-support equipment

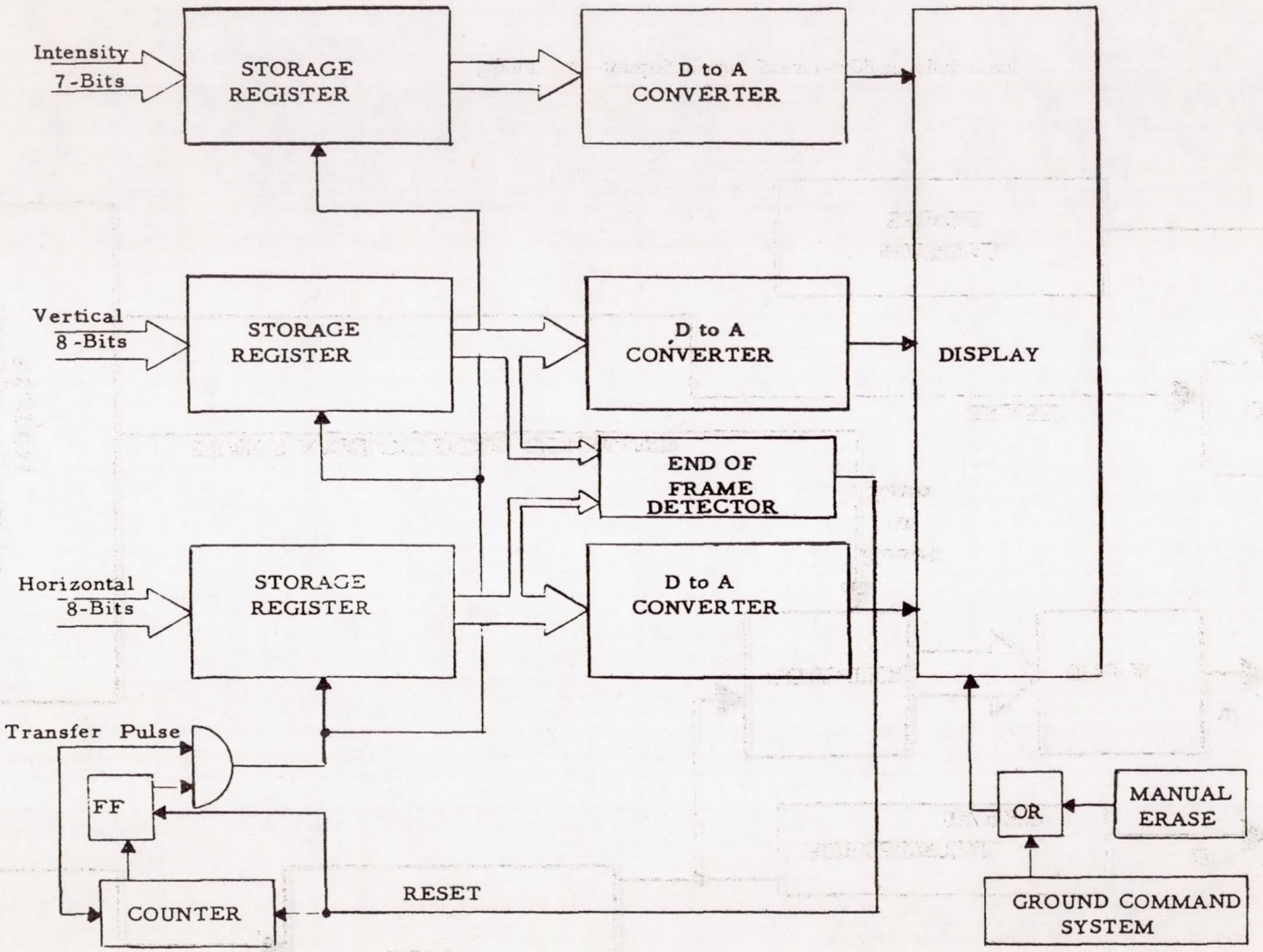

Figure 51.--Digital-store mode, ground-support equipment

Since, in the digital-store mode, data are transmitted only if a star is encountered, some means of determining the end of a frame must be provided. The simplest method is always to transmit the last element position in each picture, thus completely filling the horizontal and vertical storage registers and signifying the end of a frame. A counter, preset to count the proper number of status words, is reset by the end-of-frame signal. These status words will follow each television frame. The counter, in turn, changes the state of a flip-flop to permit scanning to resume. As in the analog mode, the signal to erase the displayed information is normally generated by the ground-command system.

The digital-direct mode, as shown in figure 52, uses pulse code modulation (PCM). Intensity is presented as a 7-bit word as in the digital-store mode, and vertical position is presented as an 8-bit word. Horizontal position is obtained by counting the word-sync pulses used to transfer intensity data from the PCM ground station to the storage register. The counter is reset by the line code transfer gates, which also transfer the vertical position data from PCM ground station to the storage register. As in the other two modes, erasure is normally commanded by the ground-command system.

When the portable ground equipment is connected directly to the Celescope package for system checkout and the system is operating in digital-direct mode, the information from Celescope is presented in serial form. Thus the portable ground equipment must provide the serial-to-parallel conversion and the storage registers to provide isolation between the digital-to-analog converters and the serial-to-parallel conversion. To accomplish this serial-to-parallel conversion, Celescope will provide the ground equipment with gate pulse W-6 and bit times 1 through 8 from the digital processing unit.

We will use a Hughes type H-1033AP20 Tonotron as the storage tube. This is a 10-inch direct-view storage tube with a useful screen diameter of 8.5 inches minimum. It uses electrostatic focusing and magnetic deflection.

Figure 53 shows the intensity amplifier for the Tonotron. The delay monostable flip-flop delays the transfer pulse for 70 microseconds. This allows the sweeps to be positioned and all transients to die out. The unblanking monostable flip-flop then allows the astable flip-flop to operate for 20 microseconds. The astable flip-flop operates the chopper at a one megacycle/sec rate, thus enabling the intensity information to be AC-amplified and applied to the grid of the tube.

For protection of the Tonotron, transistor switches turn off the intensity astable flip-flop if either the write beam or the flood beam is lost. In the event of a loss of horizontal sweep voltage, the intensity is turned off because of the action of two Schmidt triggers. The first Schmidt trigger is driven from the horizontal amplifier and alternately charges and discharges a capacitor. The capacitor time is about 300 microseconds, and it discharges in about three milliseconds. The voltage across the capacitor controls the second Schmidt trigger. The intensity will be turned off three milliseconds after a loss of sweep.

Most of the digital and storage display circuitry has been completed. Electro-Mechanical Research Model 185-0055 cards will be used for the registers, Model 185-0013 for the counter. The Model 185 cards will have to be modified slightly by adding one more stage for the horizontal and vertical circuitry and removing one stage for the intensity circuitry. For the horizontal and vertical controls, the additional stage will become the least significant bit of the binary-to-analog converter, and in the intensity loop the least significant bit of the binary-to-analog converter will be clamped at -1 volt for the binary zero. Since the Model 185 shift registers require a double-ended input, they will require flip-flops for drivers. The flip-flops are placed between the mode relays and the registers.

The erase circuitry consists of a monostable flip-flop coupled through an emitter-follower to the backing electrode of the storage tube. The final erase time will have to be determined later; it will be 0.5 second or shorter.

The NASA ground station will provide a printed output of status data as it is received. We will use this printed sheet for quick-look analysis of Celescope status during the emergency or adjustment modes of operation.

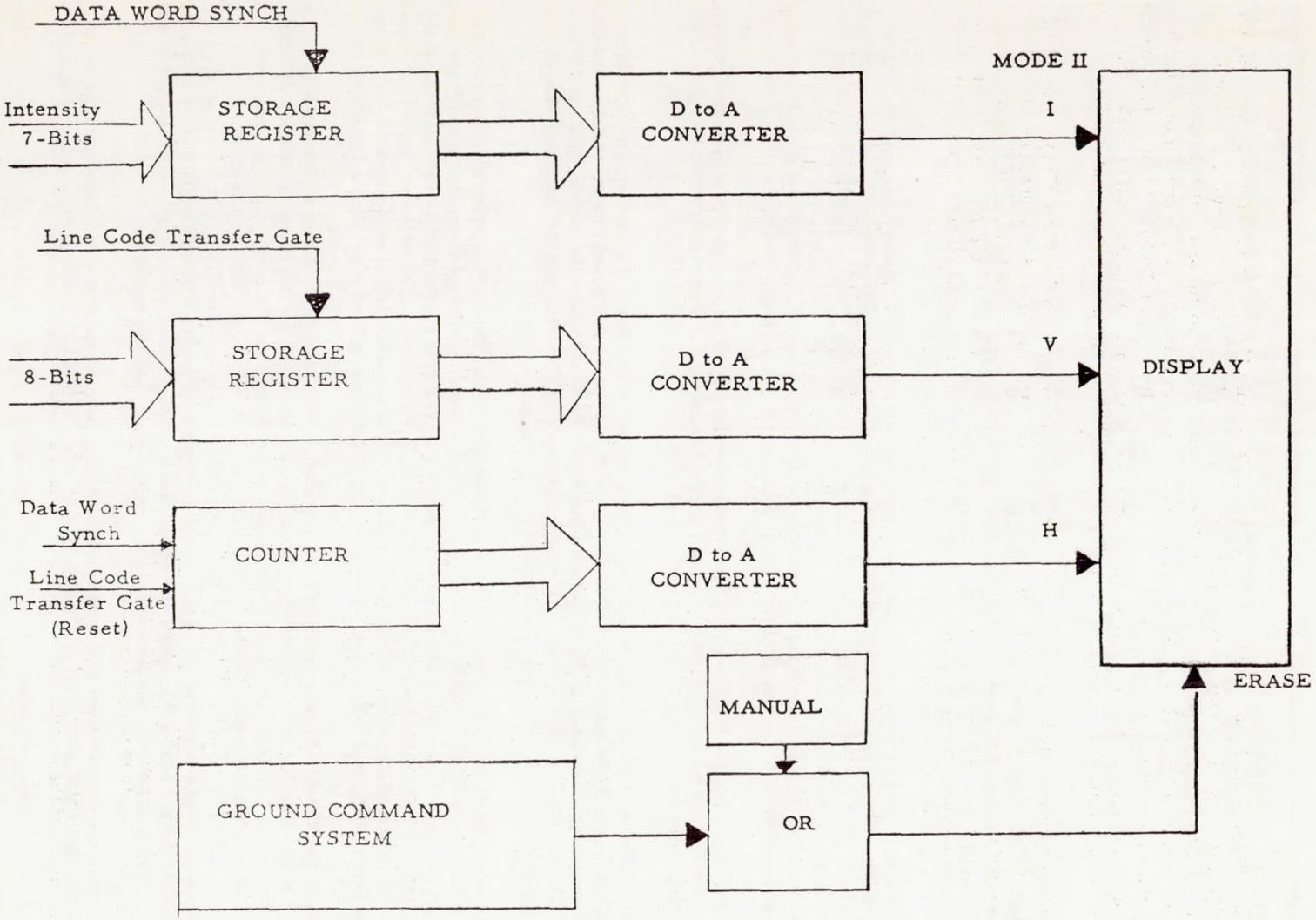

Figure 52. --Digital-direct mode, ground-support equipment

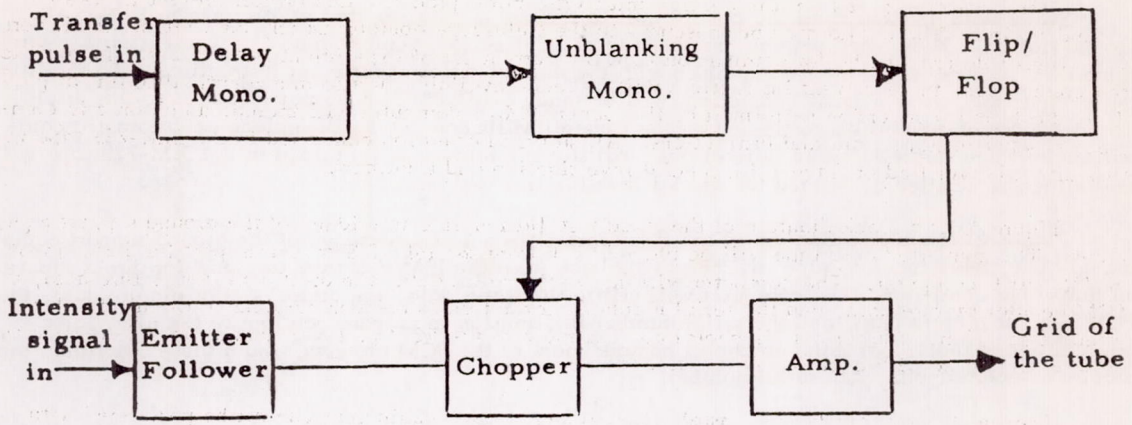

Figure 53. --Block diagram of intensity amplifier for the Tonotron

The portable ground-support equipment will be divided into three main drawers and will be housed in a Premier sloped-front console FS1001, shown in figure 54. One drawer will contain the ±12-volt and ±50-volt power supplies. This console will weigh about 200 pounds. It can thus be transported by two men and a station wagon. It will require 1000 watts of 110-volt, 60-cycle, single-phase alternating current. Our portable ground-support equipment will also include a Tektronix Model 536 oscilloscope of standard dimensions (13 x 16 x 23 inches), equipped with a standard stand 15 x 24 x 39 inches.

The equipment will include, as well, a spacecraft-command simulator for controlling the Celescope prior to mating with the spacecraft. It will be able to receive the direct output from the Celescope, or alternatively it will be qble to receive the output from NASA's PCM ground station, but the equipment will not be able to handle directly the output of NASA's spacecraft simulator, or the direct output from the spacecraft.

There are three types of operation of the Celescope in orbit: routine, corrective, and emergency. The emergency method of operation sets the most stringent requirements on the ground-support equipment. In this method, prior to the pass, the Celescope operator has had the full range of commands for one maladjusted telescope entered into the command memory of the AD/ECS computer at the NASA ground station. The NASA operator has individual cards for calling any one of these commands and an "execute" button for transmitting that command from the AD/ECS computer to the OAO. These commands are made by verbal order from the Celescope operator in much the same way as he has previously adjusted the Celescope in the laboratory. The emergency method will be used only to correct a picture that is suddenly far out of focus; the most probable times for such an operation would be at the time of first turn-on after achieving orbit, and subsequent to any later emergency that would require long-term shutdown of the Celescope equipment.

The corrective mode of operation, to be made when the Celescope focus begins to drift away from its acceptable limits, calls a short series of adjustment commands from the AD/ECS computer aimed at determining the new settings for optimum focus. Here the pictures from one pass are studied, the correction adjustment series is inserted into the AD/ECS memory, and the pictures resulting from the corrective pass are again studied to determine the commands required on the following pass for recommencing data acquisition.

The routine mode of operation uses a predetermined series of commands to control the acquisition of data in some such sequence as that shown in figure 26. This method will be used for any pass following one in which the operator could detect no inadequacies on the picture or status data.

Status data are sent from the control unit to the status processor and printer present in NASA's ground station. These data may be presented to the Celescope operator in any convenient visible form, since their sole use will be for comparison with the current set of experiment instructions. To facilitate the comparison, these current instructions will be made available in a format identical to this display. The data format conversion performed by the General Mills computer will include an automatic comparison between status data and instructions. All status information contained in the IBM-729 tape will thus either be verified or flagged for special investigation and treatment.

Figure 49 is a block diagram of the fixed installation, in Cambridge, of the ground support equipment. The converted data tape will be played back from the IBM-729 tape transport for direct input to an IBM-7090 computer. The computer will utilize the status data, the digital stellar picture data, the PCM nebular picture data, and the serial number information to prepare catalogs of the ultraviolet brightnesses of individual stars, isophotal contour maps of the PCM pictures, and a table describing the picture associated with each serial number.

The functions of our fixed - installation ground-support equipment can all be performed with standard peripheral equipment for IBM installation.

VI. Data Reduction

Our astrophysical analysis would be accomplished by running the digital record as the data input to a digital computer program for the generation of our star catalog, and by measuring the isophotal contours for investigating the nebulosities. We feel that we must be able to use simultaneously scientific judgment for a subjective data analysis, and the automatic computing methods for an objective data analysis. Our main provision for the former is to make no decisions that will prevent useful data available in the satellite from reaching the ground. Our main provision for the latter is our digitization of information on board the satellite. The digital information will be more accurate and easier to handle than the analog information. We plan to organize a digital computer program for processing these data into a printed star catalog. The magnetic-tape equivalent of this printed catalog can then easily be used for further studies of stellar atmospheres, and for use in computing programs that, because of our present inadequate knowledge of stellar ultraviolet fluxes, cannot be specified in advance. We will also produce ultraviolet maps of the sky, showing both stars and nebulosities.

We believe that the catalog and maps will provide a wealth of data on which to base theoretical papers. We will therefore publish them without undue delay, to allow study by other members of the astronomical community.

In our laboratory we have prepared a breadboard model of both the space-borne and ground-based data-handling equipment shown in figure 45. We are utilizing two types of display for evaluation of these data-handling techniques, as illustrated in figures 55, 56, 57.

The multiple A-scope presentation of figures 55 and 56 enables us to measure the brightnesses of nebulae and stars as a function of position, throughout the entire field of view, by standard astronomical measuring engines. This multiple A-scope monitor has independent controls for its intensity and its amplitude modulation. Under the low magnification shown in figure 55 we can examine the intensity-modulated picture directly to see what it looks like. Under the high magnification shown in figure 56 we can measure the amplitude and waveform of the signal precisely. In the operational version of the ground-support equipment, these functions will be accomplished by the PCM encoding, followed by analysis with the 7090 computer.

In the operational version of the ground-support equipment, the digital presentation of figure 57 will not normally be presented in visible form, but rather will be fed directly to a computer. Each column of dots represents a picture element for which the intensity was above threshold. The first 18 bits give the position of the picture element, and the last 7 bits give its intensity.

Tables 11 and 12 are prototype samples of the catalogs we plan. Figure 58 shows a sample of the pictures that will be published and studied along with these catalogs. Note that figures 55, 56, 57 consist of photographs of a breadboard display system used to evaluate the data-processing equipment philosophy; figure 58 is our conception of how the actual display will look.

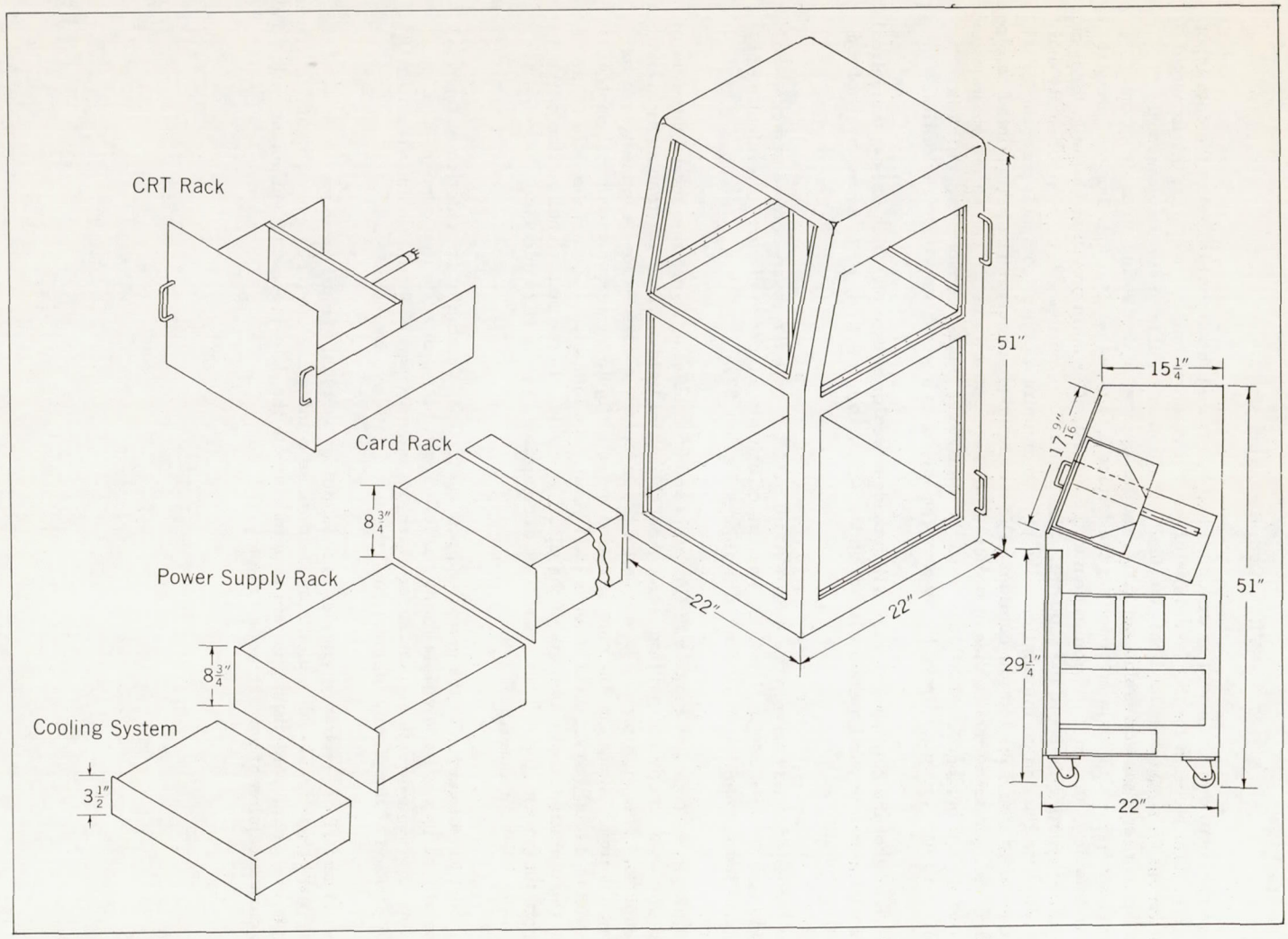

Figure 54.--Dimensions of console for ground-support equipment

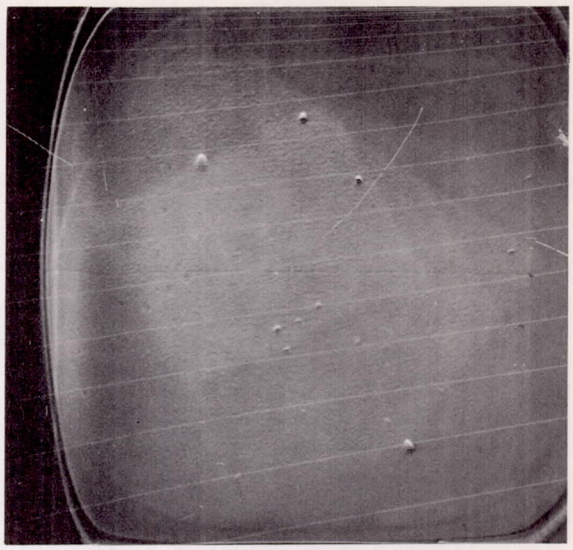

Figure 55.(right)--Multiple A-scope television display

Figure 56.(below)--Enlargement of portion of figure 55

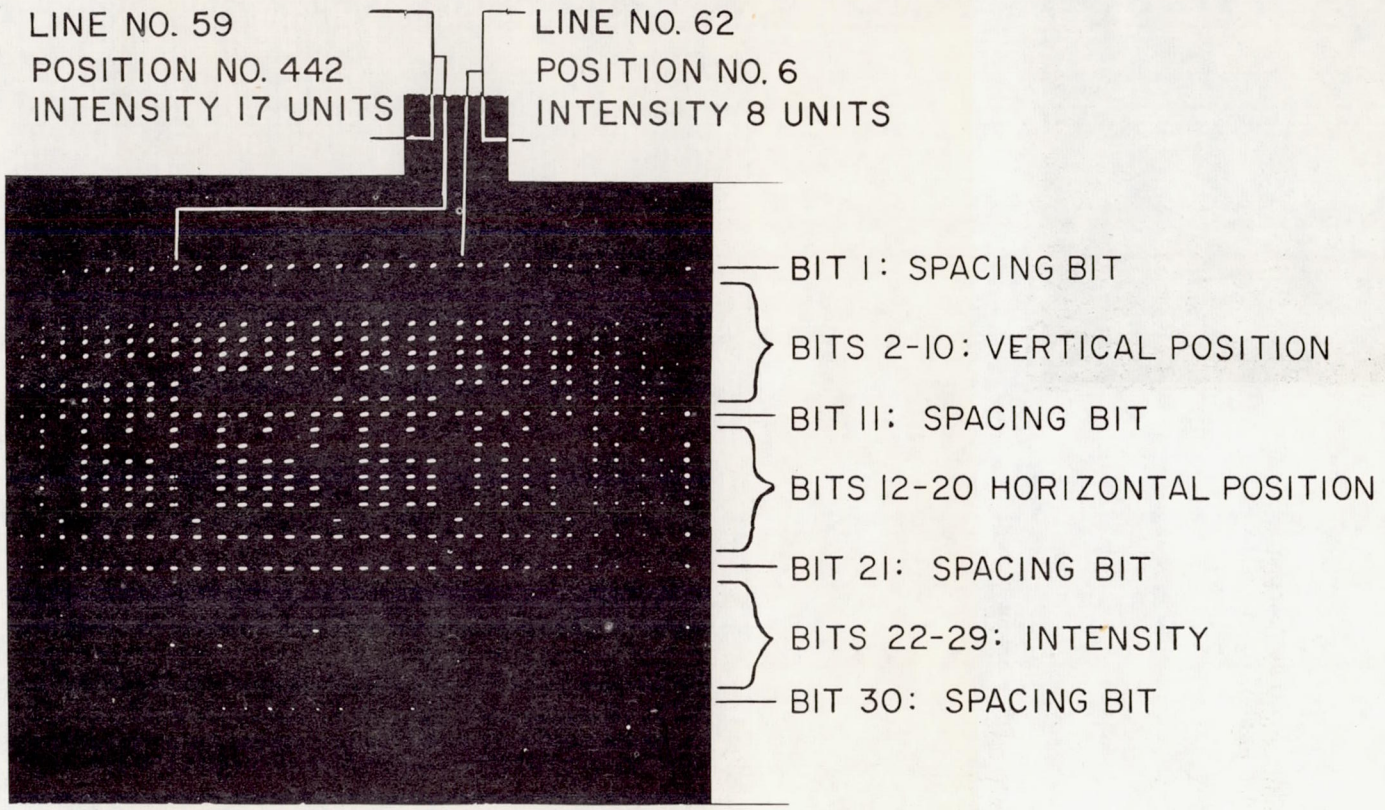

Figure 57. --Visual representation of digital-store television display

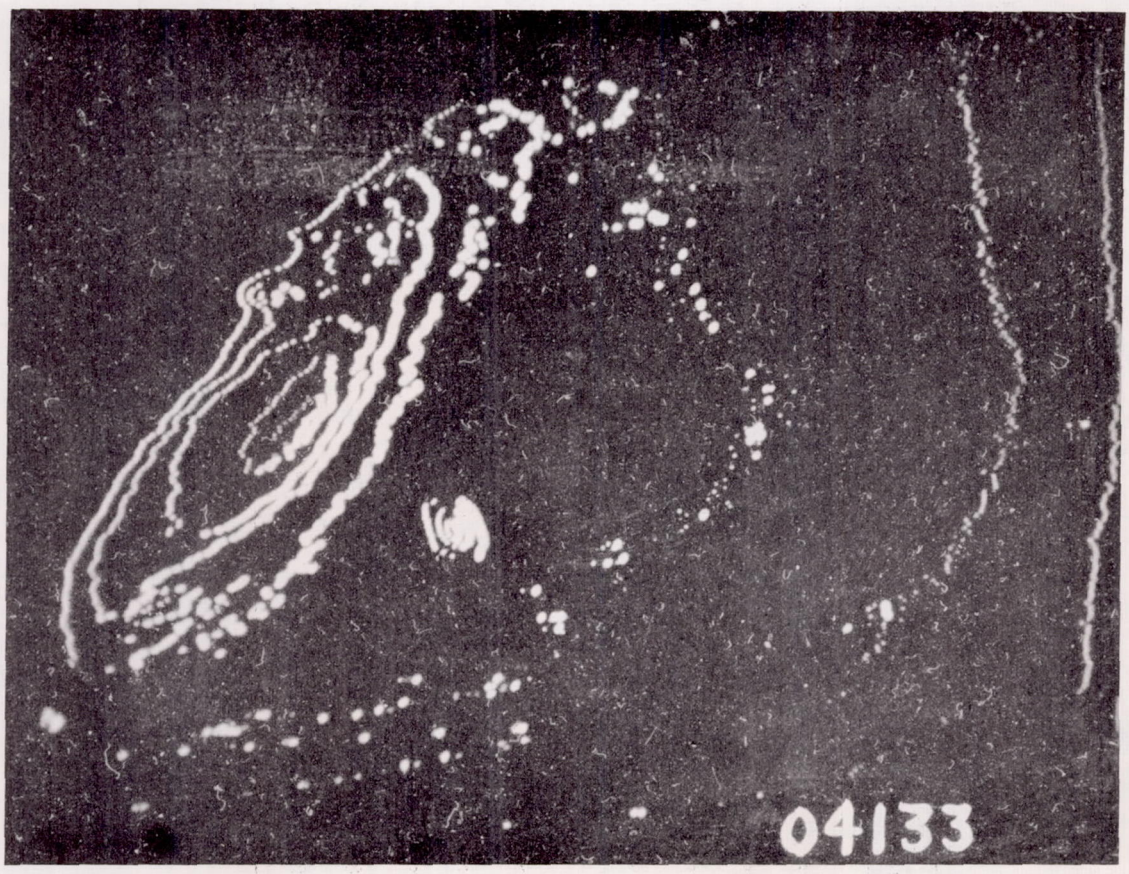

Figure 58.--Artist's conception of television display by means of isophotal contours

Table 11. --Sample catalog of ultraviolet stellar magnitudes

Celescope catalog number	(1950.0) Right ascension	Declination	m_{u1} (2600)	m_{u2} (2300)	m_{u3} (1500)	m_{u4} (1400)	Spectrum	m_{pv} (5300 A)
18100	$5^h\ 33.^m5$	+07?93	8.7	9.3	---	9.3	---	---
18101	5 33.6	-13.06	---	---	9.5	---	---	---
18102	5 33.7	-01.23	0.3	-1.0	-2.3	-2.0	cB0eI	1.8
18103	5 33.9	+15.57	9.5	---	---	---	---	---
18104	5 33.9	-53.49	---	9.5	9.5	---	---	---
18105	5 34.0	+00.27	7.9	7.5	7.8	---	---	---
18106	5 34.2	+61.55	8.9	9.6	---	9.9	---	---
18107	5 34.3	+21.12	1.9	0.9	-0.1	-0.3	B3pe	3.1
18108	5 34.3	-06.09	4.8	3.1	1.8	2.5	B1	5.8
18109	5 34.5	-03.32	---	9.8	7.5	8.1	---	---

Table 12. --Sample table describing published pictures

Serial number	Center coordinates (1950.0)		Exposure time	Camera number	Zenith distance	Scanning mode	Threshold (stellar magnitude)	Exposure start time
	Right ascension	Declination						
								JD2438456 +
04130	$0^h\ 38^m.7$	+28°.17	10^s.0	3	80°	DD	10.0	.93700
04131	0 38.7	+30.37	5.7	1	79	DD	9.5	.93778
04132	0 38.7	+30.37	8.3	2	79	DD	9.8	.93778
04133	0 38.7	+30.37	30.0	3	79	DD	----	.93778
04134	0 38.7	+30.37	30.0	4	79	DD	9.6	.93778
04135	0 38.7	+30.37	29.3	1	79	DD	----	.93795
04136	0 38.7	+30.37	25.8	2	80	DD	----	.93801
04137	0 38.7	+30.37	10.0	3	80	DD	10.0	.93813
								JD2438457 +
04138	0 47.5	+25.95	5.7	1	60	DD	9.5	.00454
04139	0 47.5	+25.95	8.3	2	60	DD	9.8	.00454

General references

In addition to the specific references in the text, the following general reviews may prove helpful:

BERKNER, L. V., and ODISHAW
1961. Science in space. McGraw-Hill Book Company, New York, 458 pp.

SCHATZMAN, E.
1960. Les applications de l'astronautique à l'astrophysique. Astronautica Acta, vol. 6, pp. 159-166.

SWINGS, P.
1961. Report of Commission 44, In Agenda and draft reports, 11th General Assembly, International Astronomical Union, Willmer Bros. and Hara Ltd., Birkenhead, England, pp. 521-555.

WHIPPLE, F. L., and DAVIS, R. J.
1960. Proposed stellar and interstellar survey. Astron. Journ., vol. 65, pp. 285-290.

Specific references

ALEXANDER, J. D. H., BOWEN, P. J., and HEDDLE, D. W. O.
1962. Southern hemisphere observations of ultraviolet from celestial objects. Paper given at COSPAR meeting, May 1962.

ALLEN, C. W.
1955. Astrophysical quantities. Athlone Press, London, 263 pp.

ANGEL, D. W., HUNTER, W. R., TOUSEY, R., and HASS, G.
1961. Extreme ultraviolet reflectance of LiF-coated aluminum mirrors. Journ. Opt. Soc. America, vol. 51, pp. 913-914.

BAEZ, A. V.
1960a. A self-supporting metal Fresnel zone-plate to focus extreme ultra-violet and soft X-rays. Nature, vol. 186, p. 958.

1960b. A proposed X-ray telescope for the 1- to 100-A region. Journ. Geophys. Res., vol. 65, pp. 3019-3020.

1961. Fresnel zone plate for optical image formation using extreme ultraviolet and soft X radiation. Journ. Opt. Soc. America, vol. 51, pp. 405-412.

BERNING, P. H., HASS, G., and MADDEN, R. P.
1960. Reflectance-increasing coatings for the vacuum ultraviolet and their applications. Journ. Opt. Soc. America , vol. 50, pp. 586-597.

BLAAUW, A.
1961. On the origin of the O- and B-type stars with high velocities (the "run-away" stars), and some related problems. Bull. Astron. Inst. Netherlands, vol. 15, pp. 265-290.

BYRAM, E. T., CHUBB, T. A., and FRIEDMAN, H.
1961. Ultraviolet Light from Celestial Sources. Mèm. Soc. R. Sc. Liège, 5 Ser., vol. 4, pp. 469-475.

1962. Private communication from Dr. Chubb.

CANAVAGGIA, R., and PECKER, J. C.
1953. Les gèantes jaunes. II. Spectres continus. Ann. d'Ap., vol. 16, pp. 47-59.

CARRIER, G. F., and AVRETT, E. H.
1961. A non-gray radiative-transfer problem. Astrophys. Journ., vol. 134, pp. 469-481.

CROSSWHITE, H. M., ZIPF, E. C., Jr., and FASTIE, W. G.
1962. Far-ultraviolet auroral spectra. Journ. Opt. Soc. America, vol. 52, pp. 643-648.

DAVIS, R. J., and GODFREDSON, E. A.
1961. Optimum resolving power for an ultraviolet space telescope. Journ. Planet. Space Sci., vol. 5, pp. 207-212.

ELECTRONIC PREVIEW AND SCIENCES REVIEW
1962. Description of Westinghouse's new uvicon target, vol. 3, no. 8, p. 4, August 1962.

GREENBERG, J. M.
1960. The sizes of interstellar grains. Astrophys. Journ., vol. 132, pp. 672-676.

HARTMANN, J.
1904. Investigations on the spectrum and orbit of δ Orionis. Astrophys. Journ., vol. 19, pp. 268-286.

HAYAKAWA, S.
1960. A possible origin of the ultraviolet radiation from galactic clouds. Publ. Astron. Soc. Japan, vol. 12, pp. 113-114.

HEDDLE, D. W. O.
1962. Observations in the southern hemisphere of ultraviolet light from celestial objects. Nature, vol. 193, p. 861.

HINTEREGGER, H. E.
1961. Telemetering monochromator measurements of extreme ultraviolet radiation. Part II: Physical applications. In Space astrophysics, W. Liller, ed., McGraw-Hill, New York, pp. 74-95.

HUNGER, K.
1955. Die Atmosphäre des AO-Sternes Alpha Lyrae. Zeitschr. f. Astrophys., vol. 36, pp. 42-97.

JOHNSON, F. S.
1961. Solar radiation. In Satellite environment handbook, F. S. Johnson, ed., Stanford University Press, Stanford, pp. 77-81.

KAMIYAMA, H.
1959. Vertical distribution of molecular oxygen. Sci. Rep. Tohoku Univ., ser. 5, vol. 11, pp. 84-97.

KUPPERIAN, J. E., Jr., BOGGESS, A., III, and MILLIGAN, J. E.
1958. Observational astrophysics from rockets. I. Nebular photometry at 1300 A. Astrophys. Journ., vol. 128, pp. 453-464.

KUPPERIAN, J. E., Jr., BYRAM, E. T., CHUBB, T. A., and FRIEDMAN, H.
1958. Extreme ultraviolet radiation in the night sky. Ann. de Geophysique, vol. 14, pp. 329-333.

McNAMARA, D. H., and HANSEN, K.
1961. Stellar rotation and the Beta Canis Majoris Stars. Astrophys. Journ., vol. 134, pp. 207-213.

MALITSON, H. H., PURCELL, J. D., TOUSEY, R., and MOORE, C. E.
1960. The solar spectrum from 2635 to 2085 A. Astrophys. Journ., vol. 132, pp. 746-766.

PIKEL'NER, S. B., SHKLOVSKII, I. S., and IVANOV-KHOLODNYI, G. S.
1959. On possible mechanisms of emission of discrete galactic objects in the spectral region 1225-1350 A. Astron. Journ. U.S.S.R., vol. 36, pp. 264-268.

SCHWARZSCHILD, K.
1905. Untersuchungen zur geometrischen Optik. II. Theorie der Spiegeltelescope. Mitt. Astron. Sternw. Göttingen, no. 10, 28 pp.

SCIENTIFIC AMERICAN
1960. Ultraviolet stars, vol. 202, no. 3, pp. 88-89.

SHKLOVSKII, I. S.
1959. Corpuscular emission from early-type stars as a possible cause of emission from nebulae in the region 1225-1350 A. Astron. Journ. U.S.S.R., vol. 36, pp. 579-584.

SKORINKO, G., DOUGHTY, D. D., and FEIBELMAN, W. A.
1961. An ultraviolet sensitive image tube. Westinghouse Res. Lab., Scientific Paper 912-J902-P1, 6 pp; in press Journ. Opt. Soc. America.

STECHER, T. P., and MILLIGAN, J. E.
1961. Stellar spectrophotometry below 3000 Angstroms. Astron. Journ., vol. 66, p. 296.

STONE, P. H., and GAUSTAD, J. E.
1961. The application of a moment method to the solution of non-gray radiative-transfer problems. Astrophys. Journ., vol. 134, pp. 456-468.

STROM, S. E., and STROM, K. M.
1961. Interstellar absorption below 100 A. Publ. Astron. Soc. Pacific, vol. 73, pp. 43-45.

TOUSEY, R.
1961. Ultraviolet spectroscopy of the sun. In Space astrophysics, W. Liller, ed., McGraw-Hill, New York, pp. 1-16.

TRAVING, G.
1955. Die Atmosphäre des BO-Sternes τ Scorpii. Zeitschr. f. Astrophys., vol. 36, pp. 1-41.

UNDERHILL, A. B.
1951. A model atmosphere for an early O-type star. Publ. Dominion Astrophys. Obs. Victoria, vol. 8, pp. 357-384.

VIGROUX, E.
1960. L'ozone atmosphérique. L'Astronomie, vol. 74, pp. 241-255.

VITENSE, E.
1951. Der Aufbau der Stern atmosphären. IV. Kontinuierliche Absorption und Streuung als Funktion von Druck und Temperatur. Zeitschr. f. Astrophys., vol. 28, pp. 81-112.

WILSON, N. L., TOUSEY, R., PURCELL, J. D., JOHNSON, F. S., and MOORE, C. E.
1954. A revised analysis of the solar spectrum from 2990 to 2635 A. Astrophys. Journ., vol. 119, pp. 590-612.

ZIEMER, R. R.
1961. Orbiting astronomical observatories. Astronautics, vol. 6, no. 5, pp. 36 ff.

NOTICE

This series of Special Reports was instituted under the supervision of Dr. F. L. Whipple, Director of the Astrophysical Observatory of the Smithsonian Institution, shortly after the launching of the first artificial earth satellite on October 4, 1957. Contributions come from the Staff of the Observatory. First issued to ensure the immediate dissemination of data for satellite tracking, the Reports have continued to provide a rapid distribution of catalogues of satellite observations, orbital information, and preliminary results of data analyses prior to formal publication in the appropriate journals.

Edited and produced under the supervision of Mr. E. N. Hayes, the Reports are indexed by the Science and Technology Division of the Library of Congress, and are regularly distributed to all institutions participating in the U.S. space research program and to individual scientists who request them from the Administrative Officer, Technical Information, Smithsonian Astrophysical Observatory, Cambridge 38, Massachusetts.